The Secret of Sailing (Draft)

Claes Johnson

Contents

Foreword

> Northern California has a storied, 500-year history of sailing. But despite this rich heritage, scientists and boat designers continue to learn more each day about what makes a sail boat move. Contrary to what you might expect, the physics of sailing still present some mysteries to modern sailors. (The Physics of Sailing [**?**])

In this book we present a mathematical theory of sailing based on a combination of analysis and computation. By computing and analyzing turbulent solutions of the incompressible Navier-Stokes equations for slightly viscous flow subject to force boundary conditions, we uncover the combined mechanisms of a sail and keel of generating lift and drag with crucial lift/drag ratio > 6 for the sail and > 10 for the keel, which can drive a sailing boat into the wind (with an upwind velocity component). This new theory is fundamentally different from that envisioned in the classical theories by Kutta-Zhukovsky for lift in inviscid flow and by Prandtl for drag in viscous flow. We show that lifting flow with large lift/drag ratio, results from an instability mechanism at rear separation of slightly viscous flow generating counter-rotating low-pressure rolls of streamwise vorticity inititated as surface vorticity resulting from meeting opposing flows. This mechanism is entirely different from the circulation mechanism of Kutta-Zhukovsky theory. We show that the new theory allows accurate *ab initio* computation of lift, drag and heeling moments of an entire sailing boat using a million mesh-points, instead of the impossible quadrillions of mesh-points required according to state-of-the-art following Prandtl's dictate of resolution of very thin boundary layers connected with no-slip velocity boundary conditions. The new theory thus offers a way out of the present deadlock of computational fluid mechanics of slightly viscous turbulent flow, and opens new possibilities of realistic simulation of sailing.

Stockholm Dec 2011

Claes Johnson

Figure 1: Seeking to balance the heeling on a beat.

Part I

Basics

Chapter 1

The Miracle of Sailing

> The pessimist complains about the wind; the optimist expects it to change; the realist adjusts the sails. (William Arthur Ward)

> He is the best sailor who can steer within the fewest points of the wind, and extract a motive power out of the greatest obstacles. Most begin to veer and tack as soon as the wind changes from aft, and as within the tropics it does not blow from all points of the compass, there are some harbors which they can never reach. (Henry David Thoreau)

The use of boats and in particular sailing boats has been instrumental in the development of human civilization. The big sail ships enabling World trade were replaced by a motored ships in the late 19th century, but may come back with increasing shortage of fuel.

The earliest representation of a ship under sail appears on an Egyptian vase from about 3500 B.C. Advances in sailing technology from the Middle Ages onward enabled Arab, Chinese, Indian and European explorers to make longer voyages into regions with extreme weather and climatic conditions. Improvements were made in the design of sails, masts and rigging, and navigational equipment became more sophisticated. From the 15th century onwards, European ships went further north, stayed longer on the Grand Banks and in the Gulf of St. Lawrence, and eventually began to explore the Pacific Northwest and the Western Arctic.

A *sailing boat* is a boat with a *sail* and usually also a *keel* attached to the hull under water. Depending on the direction of the wind to the direction of motion of the boat, sailing relies on different physical principles.

Sailing the boat within roughly 30 degrees either side of *dead downwind* (wind straight from behind) is called a *run*. In this case the sail is mounted roughly perpendicular to the wind direction and propels the boat simply by the *drag* from the airflow around the sail in the direction of the wind, and a keel is not really necessary.

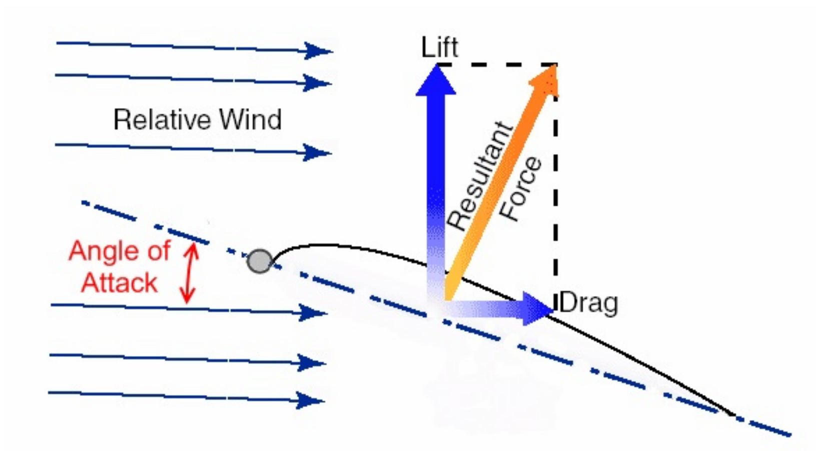

Figure 1.1: Lift L and drag D forces on a sail.

It is possible to also sail upwind (against the wind) by *beating* with *close-hauled* sails at 35-80 degrees off the wind depending on the boat, and repeatedly changing direction by *tacking*, but this requires a keel. In beating both the sail and keel act like *airfoils* generating forces of *lift* L and *drag* D at certain *angles of attack* of the sail to the wind direction and of the keel to the the motion of the boat through the water. A forward component of the lift from the sail (*drive*) propels the boat forward, while the side component (*heeling*) is balanced by lift in the opposite direction from the keel. The drive is balanced by drag forces from sail, keel and hull.

A good, modern *sloop* can sail within 25 degrees of the *apparent wind*, which is the real wind meeting the sail taking the boat velocity into account. An America's Cup racing sloop can sail within 16 degrees under ideal conditions. Those figures might translate into 45 degrees and 36 degrees relative to the actual wind, depending on boat speed.

The lift-to-drag quotient $\frac{L}{D}$ of both sail and keel needs to larger than 6-8 to allow beating at 45 degrees, and the miracle of sailing can thus be said to be to explain why a sail and a keel is capable of generating $\frac{L}{D} > 6 - 8$ with a larger value the better.

A boat traveling approximately perpendicular to the wind, that is between beating and running, is *reaching* with again both sail and keel acting like airfoils, with the difference to beating that sails are not close-hauled.

We focus in this book first on beating and reaching with both sail and keel acting like the wing on an airplane with $\frac{L}{D} > 6 - 8$ at maximal lift. The miracles of sailing and flying are thus closely connected.

When sailing dead downwind the speed of the boat is limited to the wind speed, since drive in this case comes from drag, but in reaching with drive from lift it is possible to go quicker than the wind speed, in which case the apparent wind is quite different from the true wind and sails have to be more close-hauled than with less speed. This effect(which is particularly pronounced in high-speed ice-sailing with the sails always close-hauled independent of the direction to the true wind.

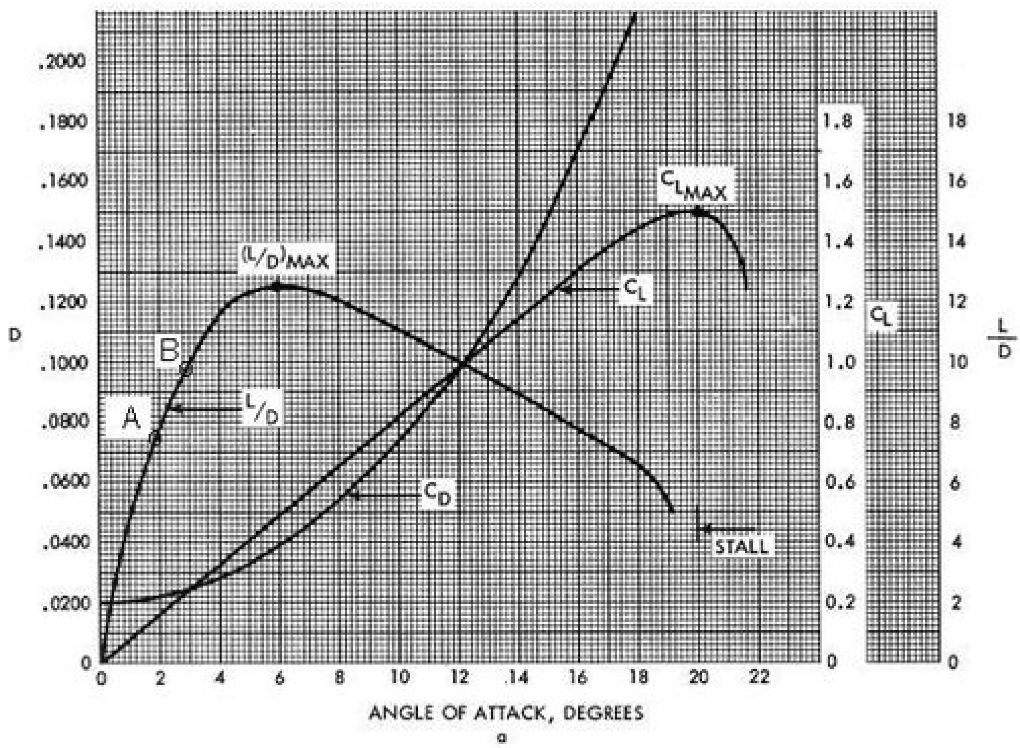

Figure 1.2: The secret of sailing: Lift L, drag D and lift-to-drag $\frac{L}{D}$ for different (apparent) angles of attack. Note that $\frac{L}{D} \approx 6$ at maximal lift at an angle of attack of 20 degrees, while maximum $\frac{L}{D} \approx 13$ is obtained at an angle of attack of 6 degrees.

Chapter 2

The Miracle of Beating

2.1 The Principle of Drive from Lift

Let us now do some simple mathematics showing the *principle of beating* under the assumption that $\frac{L}{D} > 10$ for both sail and keel. We then proceed as a main part of the book to explain in detail how sail and keel act to generate $\frac{L}{D} > 10$. Together this explains the miracle of sailing based on the miracle of beating.

We consider beating at speed v against a wind of speed w (both vs the water) under forces from a close-hauled sail (with beam parallel to the midline of the boat) at a given apparent angle of attack $\alpha \approx 15-20$ degrees, from a keel at a certain angle of attack (leeway) $\beta \approx 5-10$ degrees and from drag of the hull.

Commonly $v \approx \frac{2}{3}w$ corresponding to a speed of about $0.5w$ in the direction opposite to the wind, which is roughly the same as the speed in full downwind in the wind direction. A higher speed may thus be reached in beating than in full downwind, while the effective speed in the full upwind direction is the same as in the full downwind direction.

The forward drive force is given as the component $F = \sin(\alpha)L$ of the lift force L acting on the sail in a direction perpendicular to the apparent wind direction with F the component of L in the forward direction of the boat as shown in Fig. 2.1. The component $H = \cos(\alpha)L$ perpendicular to the direction of the boat creates heeling. The drag force D from the sail has a component $\cos(\alpha)D$ opposite to the drive F, and a (small) component $\sin(\alpha)D$ adding to the heeling, see Fig. 2.1.

The lift and drag forces on the sail from the wind are balanced by lift and drag forces on the keel from the motion of the boat through the water at the angle β off the direction of the midline of the boat, as shown in Fig. 2.1.

The lift coefficient L_S scales with the angle of attack α until stall at an angle of attack of $15-20$ degrees, that is $L_S(\alpha) \approx \bar{L}_S\alpha$ with $\bar{L}_S$ a certain constant for $\alpha < 15-20$. The drag coefficient increases quadratically from a positive minimal value for α, that is $D_S(\alpha) \approx D_S(0) + \bar{D}_S\alpha^2$ with A_D a constant. The lift and drag coefficients of the keel have the same dependence on the leeway β. The drag coefficient D_H for the hull is roughly constant up to a certain maximal speed determined by the length of the boat (scaling roughly with the squareroot of the length).

2.2 Balance of Heeling and Drive-Drag

Balancing heeling forces from sail and keel using that $\cos(\alpha) \approx \cos(\beta)$ and $\sin(\alpha)D \approx 0$, we have

$$L = L_S(v+w)^2 = L_K v^2, \tag{2.1}$$

where L_S is the *lift coefficient* of the sail for a given a given apparent angle α with $L = L_S(v+w)^2$ the lift force scaling quadratically with the approximate wind speed $v+w$ vs the sail, and L_K the corresponding lift coefficient for the keel at its angle of attack β.

Balancing the drive force F with the opposite drag forces using that $\cos(\alpha) \approx \cos(\beta) \approx 1$ and that the keel lift has a forward drive component, we have

$$\begin{aligned} F &= \sin(\alpha)L_S(v+w)^2 \\ &= D_S(v+w)^2 + \frac{D_K}{L_K}L_K v^2 - \sin(\beta)L_K v^2 + D_H v^2 \\ &= D_S(v+w)^2 + (\frac{D_K}{L_K} - \sin(\beta))L_S(v+w)^2 + D_H v^2, \end{aligned} \tag{2.2}$$

where we used (2.1) and D_S, D_K and D_H denote drag coefficients for sail, keel and hull. We thus find the following balance of drive and drag forces:

$$(\sin(\alpha) + \sin(\beta) - \frac{D_K}{L_K} - \frac{D_S}{L_S})L_S(v+w)^2 = D_H v^2, \tag{2.3}$$

which together with (2.1) determines the boat speed v and leeway β for each given apparent angle of attack α, with $\beta < \alpha$ for normal keels. With v determined the true angle of attack $\bar{\alpha}$ can be computed as $\bar{\alpha} \approx (1+\frac{v}{w})\alpha$. The boat speed in the direction opposite to the wind is then given as $\cos(\bar{\alpha}+\beta)v$, which is to be maximized in α to give maximal speed in the direction opposite to the wind.

We see that the drive $F = \sin(\alpha)L_S(v+w)^2$ has to balance the drag forces from sail, keel and hull, with thus $\sin(\alpha) + \sin(\beta) \approx \alpha + \beta$ at least twice as large as $\frac{D_S}{L_S} + \frac{D_K}{L_K}$ to overcome the drag $D_H(v)$ from the hull.

With $\alpha \approx\approx 20$, $\beta \approx 10$ and $\sin(\alpha) + \sin(\beta) \approx 0.5$, this requires $\frac{L_S}{D_S}$ and $\frac{L_K}{D_K}$ to be larger than $6 - 8$.

2.3 The Miracle: $\frac{L}{D} > 10$

The miracle of sailing is that lift-to-drag ratios of sail and keel can be as large as 10. This book gives a new explanation of the physics of this miracle, which is not correctly described in the literature. The new explanation is expected to open to new designs of sails and keels.

2.4 Analysis of Standard Case

Simplifying (2.4) to

$$\sin(\alpha)L_S(v+w)^2 = D_H v^2, \tag{2.4}$$

and using that $L_S = \bar{L}_S\,\alpha$ and $\sin(\alpha) \approx \alpha$ (measuring here α in radians), we find that

$$v = \gamma w, \quad \gamma = \frac{A\alpha}{1 - A\alpha}, \quad A = \sqrt{\frac{\bar{L}_S}{D_H}}. \tag{2.5}$$

With $\alpha = 0.25$ as maximal value and $A = 1.6$, we have $A\alpha = 0.4$ and $\gamma = \frac{2}{3}$ representing a standard case.

To check if the upwind velocity $\bar{v}(\alpha) \equiv \cos(\alpha)v$ is maximized for $\alpha = 0.25$, we differentiate to get

$$\frac{d\bar{v}}{d\alpha} = \cos(\alpha)\frac{dv}{d\alpha} - \sin(\alpha)v, \quad \frac{dv}{d\alpha} = \frac{Aw}{(1 - A\alpha)^2}, \tag{2.6}$$

which shows that $\frac{d\bar{v}}{d\alpha} > 0$ for $\alpha = 0.25$.

The progress upwind with the lift-drag curves according to Fig. 1.2 is thus optimized at maximal lift L_S from the sail at maximal angle of attack $\alpha \approx 18$ slightly before stall with $\frac{L_S}{D_S} = 6 - 8$, while the angle of attack of the keel β typically is smaller $(5 - 10)$ and $\frac{L_K}{D_K}$ larger ≈ 12.

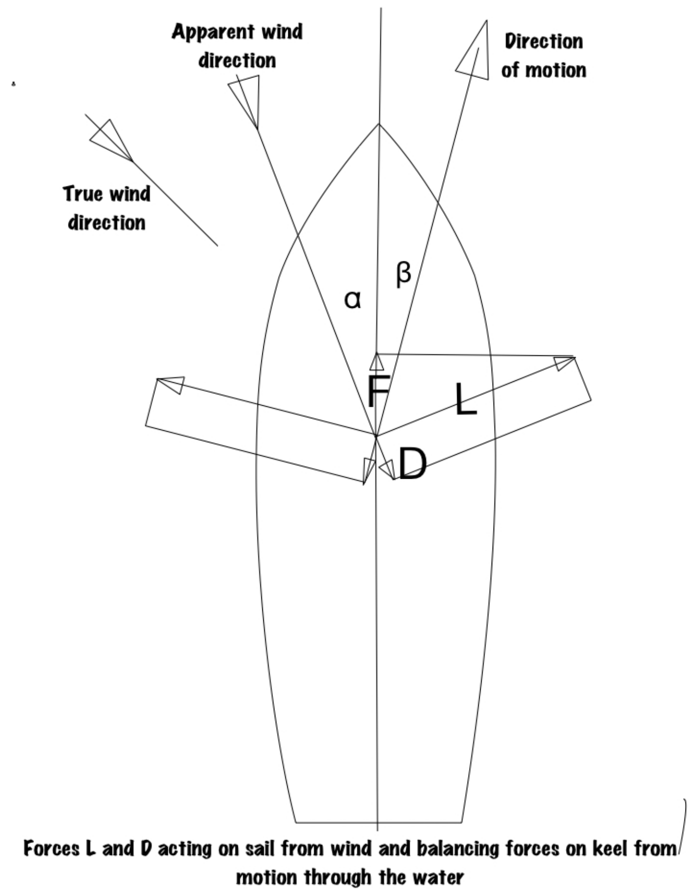

Figure 2.1: Lift L and drag D from sail at beating with drive $F = \sin(\alpha)L$ at angle of attack α, balanced by lift and drag from the keel at the angle of attack β (plus drag from the hull). Notice that the wind approaches the sail from the left, while the water approaches the keel from the right, giving opposite lift forces.

Chapter 3

Americas Cup Wing-Sail

AC45 is a forerunner to the next generation of Americas Cup boats: A wing-sailed catamaran designed for speed over 30 mph and close racing.

Figure 3.1: AC 45 wing sail.

- AC45, Capsize, Wing sail

Figure 3.2: AC 45 beating.

Chapter 4

Empty State-of-the-Art Theory

To get motivation to go into the new theory of sailing it may help to understand that state-of-the-art has very little to offer to explain the miracle of sailing. Here is what the web offers:

- School of Physics U of New South Wales: Newton's old theory (incorrect)
- physicstoday: Bernoulli or Newton? (both incorrect or empty)
- Wikipedia: Like an airplane wing (empty)
- U of Alaska-Fairbanks: Bernoulli (incorrect or empty)
- Real World Physics Problems: Newton (incorrect)
- Teacher's Domain: Like an airplane wing, Bernoulli (incorrect or empty)
- U of North Carolina: Bernoulli (incorrect or empty)
- howstuffworks: Bernoulli (incorrect or empty)
- The Physics of Sailing Explained: Bernoulli (incorrect or empty)

The most ambitious treatment is given in Physics of Sailing by J. Kimball, where both Bernoulli and Kutta-Zhukovsky's circulation theory (incorrect) are presented, but with a disappointing sum-up on p 163:

- *The sail experiences lift because the sail deflects the wind. Equal and opposite forces mean that is the sail pushes the wind in one direction, the wind pushes the sail the other way.*
- *This explanation, which relies only on the rule of equal and opposite forces, is surely correct.*

Yes, it is surely correct, as any empty theory which explains nothing, as illustrated in the above picture.

We see that there is surely a great need for a correct theory which explains the physics of sailing and that there is no such theory in state-of-the-art. Our work fills this gap in physics theory and in particular shows that the state-of-the-art explanations represented by Newton, Bernoulli or Kutta-Zhukovsky are all incorrect.

Of course, the physics of flying and sailing is not of any interest to physicists of today paralyzed by string theory, but it is an interesting problem of physics of importance to many.

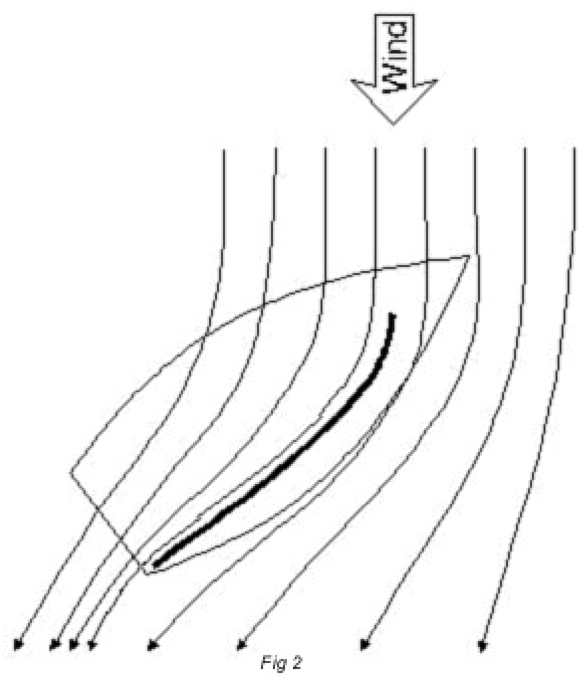

Figure 4.1: Empty explanation of lift of a sail as a reaction force from redirection of airflow.

Chapter 5

Sailboats

> If one does not know to which port one is sailing, no wind is favourable. (Seneca)
>
> When everything seems to be going against you, remember that the airplane takes off against the wind, not with it. (Henry Ford)
>
> A certain amount of opposition is a great help to a man. Kites rise against and not with the wind. Even a head wind is better than none. No man ever worked his passage anywhere in a dead calm. Let no man wax pale, therefore, because of opposition. (John Neal)

Since ancient times, people have been sailing in sailboats, as a quicker way to get across body of water then using a row boat. The ancient Romans combined both rowing and sailing into one boat and built a formidable navy of booats with many sails and slaves at oars in the hull. When man fitted his ship with a sail he probably made the most cost efficient way to travel. The fastest and most efficient sail boats of the 19th century were the *clipper ships* relying only on wind power.

Ancient sail boats used hand woven sails that were very durable and could stand the onslaught of the salty waves and the wind. Modern sails are made of lightweight polyester which can withstand dampness better than the sails made from natural fiber.

5.1 Phoenician Ships

The best seafarers and ship builders of the ancient world were the Phoenicians using well designed ships for carrying both cargo and supplies needed by the sailors. Both war and merchant ships were made with foresails, the sail hung on the forward mast or stay, with the mainsail in the centre of the boat. The keeled boat or ship is very likely a Phoenician invention. Both with oars and sails they plied the waters of the Mediterranean and eager for scarce trade goods, the Phoenicians passed the pillars of Hercules to the Atlantic, and south to trade ivory with the West Africans, and north to the British Isles seeking tin and lead.

The history of the Phoenicians spans centuries. From crude dugout canoes through keeled oared boats and on to keeled ships with both sail and oars. There are images of Phoenician ships on many ancient coins. The Phoenicians of Tyre had the great benefit of being a port city at the end of great caravan routes. They exploited this to the extreme, and founded trading colonies in many locations around the Mediterranean. The Phoenicians are the forebears of the Carthaginians, and they invented double decked war galleys called biremes whose bronze beaks or rams were greatly feared by opposing ships. The Greeks of Corinth are said to have one upped this idea with the invention of the trireme, and by the time of the Carthaginians the idea of extra oar decks for increased power and speed had been pushed to the extreme in the form of four and five decked warships.

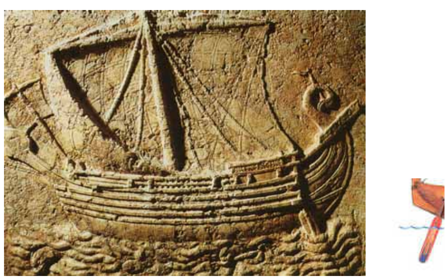

Figure 5.1: Phoenician round ships.

5.2 Polynesian Outriggs

The Polynesian people are considered to be by ancestry a subset of the sea-migrating Austronesian people and the tracing of Polynesian languages places their prehistoric origins in the Malay archipelago some 3000-8000 years ago.

Between 300 and 500 AD, the Polynesians discovered and settled Rapa Nui (Easter Island). Around AD 500 Hawai'i was settled by the Polynesians and around AD 1000 Aotearoa (New Zealand). The migration of the Polynesians is impressive considering that the islands settled by them are spread out over great distances the Pacific Ocean covers nearly a half of the Earth's surface area. Most contemporary cultures, by comparison, never voyaged beyond sight of land. Polynesians used outriggs, the predecessors of todays catamarans:

Figure 5.2: Zanzibar outrigg with lateen sail still common.

5.3 Viking Longships

Viking *longships* were ships primarily used by the Scandinavian Vikings and the Saxon people to raid coastal and inland settlements during the European Middle Ages. The vessels were also used for long distance trade and commerce, and for exploratory voyages to Iceland, Greenland, and beyond. Longship design evolved over several centuries and was fully developed by about the 9th century. The character and appearance of these ships have been reflected in Scandinavian boat-building traditions until today.

The longship was characterized as a graceful, long, narrow, light wooden boat with a shallow draft hull designed for speed. The ship's shallow draft allowed navigation in waters only one meter deep and permitted beach landings, while its light weight enabled it to be carried over portages. Longships were also double-ended, the symmetrical bow and stern allowing the ship to reverse direction quickly, without having to turn around. Longships were fitted with oars along almost the entire length of the boat itself. Later versions sported a rectangular sail on a single mast which was used to replace or augment the effort of the rowers, particularly during long journeys. Longships were the epitome of Scandinavian naval power at the time, although earlier shipbuilding techniques in ancient Greece and Rome, were far more sophisticated and varied, especially in terms of joinery.

Figure 5.3: Reconstructed viking longship.

Even though no longship sail has been found, accounts verify that longships had square sails. Sails measured perhaps 35 to 40 feet (12 m) across, and were made of wadmill (rough wool) which was woven by looms. Unlike the knarrs, the longship sail was not stitched. The sail was held in place by the mast. The mast was supported by a large block of wood called "kerling" ("Old Woman" in Old Norse). (Trent) The kerling was made of oak, and was as tall as a Viking man. The kerling lay across the two ribs and ran width-wise along the keel. The kerling also had a companion: the "mast fish", a wooden piece above the kerling that provided extra help in keeping the mast erect.

The longship had two methods of propulsion: oars and sail. At sea, the sail enabled longships to travel faster than by oar and to cover long distances overseas. Sails could be raised or lowered quickly. Oars were used when near the coast or in a river, to gain speed quickly, and when there was an adverse (or insufficient) wind. In combat, the variability of wind power made rowing the chief means of propulsion. Longships were not fitted with benches. When rowing, the crew sat on sea chests (chests containing their personal possessions) that would otherwise take up space. The chests were made the same size and were the perfect height for a Viking to sit on and row. Longships had hooks for oars to fit into, but smaller oars were also used, with crooks or bends to be used as oarlocks. If there were no holes then a loop of rope kept the oars in place.

The longship was a master of all trades: it was wide and stable, yet light, fast and nimble. With all these qualities combined in one ship, the longship was unrivaled for centuries, until the arrival of the great cog.

In Scandinavia, the longship was the usual vessel for war even with the introduction of cogs in the 12th-13th century by the late 14th century, these low-boarded vessels were at a disadvantage against newer, taller vessels - when the Victual Brothers, in the employee of the Hansa, attacked Bergen in the autumn of 1393, the "great ships" of the pirates could not be boarded by the norwegian levy ships called out by Margaret I of Denmark and the raiders were able to sack the town with impunity. While earlier times had seen larger and taller longships in service, by this time the authorities had also gone over to other types of ships for warfare.

5.4 Cogs

A *cog* is a type of ship that first appeared in the 10th century, and was widely used from around the 12th century on. Cogs were generally built of oak, which was an abundant timber in the Baltic. This vessel was fitted with a single mast and a square-rigged single sail. Even though this type of rigging prohibited sailing into the wind, it could be handled by a smaller crew, which reduced operational costs. These vessels were mostly associated with seagoing trade in medieval Europe, particularly in the Baltic Sea region.

Figure 5.4: British cog.

5.5 Sailing Ships

The **caravel** was a small ship made of the common beachwood found on the shores of Europe. These ships had three masts, the mizzen carrying a lateen sail, while the fore and main were square rigged. Larger ones had a square rigged foremast, while the main, mizzen, and bonaventure were lateen rigged. Christopher Columbus' Pinta and Nina were caravels. Also, Vasco Da Gama and other Portuguese explorers used the caravel to reach India via the Cape of Good Hope. John Cabot's ship Mattew was alos a caravel. Magellan had a caravel in his posession when he commanded the first circumnavagation. Caravels were capable ships and perfect for those first voyages out from the shores of Europe by Spain, Portugal, and England. They were faster than many other ships, but carried few guns. They were essentially merchant ships ranging from 60 to 200 tons.

The **carrack** was similar in rig to the caravel. These ships usually had the same sail arrangements as a Caravel, but with the addition of a spritsail on the bowsprit, and a topsail on the main mast. Carracks were also quite larger. The Portuguese were well known around the world for their huge, if unseaworthy, carracks. In Japan, Portuguese carracks were known as 'black ships', because of the black tar that covered their sides. The fore and after castles on these ships extended much higher than they needed to be, causing them to tip over in strong winds. Columbus' Santa Maria was a small carrack. The advent of the galleon made the carrack obsolete.

The **sloop** was a small craft with almost yacht characteristics. These ships had one mast, being square rigged with a gaff-spanker and jibs. Eventually, the speed of these ships brought an entire fleet, used to hunt down pirates in the late 17th century.

Seemigly a greatly generalized term, the word **barque** applies to a number of small merchant and coastal vessels. These ships range from fully lateen rigged to square rigged ships. These ships usually did not exceed 300 tons, and sometimes had oars to propell them through poor winds or into the eye of the wind.

A very well specified ship, **flutes** had the hull qualities of the smaller ships (a shallow draft), but had more cargo space and were square rigged with a lateen sail on the mizzen. Though these ships had more space, they lacked oars so going into the wind brought them to a halt. The Dutch used these ships commonly, and the English did aswell, only to a lesser extent. Flutes were common in the Caribbean, Dutch coastal waters, and the ports of Britain. It was a very popular ship type.

The **frigate** was a light, fast, but heavily armed warship used by all European nations. Square rigged as was the sail arrangement of most ships of its size, making it a fast and formidable opponent in battle. These ships usually sailed alone but when ever pirates spotted them, the pirates would fade into the distance. Such ships had the quality of being faster than anything more heavily armed, and more heavily armed than anything faster. 20 to 30 guns was the usual weapons compliment of frigates in this age.

The **spanish galeon** most heavily armed and largest merchant vessel of the period, they were cumbersome and slow. Such ships were employed by Spanish Treasure Fleets that carried gold, silver, and jewels from the Caribbean to Spain. They often had a large compliment of guns and crews to protect them if they were ever let a-stray from the fleet. Much of the Spanish Armada was made up of such ships, totalling 64 galleons. The average galleon carried a spritsail, top and course on the fore mast, top and main on the main mast, and lateen rigged mizzen and bonaventure. These ships had reduced upper superstructure, making them seaworthy enough to travel the globe. They best sailed with the main course furled.

5.6 Chinese Junk

A *junk* is a Chinese sailing vessel originally developed during the Han Dynasty (220 BC200 AD) and further evolved to represent one of the most successful ship types in history. Unlike a traditional square rigged ship, the sails of a junk can be moved inward, toward the long axis of the ship, allowing the junk to sail into the wind. The sails include several horizontal members, called "battens", which provide shape and strength. Junk sails are controlled at their trailing edge by lines much in the same way as the mainsail on a typical sailboat; however, in the junk sail each batten has a line attached to its trailing edge where on a typical sailboat this line (the sheet) is attached only to the boom. The sails can also be easily reefed and adjusted for fullness, to accommodate various wind strengths. The battens also make the sails more resistant than traditional sails to large tears, as a tear is typically limited to a single "panel" between battens. Junk sails have much in common with the most aerodynamically efficient sails used today in windsurfers or catamarans, although their design can be traced back as early the 3rd century AD. The standing rigging is simple or absent. The sail-plan is also spread out between multiple masts, allowing for a powerful sail surface, and a good repartition of efforts. The rig allows for good sailing into the wind.

The bottom is flat with no keel (similar to a sampan), so that the boat relies on a daggerboard or very large rudder to prevent the boat from slipping sideways in the water.The largest junks were built for world exploration in the 1400s, and were over 120 metres in length.

5.7 The Swedish Ship Vasa

Vasa was a warship built for King Gustavus Adolphus of Sweden from 1626 to 1628. The ship foundered and sank after sailing less than a nautical mile (ca 2 km) into her maiden voyage on 10 August 1628. Vasa fell into obscurity after initial attempts at recovering her valuable cannons in the 17th century but was located again in the late 1950s and salvaged with a largely intact hull and later put into the Vasa Museum in Stockholm.

Vasa was too top-heavy with two gun-decks and insufficient ballast and was known to be unstable already in port. Nevertheless, because King Gustavus Adolphus was impatient to see Vasa join the Baltic fleet in the Thirty

Figure 5.5: Junk.

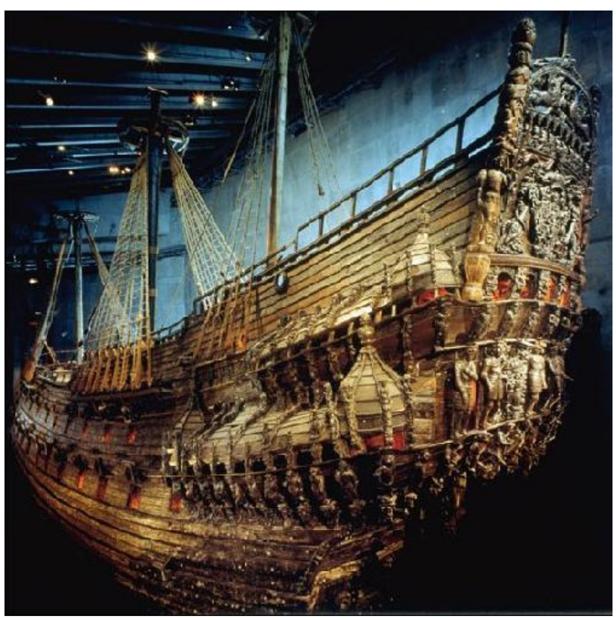

Figure 5.6: The stern of the Vasa Ship with excessive decoration.

Years' War, she was allowed to set sail and foundered a few minutes later when she first encountered a wind stronger than a breeze.

5.8 Arabian Dhow

A *dhow*is a traditional Arab sailing vessel with one or more *lateen sails*, as described below. They are primarily used along the coasts of the Arabian Peninsula, Pakistan, India, and East Africa. Larger dhows have crews of approximately thirty, while smaller dhows typically have crews of around twelve.

Up to the 1960s, dhows made commercial journeys between the Persian Gulf and East Africa using sails as their only means of propulsion. Their cargo was mostly dates and fish to East Africa and mangrove timber to the lands in the Persian Gulf. They sailed south with the monsoon in winter or early spring and back again to Arabia in late spring or early summer. The term "dhow" is also applied to small, traditionally-constructed vessels used for trade in the Red Sea and the Persian Gulf area and the Indian Ocean from Madagascar to the Gulf of Bengal. Such vessels typically weigh 300 to 500 tons, and have a long, thin hull design.

Figure 5.7: Dhow with lateen sail.

Figure 5.8: Building a dhow on Zanibar in 2005.

Chapter 6

Riggs

6.1 Lateen Sail

The lateen sail was used in Arabian Seas at least since the fourth century B.C. A lateen (from a la trina, meaning triangular) or latin-rig is a triangular sail set on a long yard mounted at an angle on the mast, and running in a fore-and-aft direction.

In western culture, the rig is originally reported found on sailing ships about the Mediterranean Sea, where the sail plan may have originated with the Arab traders plying the coastal routes of the spice trade across the Red Sea and Indian Ocean. The lateen is used today in a slightly different form on small recreational boats like the highly popular Sunfish, but is still used as a working rig by coastal fishermen in the Mediterranean outside East Africa and the northwestern parts of the Indian Ocean, where it is the standard rig for feluccas and dhows.

Until the 14th century, the lateen sail was employed primarily on the Mediterranean Sea and Indian Ocean, while the Atlantic and Baltic vessels relied on square sails. The Northern European adoption of the lateen in the Late Middle Ages was a specialized sail that was one of the technological developments in shipbuilding that made ships more maneuverable, thus, in the historian's traditional progression, permitting merchants to sail out of the Mediterranean and into the Atlantic Ocean; caravels typically mounted three or more lateens. However, the great size of the lateen yardarm makes it difficult and dangerous to handle on large ships in stormy weather, and by the eighteenth century the lateen was restricted to the mizzen mast. In the

Figure 6.1: Contemporary version of lateen sail.

early nineteenth century the lateen was replaced in European ships by the driver or spanker.

One of the disadvantages of the lateen, especially in the modern form described below, is the fact that it has a "bad tack". Since the sail is to the side of the mast, on one tack that puts the mast directly against the sail on the leeward side, where it can significantly interfere with the airflow over the sail. On the other tack the sail is pushed away from the mast, greatly reducing the interference. On modern lateens, with their typically shallower angles, this tends to disrupt the airflow over a larger area of the sail.

The lateen rig was also the ancestor of the Bermuda rig, by way of the Dutch bezaan rig. In the 16th Century, when Spain ruled the Netherlands, Moorish lateen rigs were introduced to Dutch boat builders who soon modified the design by omitting the mast and fastening the lower end of the yard directly to the deck, the yard becoming a raked mast with a full-length, triangular (leg-of-mutton) mainsail aft. Introduced to Bermuda early in the 17th Century, this developed into the Bermuda rig, which, in the 20th Century, was adopted almost universally for small sailing vessels.

6.2 Gaff Rig

Gaff rig is a sailing rig (configuration of sails) in which the sail is four-cornered, fore-and-aft rigged, controlled at its peak and, usually, its entire head by a spar (pole) called the gaff. The gaff enables a fore and aft sail to be four sided, rather than triangular, and as much as doubles the sail area that can be carried by that mast and boom (if a boom is used in the particular rig). A sail hoisted from a gaff is called a gaff rigged sail. Gaff rig remains the most popular rig for schooner and barquentine mainsails and other course sails, and spanker sails on a square rigged vessel are always gaff rigged. On other rigs, particularly the sloop, ketch and yawl, gaff rigged sails were once common but have now been largely replaced by the Bermuda rig sail.

Figure 6.2: Gaff rigg

6.3 Bermuda/Marconi Rig

The term Bermuda rig refers to a configuration of mast and rigging for a type of sailboat and is also known as a Marconi rig; this is the typical configuration for most modern sailboats. Developed in Bermuda in the 17th century, the

Figure 6.3: Bermuda rig with masthead jib.

term Marconi was a much later reference to the inventor Guglielmo Marconi, whose wireless radio masts the Bermuda rigs were said to resemble.

The rig consists of a triangular sail set aft of the mast with its head raised to the top of the mast; its luff runs down the mast and is normally attached to it for its entire length; its tack is attached at the base of the mast; its foot controlled by a boom; and its clew attached to the aft end of the boom, which is controlled by its sheet. Originally developed for smaller Bermudian vessels, and ultimately adapted to the larger, ocean-going Bermuda sloop, the Bermuda sail is either set as a mainsail on the main mast, or as the course (the principal sail) on another mast. The Bermuda rigging has largely replaced the older gaff rigged fore-and-aft sails, except notably on schooners.

The traditional design as developed in Bermuda featured very tall, raked masts, long bowsprits and booms, and vast areas of sail. Modern design has omitted the bowsprit (although it is coming back in the Volvo Ocean Race) and otherwise become less extreme.

The main controls on a Bermuda sail are: The halyard used to raise the head, and sometimes to tension the luff. The outhaul used to tension the foot by hauling the clew towards the end of the boom. The sheet used to haul the boom down and towards the center of the boat. The vang or kicking strap which runs between a point partway along the boom and the base of the mast, and is used to haul the boom down when on a run.

Figure 6.4: Beating in Volvo Ocean Race.

Figure 6.5: Reaching in Volvo Ocean Race

Figure 6.6: Main sail and jib in beating.

Figure 6.7: Main sail and jib in beating.

6.4 Sloop

Today, the most common sailboat is the sloop which features one mast and two sails, a normal mainsail and a foresail. This simple configuration is very efficient for sailing towards the wind. The mainsail is attached to the mast and the boom, which is a spar capable of swinging across the boat, depending on the direction of the wind. Depending on the size and design of the foresail it can be called a jib, genoa, or spinnaker; it is possible but not common for a sloop to carry two foresails from the one forestay at one time (wing on wing). The forestay is a line or cable running from near the top of the mast to a point near the bow.

Figure 6.8: Beating optimist.

6.5 Clipper, Ketch, Yawl, Scooner

Figure 6.9: Reaching windsurfer

Figure 6.10: The author's P28 on a beat outside Tjörn on the West Coast of Sweden.

Chapter 7

Americas Cup

> Design has taken the place of what sailing used to be. (Dennis Conner)

> Writing criticism is to writing fiction and poetry as hugging the shore is to sailing in the open sea. (John Updike)

7.1 America of New York Yacht Club

The Americas Cup is the most prestigious regatta and match race in the sport of sailing, and the oldest active trophy in international sport, predating the Modern Olympics by 45 years. The regattas origins date back to 1851 when the 31 m schooner-yacht *America*, owned by a syndicate that represented the New York Yacht Club, raced 15 yachts representing the Royal Yacht Squadron around the Isle of Wight. America won by 20 minutes. Apocryphally, Queen Victoria asked who was second; the answer famously was: "Ah, Your Majesty, there is no second". The trophy remained in the hands of the New York Yacht Club of the United States from 1852 until 1983 when the Cup was won by the challenger, *Australia II* of Australia.

The Americas Cup regatta is a challenge-driven series of match races between two yachts. Since the 1992 match, the regatta has been sailed with the International Americas Cup Class (IACC) sloop monohull class. Boats that conform to the IACC rules typically have a length of about 23 m.


Valkyrie III

Figure 7.1: Americas Cup 1895

7.2 Shamrock

One of the most famous and determined challengers was Scottish tea baron Sir Thomas Lipton. Between 1899 and 1930 he mounted five challenges, all in yachts named *Shamrock*, to gain publicity for his company, though his original entry was at the personal request of the Prince of Wales in hopes of repairing trans-Atlantic ill-will generated by the contentious earlier challenger, who had accused the NYYC of cheating. Lipton was preparing for his sixth challenge when he died in 1931. The yachts used during the Lipton era were very large sailing sloops in the *J-class* with *Shamrock V* still sailing today measuring 36 m long.

7.3 The 12-metre Class

After World War II, the huge and expensive J-class yachts were replaced by the much smaller *12-metre class* yachts, which measure from approximately 20 to 23 m overall. The New York Yacht Club's unbeaten streak continued in eight more defenses, running from 1958 to 1980. The inventor of the cunningham sail control device to increase performance, Briggs Cunningham, skippered the *Columbia* during its 1958 victory against *Sceptre* in the first challenge after 1937. In 1983 *Australia II* won the Americas Cup 4-3 breaking the 132-year winning streak, sporting a new innovative winged keel. Beaten skipper Dennis Conner won the Cup back four years later with *Stars&Stripes*.

7.4 The 1988 Big Boat Cup

In 1988 a New Zealand syndicate lodged a surprise *Big Boat* challenge under the original rules of the Cup Trust Deed with a gigantic yacht named *New Zealand* even larger than a J-class yacht. Conner's syndicate, however, recognised that a catamaran was not expressly prohibited under the rules, and the two yachts raced under the simple terms of the Deed in September 1988. New Zealand predictably lost by a huge margin in what most observers described then and since as the most controversial cup match ever.

Figure 7.2: Beating

7.5 IACC

In the wake of the 1988 challenge, the International Americas Cup Class *IACC* of yachts was introduced, replacing the 12-metre class that had been used since 1958. First raced in 1992, the IACC yachts were used until the 2007 America's Cup. In 1992, *USA-23* skippered by billionaire Bill Koch defeated the Italian challenger *Il Moro di Venezia* owned by billionaire Raul Gardini 5-1.

In 1995, The Royal New Zealand Yacht Squadron syndicate Team New Zealand with *Black Magic* skippered by Russell Coutts defeated Dennis Connors *Stars&Stripes* 5-0, and at Auckland in 1999-2000 defeated Italy's *Challenger* in the first America's Cup without an American challenger or defender. In 2003, several strong challengers vied for the cup in Auckland during the challenger selection series. Notably a number of original members of Team New Zealand including previous helmsman Russell Coutts were key members of the Swiss challenge *Alinghi* sponsored by pharmaceutical billionaire Ernesto Bertarelli, and won the Cup with surprising ease 5-0. *Alinghi* successfully defended the Cup 2007 by beating Emirates Team *New Zealand* 5-2 in Valencia.

The status of the 33rd America's Cup regatta is currently being litigated, with a resolution expected by April, 2009.

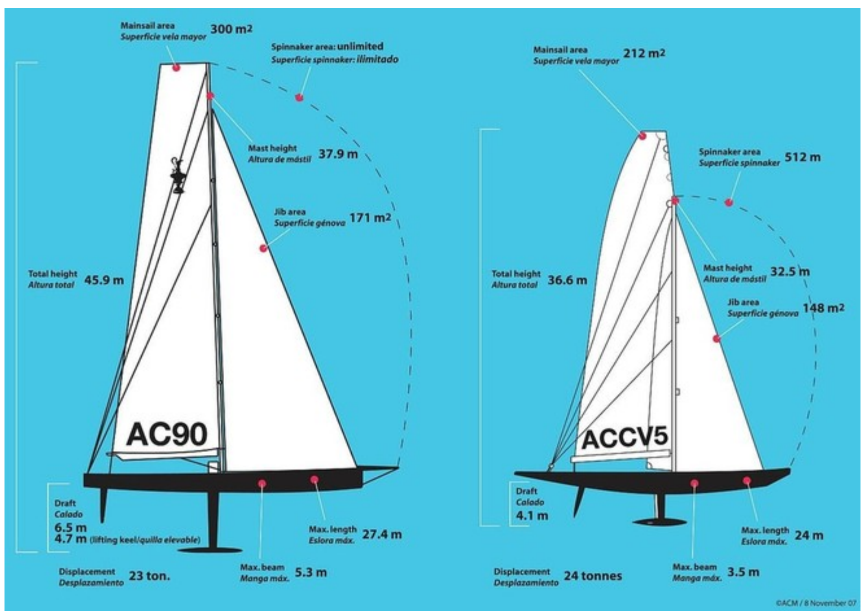

Figure 7.3: Old and new design

Part II

Lift and Drag

Chapter 8

The Mystery of Flight

> Few physical principles have ever been explained as poorly as the mechanism of lift [90].

8.1 What Keeps Airplanes in the Air?

The mystery of the flight of birds must have captured already the imagination of the early cave man, but it has remained a mystery from scientific point of view into our days of airborne mass transportation. How can that be? Isn't it known what keeps an airplane in the air? Is there no answer to give a curious child or someone with fear of flying? No, not if we seek a real answer [91]:

- *How do airplane wings really work? Amazingly enough, this question is still argued in many places, from elementary school classrooms all the way up to major pilot schools, and even in the engineering departments of major aircraft companies. This is unexpected, since we would assume that aircraft physics was completely explored early this century. Obviously the answers must be spelled out in detail in numerous old dusty aerodynamics texts. However, this is not quite the case. Those old texts contain the details of the math, but it's the interpretation of the math that causes the controversy. There is an ongoing Religious War over both the way we should understand the functioning of wings, and over the way we should explain them in children's textbooks.*

Of course you don't expect birds to understand why they can fly. You probably believe that somehow evolution has designed birds so that they can fly, presumably by some trial and error process over millions of year, while keeping human beings on the ground despite many efforts until Orwille and Wilbur Wright in 1903 showed that powered human flight in fact is possible by getting their *Flyer* into sustained flight with the help of a 12 horse-power engine.

But like the birds, Orwille and Wilbur did not have to really understand *why* what they managed to do was possible; they just managed somehow to do it by trial and error, building on the careful studies of bird wings by Lilienthal from the 1890s.

Orwille and Wilbur had computed that with a lift to drag ratio of 10 and a velocity of 10 meter per second, 4 effective horse-powers would get the 300 kg of the *Flyer* off ground at an effective thrust of 30 kp, and it worked! A human being of 75 kg capabable of delivering 1 horse power should also be able to take off...

Science is about understanding and understanding flight is to be able to explain from the principles of fluid mechanics how a wing can generate large lift at small drag, that is, to explain the miracle of Fig. [**?**].

Figure 8.1: How can a 400 ton Airbus380 take off at an engine thrust of 40 tons?

8.2 Understand a Miracle

The challenge from a scientific point of view is to explain using mathematics how a fixed wing by moving horisontally through air can generate a large lift L balancing gravitation while the drag D as the horisontal force on the wing from the air is small. The lift to drag quotient L/D is typically of size $10-20$ in the *gliding flight* of birds and of airplanes at subsonic speeds, and can reach 70 for an extreme glider, which can glide 70 meters upon loosing 1 meter in altitude.

Charles Lindberg crossed the Atlantic in 1927 at a speed of 50 m/s in his 2000 kg *Spirit of St Louis* at an effective engine thrust of 150 kp (with $\frac{L}{D} = 2000/150 \approx 13$) from 100 horse powers.

By Newton's 3rd law, lift must be accompanied by *downwash* with the wing redirecting air downwards. The enigma of flight is the mechanism of a wing generating substantial downwash at small drag, which is also the enigma of sailing against the wind with both sail and keel acting like wings creating substantial lift.

Flying on wings and sailing against the wind is a miracle, and the challenge from scientific point of view is explain the miracle of $L/D > 10$. NASA pretends to explain the miracle of the flight of the *Flyer* in Fig. 8.2 as a conseqence of Newton's Third Law. Do you get it?

Flying on a barn door tilted at 45 degrees with $L/D \approx 1$ would not be a scientific miracle, but only a rocket can generate a thrust equal to its own weight and then only for a short period of time, and air transportation by rockets is nothing for birds and ordinary people, only for astronauts.

The lift force L increases quadratically with the speed and linearly with the *angle of attack*, that is the tilting of the wing from the direction of flight, until *stall* at about 15 degrees, when the drag abruptly increases and L/D becomes too small for sustained flight.

8.3 Aerodynamics as Navier-Stokes Solutions

Fluid mechanics is well described by the Navier-Stokes equations expressing conservation of mass, momentum and energy, but there are two basic issues to handle: The viscosity of the fluid is needed as input and the equations in general have turbulent solutions defying analytical description and thus have to be solved computationally using computers.

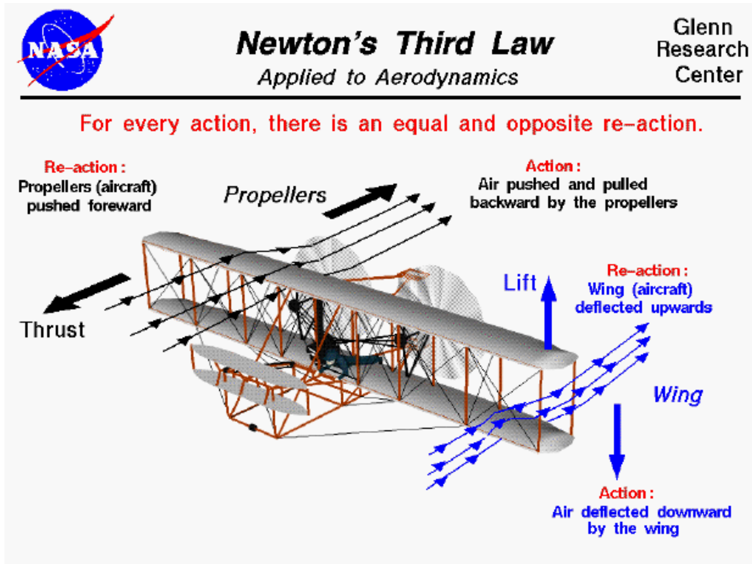

Figure 8.2: Tautological explanation of the flight of *The Flyer* by NASA:: There is upward lift on the wing from the air as a reaction to a downward push on the air from the wing.

In aerodynamics or fluid dynamics of air with small viscosity, these issues come together in a fortunate way: The precise value of the small viscosity shows to be largely irrelevant as concerns macroscopic quantities such as lift and drag, and the turbulent solutions always appearing in slightly viscous flow, show to be computable.

We shall find that there is a catch here, which we will adress shortly, but fortunately a catch which can be overcome, because in Einstein's words:

- *Subtle is the Lord, but malicious He is not.*

This means that the secret of flight can be uncovered by solving the Navier-Stokes equations and analyzing the computed solutions. We thus have at our disposal a complete fluid mechanics laboratory where we can study every aspect of the flow around a wing, or an entire airplane in the critical dynamics of take-off and landing, and also the flapping flight of bird. Nature can hide its secrets in real analog form, but not in digital simulation.

This leads to the program of this book:

- Solve the Navier-Stokes equations computationally.

- Study the computed turbulent solutions.
- Discover the mechanism creating large lift at small drag.
- Formalize the discovery into a new understandable theory of flight.

8.4 Computation vs Experiments

In Fig. 8.3 we show computed lift and drag (coefficients) C_L and C_D of a long NACA012 wing under varying angles of attack from cruising over take-off/landing to stall, obtained by solving the Navier-Stokes equations using automatically adapted meshes with less than 10^6 mesh points (blue curve) compared to measured values in wind tunnel experiments. The computational values lie within the range of the experimental values and thus evidently capture reality.

The message is that it is possible to compute the lift and drag of an airplane in the whole range of angles of attack, from small angles of stationary cruising at high speed, to large angles close to stall in the dynamics of start and landing at low speed. This is a happy new message, since state-of-the-art tells [59] that 50 years of doubled computer power every 18 months are need to make computation of lift and drag of an airplane possible by solving the Navier-Stokes equations.

We hope this gives the reader motivation to continue reading to discover how a wing generates large lift at small drag, the mystery of flight.

8.5 Many Old Theories: None Correct

Before revealing the essence of the new theory we address some of the many incorrect explanations of flight that you find in text books and media. If many different theories of a certain physical phenomenon coexist over time, which has been the case as concerns flight over a period of 100 years, it is a sign that none of the theories is correct. Right?

If there is a correct theory none of the incorrect theories can survive, as illustrated e.g. by the homogeneity of the (correct) homo sapiens without any surviving (incorrect) Neanderthalers.

To properly understand the correct theory, it is useful to study (some of the) incorrect theories, because even an incorrect theories usually contains

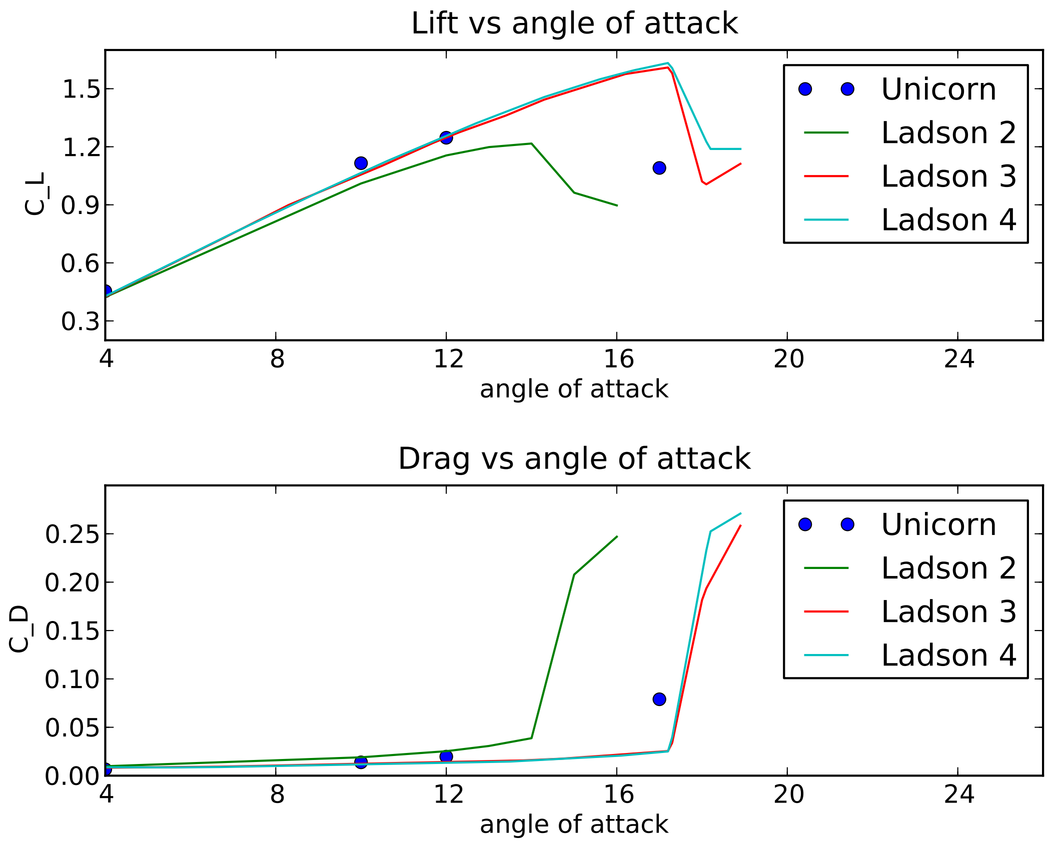

Figure 8.3: Evidence that computation of lift and drag coefficients C_L and C_D of a wing is possible from small angles of attack at crusing to large angles at start and landing: The blue curve shows computed coefficients by solving the Navier-Stokes equations by Unicorn [**?**] compared to different wind tunnel experiments by Gregory/O'Reilly and Ladson.

an element of truth, and the correct theory is the one that best captures most elements of truth.

8.6 Correct New Theory: d'Alembert's Paradox

The new flight theory to be presented can be shown to be correct as far as the Navier-Stokes equations describe fluid mechanics, because the new flight theory directly reflects properties of Navier-Stokes solutions. The key to uncover the mathematical secret of flight came from a correct resolution of d'Alembert's paradox form 1752 presented in our book [103] and article [104] 255 years later and then with the help of computation.

Our resolution of d'Alembert's paradox is fundamentally different from the one suggested by the young German physicist Ludwig Prandtl, called the father of modern fluid mechanics, timely presented after the *Flyer* had been seen flying to form the basis of 20th century theory of flight.

By studying computed Navier-Stokes solutions, which Prandtl could not do, we discover that Prandtl's resolution of d'Alembert's paradox does not correctly describe the essential physics, nor does the flight theory conceived by the father of modern fluid mechanics. A study of the new flight theory thus naturally starts with a study of the new resolution of d'Alembert's paradox.

Before proceeding to the study of the new flight theory we will to get perspective recall how flight is explained in standard scientific literature and popular science. We start out with some popular theories listed as incorrect by NASA and complete the picture with a theory due to Kutta-Zhukovsky-Prandtl viewed to offer a scientific explanation of both lift and drag, but as we will see is also incorrect.

Chapter 9

Incorrect Theories for Uneducated

> It's all one interconnected system. Unless the overall result of that system is for air to end up lower than it was before the plane flew by, there will be no lift. Wings move air downward, and react by being pushed upward. That's what makes lift. All the rest is just interesting details[90].
>
> The field of hydrodynamic phenomena which can be explored with exact analysis is more and more increasing. (Zhukovsky, 1911)

9.1 Incorrect Theories: NASA

You have probably heared some of the explanations offered in popular science, like higher velocity and lower pressure on the upper surface of the wing because it is curved and air there has a longer path to travel than below? Or maybe you are an aeroplane engineer or pilot and know very well why an airplane can fly, because lif is generated by circulation?

In either case, you should get a bit worried by reading that the authority NASA on its website [117] dismissses all popular science theories for lift, including your favorite one, as being incorrect, but then refrains from presenting any theory claimed to be correct! NASA surprisingly ends with an empty out of reach:

- *To truly understand the details of the generation of lift, one has to have a good working knowledge of the Euler Equations.*

This is just a fancy way of expressing that not even NASA [**?**] understands what keeps an airplane in the air. Of course, it is not possible to find the correct theory by removing all incorrect theories, like forming a correct sculpture out of a block of stone by removing all pieces of stone which are not correct, because there are infinitely many incorrect theories and not even NASA can list them all.

To present incorrect theories at length is risky pedagogics, since the student can get confused about what is correct and not, but signifies the confusion and misconceptions still surrounding the mechanisms of flight. If a correct theory was available, there would be no reason to present incorrect theories, but the absence of a correct theory is now seemingly covered up by presenting a multitude of incorrect theories.

The following three incorrect theories listed by NASA are commonly presented in text books directed to a general audience. Take a look and check out which you have met and if you they are convincing to you.

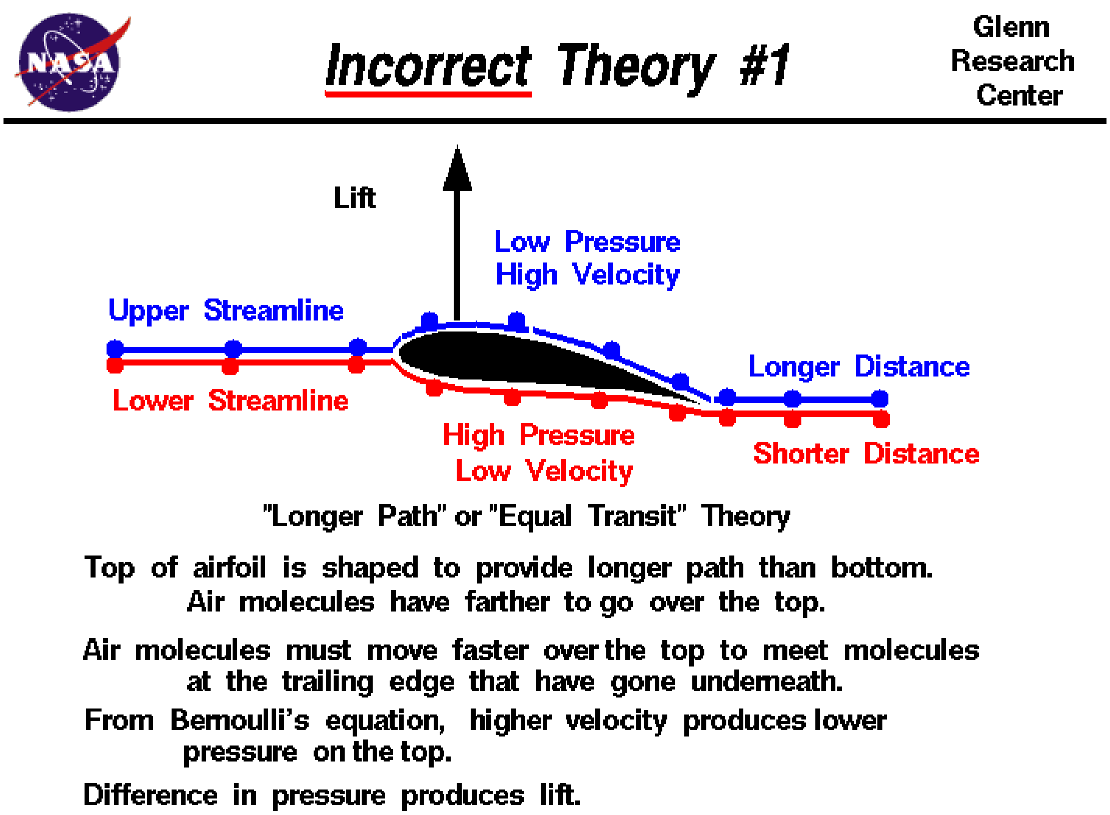

Figure 9.1: The 'longer path theory is wrong becasue an airplane can fly upside down.

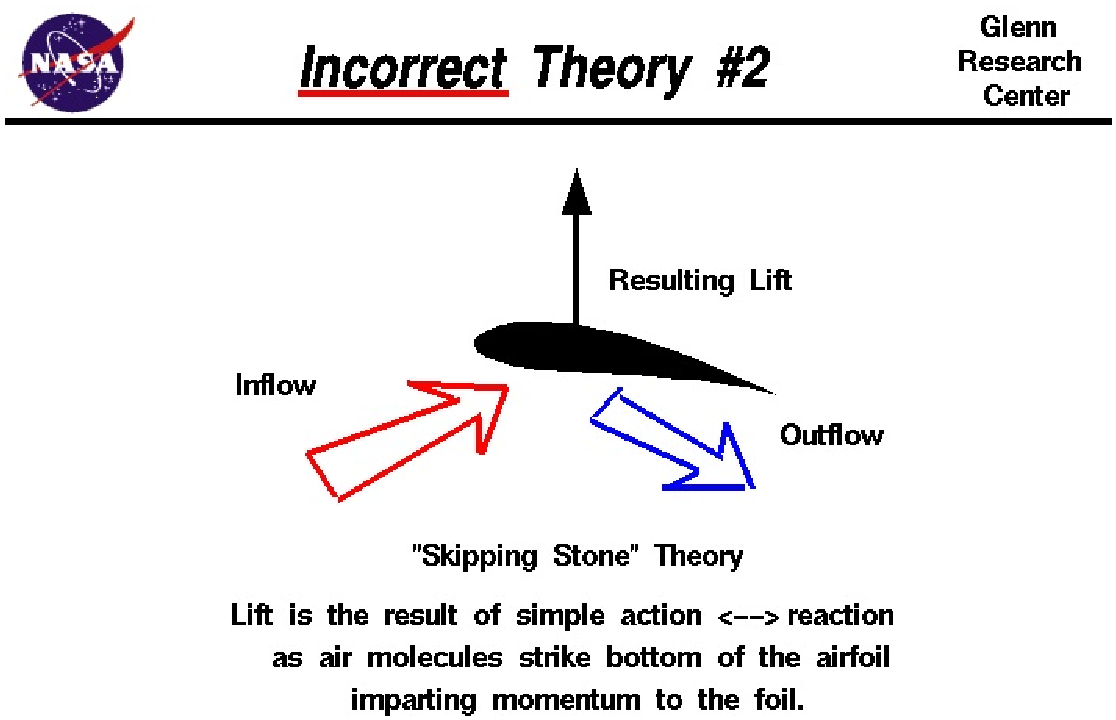

Figure 9.2: The “skipping stone is Newton’s theory, which gives a way too small lift.

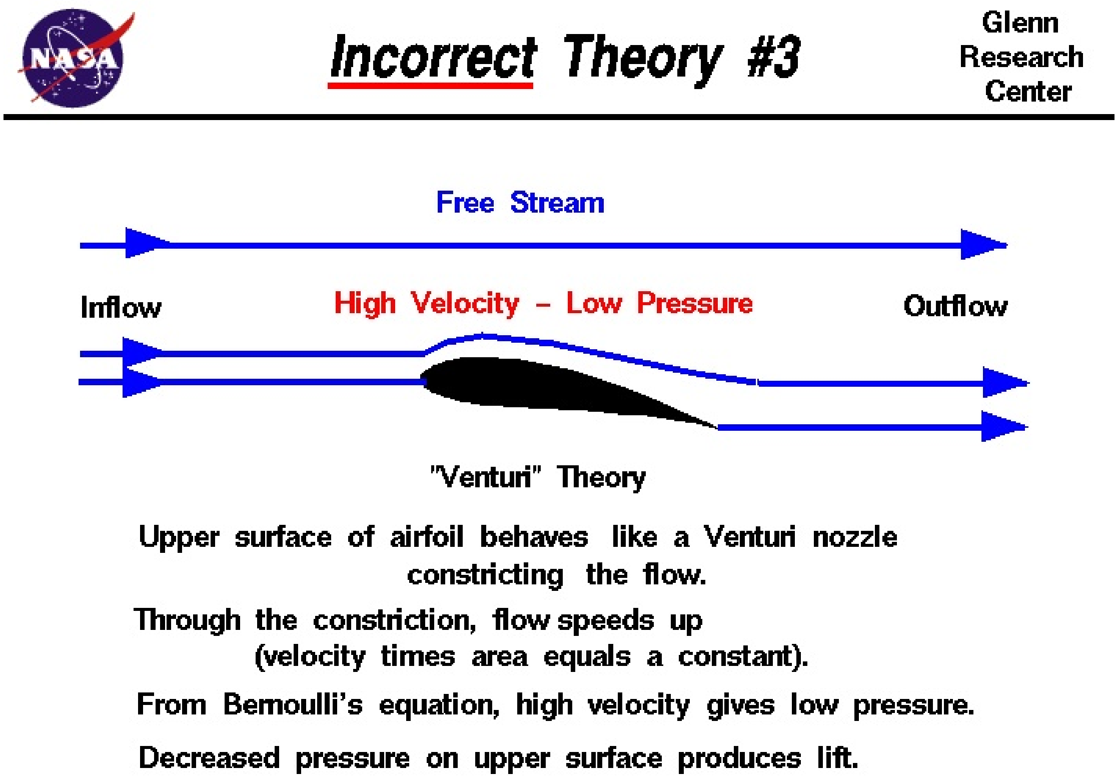

Figure 9.3: The "Bernouilli theory of higher speed above the wing and thus lower pressure because of the curvature of the wing, is wrong because an airplane can fly upside down.

9.2 Trivial Theory: NASA

The closet NASA comes to a correct theory is the trivial theory depicted in Fig. 9.4: If there is downwash then there is lift. This follows directly by Netwon's 3rd law, but the question is why there is downwash?

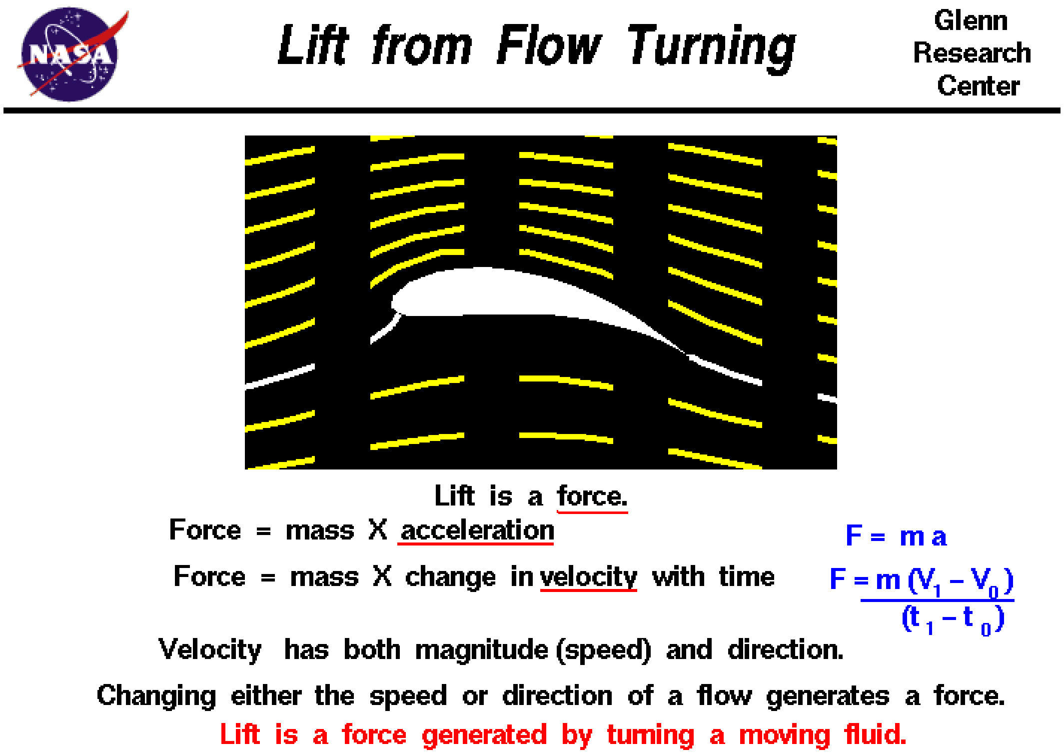

Figure 9.4: Trivial tautological theory of lift presented as correct by NASA.

Chapter 10

Incorrect Theory for Educated

> Lift is a lot trickier. In fact it is very controversial and often poorly explained and, in many textbooks, flat wrong. I know, because some readers informed me that the original version of this story was inaccurate. I've attempted to correct it after researching conflicting "expert" views on all this....If you're about fed up, rest assured that even engineers still argue over the details of how all this works and what terms to use [45].

10.1 Newton, d'Alembert and Wright

When the Wright brothers in 1903 showed that powered human flight was possible by putting a 12 hp engine on their *Flyer*, this was in direct contradiction to the accepted mathematical theory by Newton, who computed the lift from downwash of air particles hitting the lower part of the wing and found it to be so small that human flight was unthinkable.

Newton was supported by the mathematician d'Almembert who in 1755 proved that both lift and drag was zero for for *potential flow*, which seemed to describe the flow of air around a wing.

10.2 Kutta-Zhukovsky: Circulation: Lift

To save theoretical aerodynamics from complete collapse, a theory showing substantial lift had to be invented, and such a theory was delivered by Kutta in Germany and Zhukovsky in Russia 1904-6, who modified zero lift potential flow by adding a large scale *circulation* around the wing. Kutta-Zhukovsky showed that if there is circulation then there is lift, but could not explain from where the circulation came.

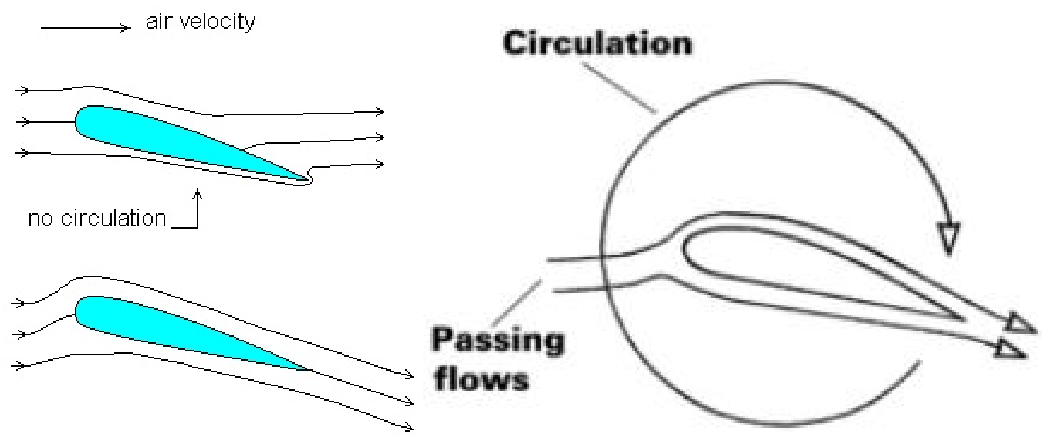

Figure 10.1: Top left figure shows potential flow without downwash (the incoming flow is not redirected) and thus no lift. The bottom left shows a flow with circulation resulting from adding a large scale rotational flow around the wing as shown in the right figure.

10.3 Prandtl: Boundary Layer: Drag King

This was timely done by the German physicists Ludwig Prandtl, who in a short note in 1904 saved aerodynamics by opening the possibility that both circulation with lift and drag somehow originiate from a thin *boundary layer*.

The theory by Kutta-Zhukovsky-Prandtl has become the theory for the educated specialists of aerodynamics, who very well understand that the theories for uneducated are incorrect. Today 100 years later, this is still the theory of flight presented in text books: Lift comes from circulation, and circulation and drag comes from a thin boundary layer.

There is an alternative to circulation as generation of lift, referred to as the *Coanda effect* stating that upper surface suction is an effect of viscosity causing the flow to stick to the surface, but the support of this theory in the literature is weak.

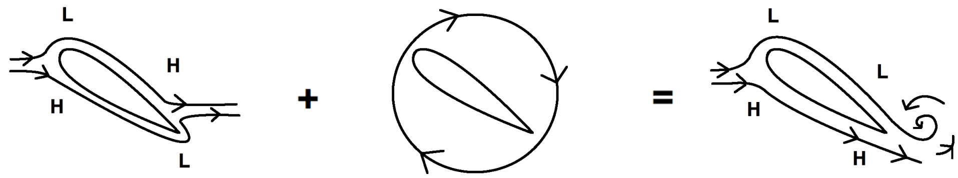

Figure 10.2: Kutta-Zhukovsky theory of lift combining potential flow (left) with large scale circulation, thus changing the zero lift pressure distribution of potential flow to lifting flow by shifting the high (H) and low (L) pressure zones at the trailing edge of the flow by unphysical circulation around the section (middle) resulting in flow with downwash/lift and starting vortex (right).

State-of-the-art thus tells you that to compute drag and lift of an airplane you need to resolve the boundary layer, which however requires 10 quadrillion (10^{16} mesh points, which will require 50 years of Moore's law improving the computational power by a factor of 10^{10}.

But is the theory of Kutta-Zhukovsky-Prandtl for educated correct? Do we have to wait 50 years to compute lift and drag of an Airbus?

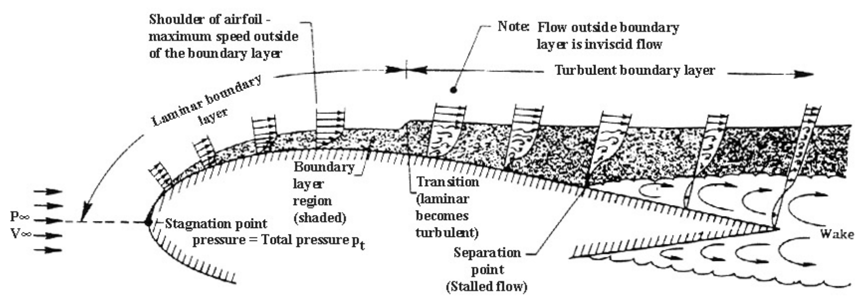

Figure 10.3: Prandtl's boundary layer theory in pictures.

10.4 More Confusion

Many sources, in addition to NASA, give witness of the lack of convincing scientific answer of how a wing can generate lift with small drag. We give here a sample starting with more from [130]:

- *"Here we are, 100 years after the Wright brothers, and there are people who give different answers to that question," said Dr. John D. Anderson Jr., the curator for aerodynamics at the Smithsonian National Air and Space Museum in Washington. "Some of them get to be religious fervor."*

- *The answer, the debaters agree, is physics, and not a long rope hanging down from space. But they differ sharply over the physics, especially when explaining it to nonscientists. "There is no simple one-liner answer to this," Dr. Anderson said.*

- *The simple Newtonian explanation also glosses over some of the physics, like how does a wing divert air downward? The obvious answer – air molecules bounce off the bottom of the wing – is only partly correct.*

- *If air has to follow the wing surface, that raises one last question. If there were no attractive forces between molecules, would there be no flight? Would a wing passing through a superfluid like ultracold helium, a bizarre fluid that can flow literally without friction, produce no lift at all? That has stumped many flight experts. "I've asked that question to several people that understand superfluidity," Dr. Anderson, the retired physicist, said. "Alas! They don't understand flight."*

- *It is important to realize that, unlike in the two popular explanations described earlier (longer path and skipping stone), lift depends on significant contributions from both the top and bottom wing surfaces. While neither of these explanations is perfect, they both hold some nuggets of validity. Other explanations hold that the unequal pressure distributions cause the flow deflection, and still others state that the exact opposite is true. In either case, it is clear that this is not a subject that can be explained easily using simplified theories. Likewise, predicting the amount of lift created by wings has been an equally challenging task for engineers and designers in the past. In fact, for years, we have relied heavily on experimental data collected 70 to 80 years ago to aid in our initial designs of wing.*[52]

- http://www.youtube.com/watch?v=uUMlnIwo2Qo

- http://www.youtube.com/watch?v=ooQ1F2jb10A

- http://www.youtube.com/watch?v=kXBXtaf2TTg

- $http://www.youtube.com/watch?v = 5wIq75_BzOQ$
- $http://www.youtube.com/watch?v = khca2FvGR - w$

Chapter 11

Summary of State-of-the-Art

> You'd think that after a century of powered flight we'd have this lift thing figured out. Unfortunately, it's not as clear as we'd like. A lot of half-baked theories attempt to explain why airplanes fly. All try to take the mysterious world of aerodynamics and distill it into something comprehensible to the lay audience–not an easy task. Nearly all of the common "theories" are misleading at best, and usually flat-out wrong [87].

11.1 Newton

Classical mathematical mechanics could not give an answer to the mystery of gliding flight: Newton computed by elementary mechanics the lift of a tilted flat plate redirecting a horisontal stream of fluid particles, but obtained a disappointingly small value proportional to the square of the angle of attack. To Newton the flight of birds was inexplicable, and human flight certainly impossible.

11.2 d'Alembert and Potential Flow

D'Alembert followed up in 1752 by formulating his paradox about zero lift/drag of *inviscid incompressible irrotational steady flow* referred to as *potential flow,* which seemed to describe the airflow around a wing since the viscosity of air is very small so that it can be viewed as being inviscid (with zero viscosity).

Mathematically, potential flow is given as the gradient of a *harmonic funtion* satisfying *Laplace's equation*.

At speeds less than say 300 km/h air flow is almost incompressible, and since a wing moves into still air the flow it could be be expected to be irrotational without swirling rotating vortices. D'Alembert's mathematical potential flow thus seemed to capture physics, but nevertheless had neither lift nor drag, against all physical experience. The wonderful mathematics of potential flow and harmonic functions thus showed to be without physical relevance: This is *D'Alembert's paradox* which came to discredit mathematical fluid mechanics from start [104, 125, 92].

To explain flight d'Alembert's paradox had to be resolved, but nobody could figure out how and it was still an open problem when Orwille and Wilbur Wright in 1903 showed that heavier-than-air human flight in fact was possible in practice, even if mathematically it was impossible.

11.3 Kutta-Zhukovsky-Prandtl

Mathematical fluid mechanics was then saved from complete collapse by the young mathematicians Kutta and Zhukovsky, called the father of Russian aviation, who explained lift as a result of perturbing potential flow by a large-scale circulating flow or *circulation* around the two-dimensional section of a wing, and by the young physicist Prandtl, called the father of modern fluid dynamics, who explained drag as a result of a *viscous boundary layer* [119, 120, 124, 93].

This is the basis of state-of-the-art [21, 72, 74, **?**, 98, 126, 137], which essentially is a simplistic theory for lift without drag at small angles of attack in inviscid flow and for drag without lift in viscous flow. However, state-of-the-art does not supply a theory for lift-and-drag covering the real case of *3d slightly viscous turbulent* flow of air around a 3d wing of a jumbojet at the critical phase of take-off at large angle of attack (12 degrees) and subsonic speed (270 km/hour), as evidenced in e.g. [47, 89, 90, 91, 130, 7, 52, 113, 116]. The simplistic theory allows an aeroplane engineer to roughly compute the lift of a wing a crusing speed at a small angle of attack, but not the drag, and not lift-and-drag at the critical phase of take-off [59, 131]. The lack of mathematics has to be compensated by experiment and experience. The first take off of the new Airbus 380 must have been a thrilling experience for the design engineers.

The state-of-the-art theory of flight can be summarized as either

- correct and trivial,
- nontrivial and incorrect,

in the following forms:

- Downwash generates lift: trivial without explanation of reason for downwash from suction on upper wing surface.
- Low pressure on upper surface: trivial without explanation why.
- Low pressure on curved upper surface because of higher velocity (by Bernouilli's law), because of longer distance: incorrect.
- Coanda effect: The flow sticks to the upper surface by viscosity: incorrect.
- Kutta-Zhukovsky: Lift comes from circulation: incorrect.
- Prandtl: Drag comes mainly from viscous boundary layer: incorrect.

11.4 Text Book Theory of Flight

The following text books all present versions of the Kutta-Zhukovsky-Prandtl theory of flight:

- Prandtl-Essentials of Fluid Mechanics, Herbert Oertel (Ed.)
- Aerodynamics of Wingd and Bodies, Holt Ashley and Marten Landahl,
- Introduction to the Aerodynamics of Flight, Theodore A. Talay, Langley Reserach Center,
- Aerodynamics of the Airpoplane, Hermann Schlichting and Erich Truckenbrodt,Mac Graw Hill
- Airplane Aerodynamics and Performance, Jan Roskam and C T Lan,
- Fundamentals of Aerodynamics, John D Anderson,
- Fuhrer durch die Stromungslehre, L Prandtl,...

- Aerodynamicss of Wind Turbins, Martin Hansen,
- Aerodynamics, Aeronautics and Flight Mechanics, McCormick,
- Aerodynamics, Krasnov,
- Aerodynamics, von Karmann,
- Theory of Flight, Richard von Mises.

The text book theory of flight has been remarkably stable over 100 year with little improvement in accuracy as if the theory once and for all was set by Kutta-Zhukovsky-Prandtl. But science does not work that way: If no progress is made on a complex scientific topic, like flight, this is a strong indication that what was hammered in stone is incorrect science. This book will help the reader to decide if such a suspicion is well founded.

Chapter 12

Shut Up and Calculate

> How can aviation be grounded in such a muddy understanding of the underlying physics? As with many other scientific phenomena, it's not always necessary to understand why something works to make use of it. We engineers are happy if we've got enough practical knowledge to build flying aircraft. The rest we chalk up to magic [87].

12.1 Naviers-Stokes vs Schrödinger

The interpretation of the wave functions of the new quantum mechanics of the atomic world as solutions of Schrödinger's wave equations, was intensely debated in the 1920s by Schrödinger, Bohr, Born and Dirac without reaching any agreement. This led a frustated Dirac in an effort to get out of the scientific dead lock to make the appeal "shut up and calculate": Simply solve the Schrödinger equation and take what you get as physics. However, Dirac's appeal did not and still does not help much because analytical solution of Schrödinger's equation is possible only for the Hydrogen atom with one electron, and computational solution involves $3N$ space dimensions for N particles, which even today is possible only for small N.

The debate thus is shifted to different techniques of solving Schrödinger's equation, considered to harbor the truth, and the debate goes on.

Similarly, solutions of the Navier-Stokes equations may be expected to tell the physics of flight, and so the question is if they are computable or as uncomputable as Schrödinger's equation?

Navier-Stokes solutions at the high Reynold's numbers of flight are turbulent and have thin boundary layers and the standard wisdom expressed by Kim an Moin [43] is that computational resolution requires quadrillions of mesh points beyond the capacity of any forseeable computer.

But there is trick, or mircale, which make the Navier-Stokes equations computable: If we combine the Navier-Stokes equations with a slip boundary condition modeling that the friction force from the air on the wing is small, which it is for slightly viscous flow, then there is no Prandtl boundary layer to resolve and then solutions of the Naviers-Stokes equations can be computed with 10^6 mesh points, and the lift and drag of these solutions agree very well with experiments. Thus Dirac's appeal works out for flight described by Navier-Stokes equations.

Chosing a slip (or small friction) boundary condition, which we can do because it is a good model of actual physics, we gain in two essential aspects: Solutions become computable and computed solutions tell the truth.

The truth we find this way is that neither lift nor drag originate from a thin boundary layer, and thus that the Kutta-Zhukovsky-Prandtl theory is unphysical and incorrect. State-of-the-art today thus presents a theory of flight which is both unphysical and uncomputable.

12.2 Compute - Analyze - Understand

Computed solutions show that a wing creates lift as a reaction force *downwash*, with less than 1/3 coming from the lower wing surface pushing air down and the major remaining part from the upper surface sucking air down, with a resulting *lift/drag quotient* $\frac{L}{D} > 10$.

You could stop here following the device of the physicist Dirac of "shut up and calculate" but as a scientist and rational human beings you would certainly like to "understand" the solutions, that is describe the "mechanism" making a wing generate large lift with small drag.

Chapter 13

Mathematical Miracle of Flight

> ...do steady ow ever occur in nature, or have we been pursuing fantasy all along? If steady flows do occur, which ones occur? Are they stable, or will a small perturbation of the ow cause it to drift to another steady solution, or even an unsteady one? The answer to none of these questions is known. (Marvin Shinbrot in Lectures on Fluid Mechanics, 1970)

Computing turbulent solutions of the Navier-Stokes equations led us to a resolution of d'Alembert's paradox, which revealed the miracle of flight as we show in this book. You will find that it is quite easy to grasp, because it can be explained using different levels of mathematics. We start out easy with the basic principle in concept form and then indicate some of the mathematics with references to more details. Supporting information is given in the Google knols [135] and [111].

To understand flight means to identify the relevant mathematical aspects of solutions to the Navier-Stokes equations, and this is what this book will help you to do. The code words of the mathematical mircale of flight:

- Non-separation of potential flow before trailing edge creating suction on the upper surface of wing and downwash.

- Slip-separation at trailing edge with small drag instead of potential flow separation destroying lift.

This principle is pictured in Fig. 13.1 supported by computational simulations in Fig. 13.2- **??**. We see the zero lift/drag of potential flow being replaced by real flow with low-pressure trailing edge slip separation with streamwise vorticity swirling flow shown in Fig. 13.3. We shall below analyze this pictures in more detail to reach a real understanding of how a wing is capable of generating at the ame time big lift and small drag, the enigma of flight. The reader may anticipate the analysis by a study of the pictures.

The enigma of flight is why the air flow separates from the upper wing surface at the *trailing edge*, and not before, with the flow after separation being redirected downwards according to the tilting of the wing or *angle of attack*. We will reveal the secret to be an effect of a fortunate combination of features of *slightly viscous incompressible flow* including a crucial *instability mechanism at separation* analogous to that seen in the swirling flow down a bathtub drain, generating both suction on the upper wing surface and drag.

We show that this mechanism of lift and drag is operational for angles of attack smaller than a critical value of about 15 degrees depending on the shape of the wing, for which the flow separates from the upper wing surface well before the trailing edge with a sudden increase of drag and decrease of lift referred to as *stall*.

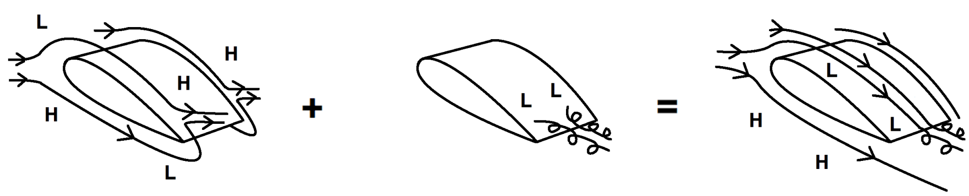

Figure 13.1: Correct explanation of lift by perturbation of potential flow (left) at separation from physical low-pressure turbulent counter-rotating rolls (middle) changing the pressure and velocity at the trailing edge into a flow with downwash and lift (right).

13.1 Mathematical Computation and Analysis

We present below a mathematical analysis of the computed solutions showing that lift and drag result from a specific 3d instability mechanism generating low-pressure rolls of streamwise vorticity attaching at separation. This analysis gives a new resolution of d'Alembert's paradox of zero drag in inviscid

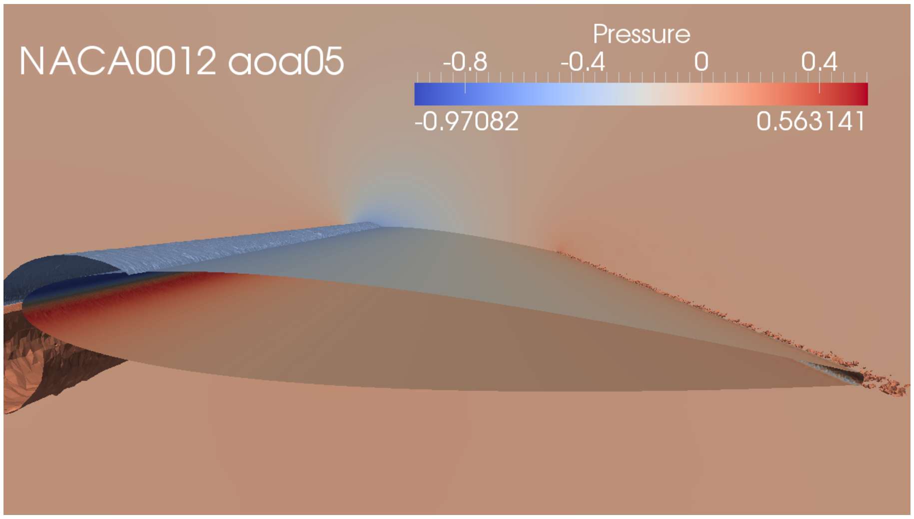

Figure 13.2: Pressure distribution with big leading edge lift (suction above and push below) and small drag at $\alpha = 5$. Notice that the high pressure at the trailing edge of potential flow is missing thus maintaining big lift.

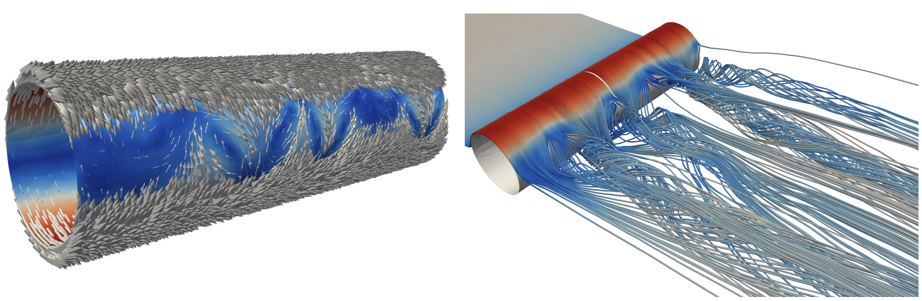

Figure 13.3: Turbulent separation by surface vorticity forming counter-rotating low-pressure rolls in flow around a circular cylinder, illustrating separation at the trailing edge of a wing [101].

flow [?], which is fundamentally different from the accepted resolution by Prandtl based on boundary layer effects.

We show that lifting flow results from an instability at rear separation generating counter-rotating low-pressure rolls of streamwise vorticity inititated as surface vorticity resulting from meeting opposing flows. This mechanism is entirely different from the mechanism based on global circulation of Kutta-Zhukovsky theory. We show that the new theory allows accurate computation of lift, drag and twisting moments of an entire airplane using a few millions of mesh-points, instead of the impossible quadrillions of mesh-points required according to state-of-the-art following Prandtl's dictate of resolution of very thin boundary layers connected with no-slip velocity boundary conditions.

The new theory thus offers a way out of the present deadlock of computational aerodynamics of slightly viscous turbulent flow.

Chapter 14

Observing Pressure, Lift and drag

14.1 Potential Flow Modified at Separation

We will now uncover the secret of flight in more detail by inspecting computational solutions of Navier-Stokes equations with a slip boundary condition. The distribution of the pressure over the wing surface determines both lift and drag. The pressure acts in a direction normal to the wing surface and its components perpendicular and parallel and perpendicular to the motion of the wing give the distributions of lift and drag over the wing surface which give the total lift L and drag D with by integration. We discover that $L/D \approx 30-50$ for $\alpha < 14$ as recorded in Fig. 8.3, which captures the miracle of flight.

We will then inspect the velocity and the vorticity and the seek to rationalize what we have seen in terms of basic fluid mechanics. We will find that the flow can be described as a modified form of potential flow with the modification resulting from a specific form of separation at the trailing edge which we will describe as *slip separation with point stagnation*.

The flow before separation thus will seen to be close to potential flow and there conform with *Bernoulli's Principle* stating that the sum of kinetic energy $\frac{1}{2}|u|^2$ with u velocity and pressure p remains constant over the region of potential flow:

$$\frac{1}{2}|u|^2 + p = \text{constant}, \tag{14.1}$$

expressing that the pressure is low where the velocity is high and vive versa.

We recall the principal description in Fig. 13.1 with full potential flow to the left with high pressure H on top of the wing and low pressure L below at the trailing edge destroying lift, and to the right the real flow modified by a certain perturbation at the trailing edge switching H and L to generate lift.

14.2 Pressure, Lift and Drag Distribution

Fig. 14.2-14.2 show the pressure distribution for $\alpha = 4, 10, 12, 17$. We observe

- low pressure on top/front of the leading edge and high pressure below as expected from potentiual flow,
- no high pressure on top of the trailing edge in contrast to potential flow,
- the pressure distribution intensifies with increasing angle of attack,
- max negative pressure (lift) 5 times bigger than max pressure (drag) on leading edge for $\alpha = 10$,

Fig. 14.5 shows the distributions of lift and drag over the surface of the wing section for $\alpha = 0, 2, 4, 10, 18$. We observe

- lift increases and peaks at the leading edge as α increases towards stall,
- both lift and drag are small att the trailing edge,
- the negative lift on the lower surface for small α shifts to positive lift for larger α,
- the lift from the upper surface is several times bigger than from the lower surface
- leading edge suction: negative/positive drag on the upper/lower leading edge balance to give small net drag,
- main drag from leading edge for smaller α.

Altogether, we see that the miracle of $\frac{L}{D} > 10$ results from the facts that

- main lift and drag come from leading edge,

- minimal pressure several times bigger than the maximal pressure on the leading edge (factor 5 say)
- leading edge suction reduces drag (another factor 2 say).

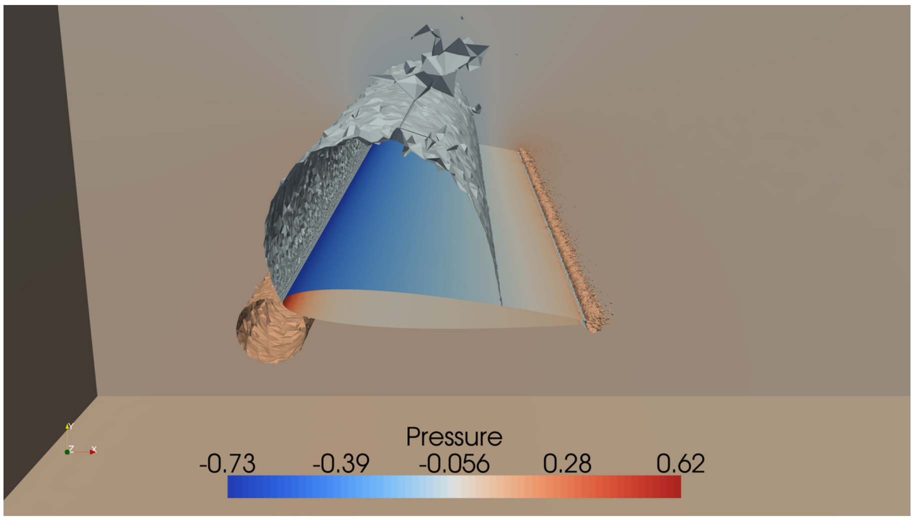

Figure 14.1: Pressure distribution at $\alpha = 4$.

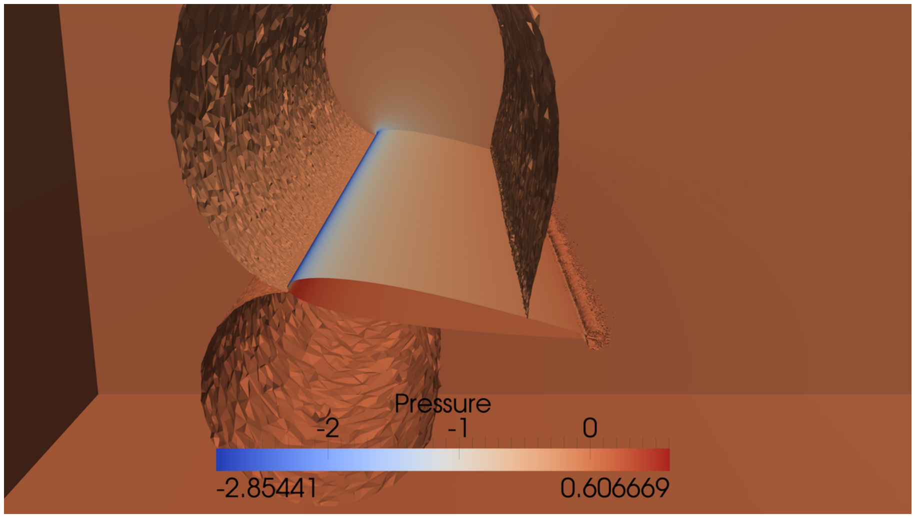

Figure 14.2: Pressure at $\alpha = 10$.

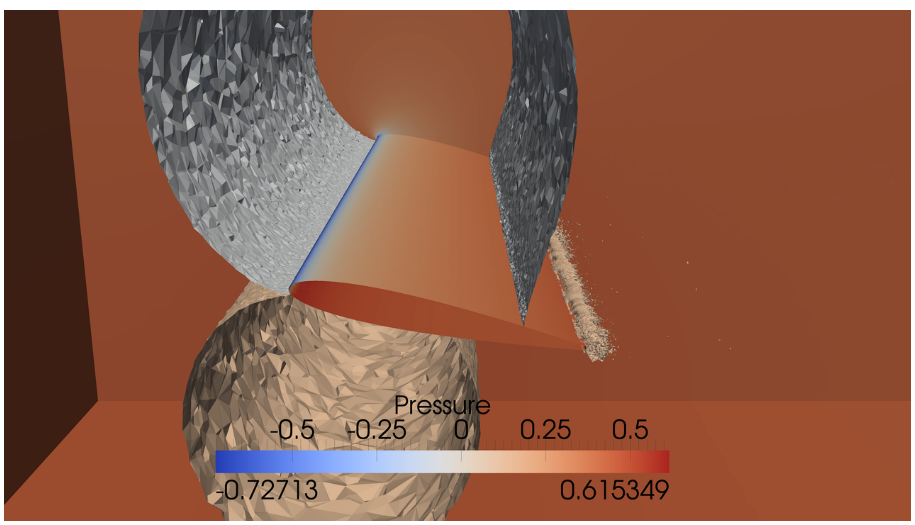

Figure 14.3: Pressure distribution at $\alpha = 12$.

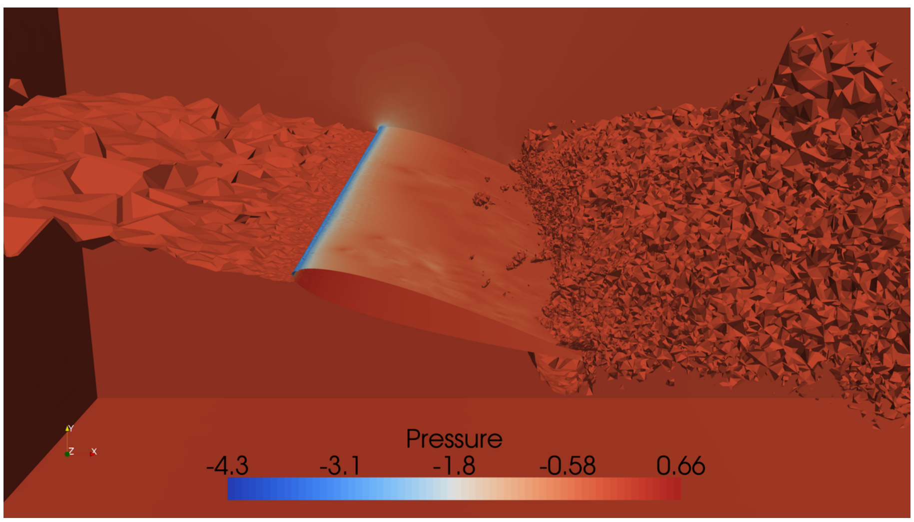

Figure 14.4: Pressure at $\alpha = 17$.

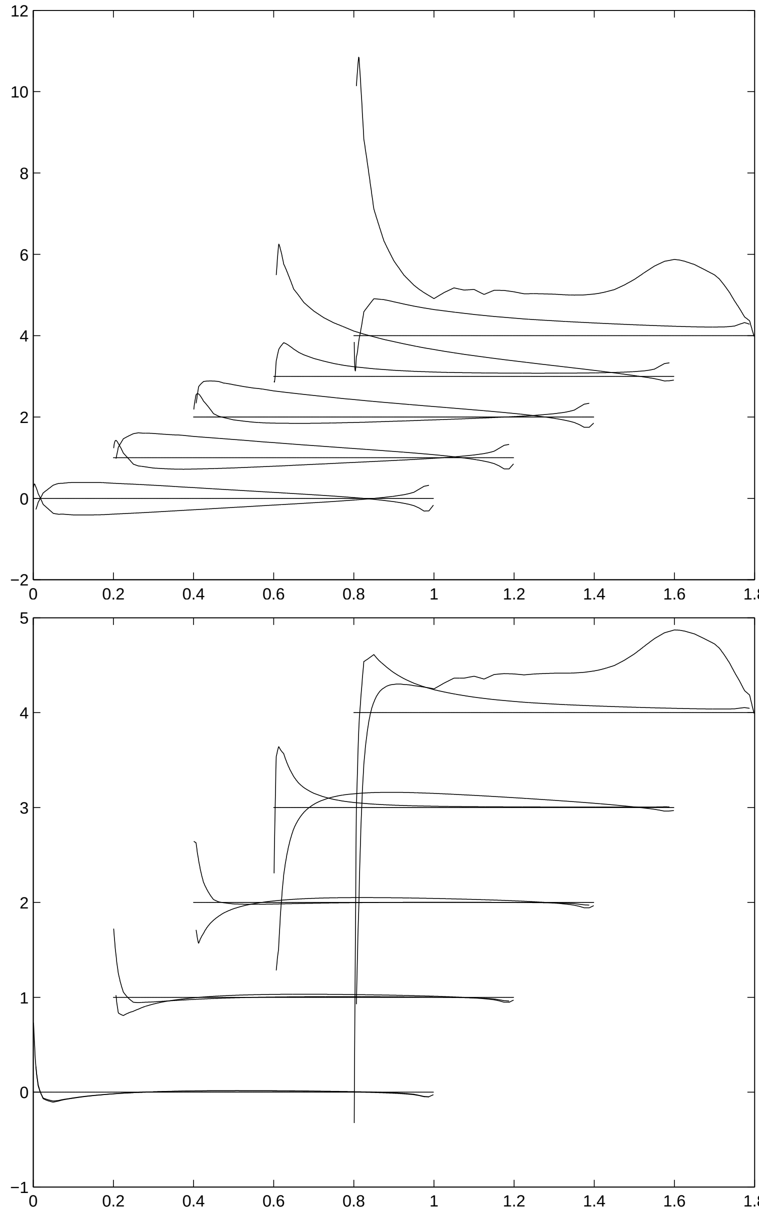

Figure 14.5: G2 computation of normalized local lift force (upper) and drag force (lower) contributions acting along the lower and upper parts of the wing, for angles of attack 0, 2 ,4 ,10 and 18°, each curve translated 0.2 to the right and 1.0 up, with the zero force level indicated for each curve.

Chapter 15

Observing Velocity

Fig. 15 and 15 show the velocity for $\alpha = 10, 14, 17$. We observe

- high velocity on top/front of the leading edge and low velocity below in conformity with Bernoulli's Principle,
- a wake with low velocity develops as stall is approached,
- well before stall the flow separates smoothly at the trailing edge and not as potential flow at stagnation before the trailing edge,
- the separation moves forward from the trailing edge on the upper surface as stall is approached.

Fig. 15.3 and 15.4 show oilfilm plots of the velocity at the trailing edge. We observe

- rotational slip separation with point stagnation in a zig-zag pattern
- generating rolls of streamwise vorticity with low pressure.

Fig. 15.6-15.10 also show the zig-zag velocity separation pattern with point stagnation.

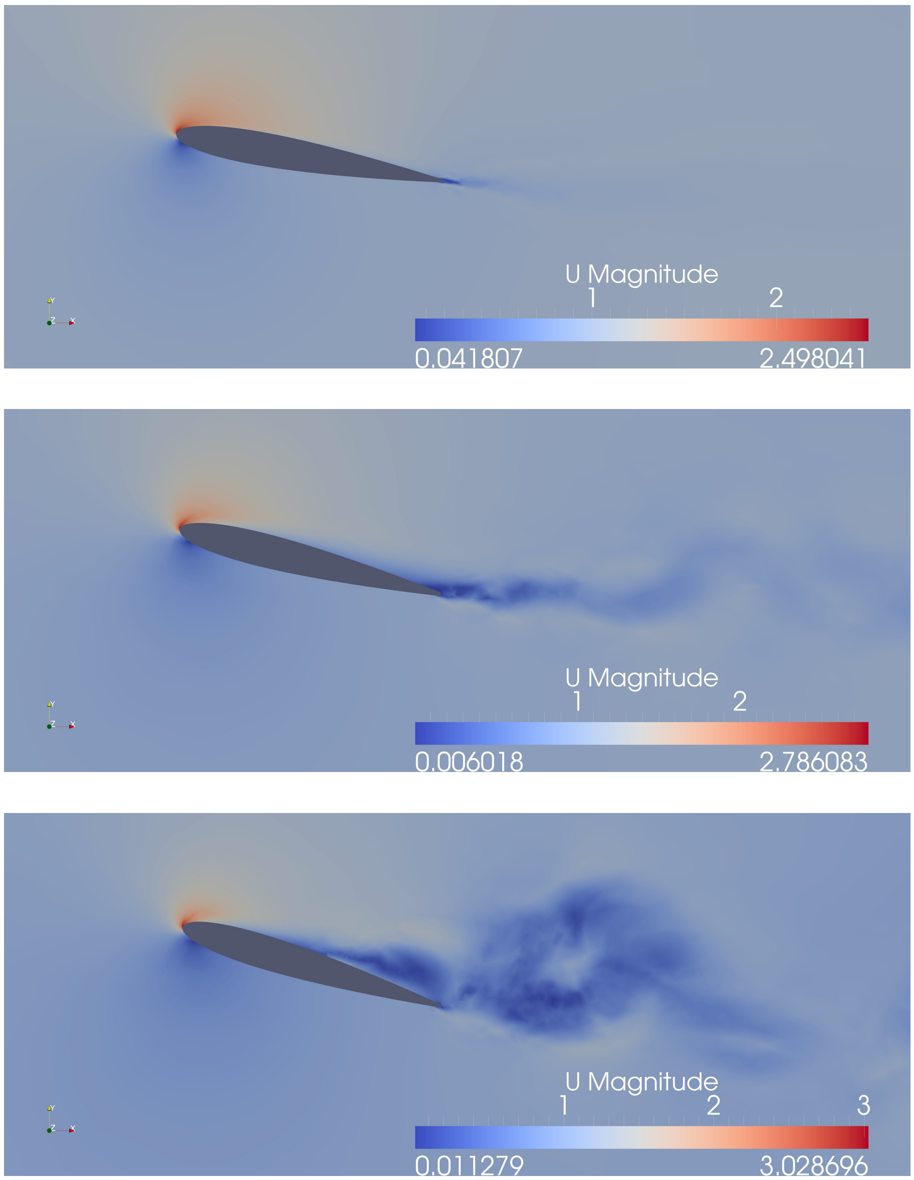

Figure 15.1: Velocity magnitude around the airfoil for $\alpha = 10$ (top), 14 (center) and 17 (bottom).

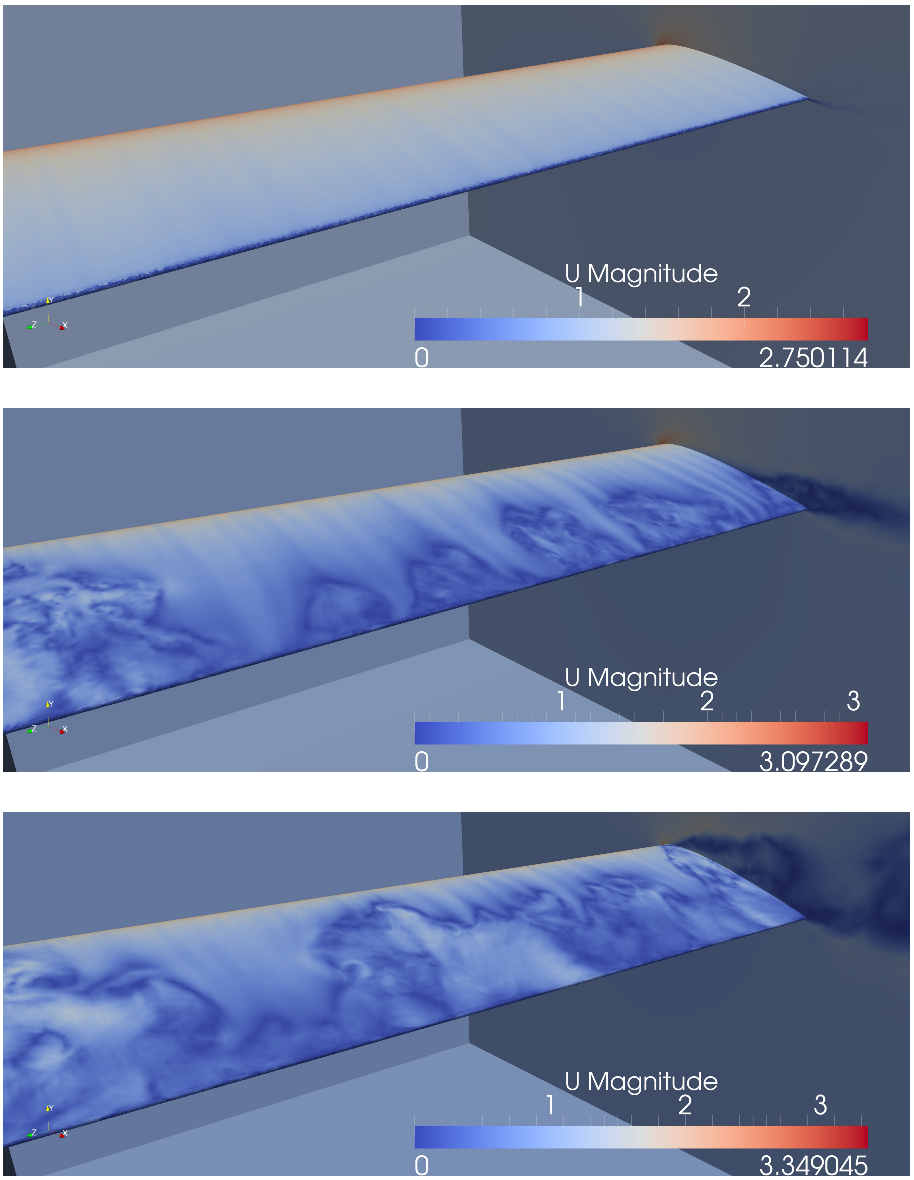

Figure 15.2: Velocity magnitude on the airfoil surface for $\alpha = 10$ (top), 14 (center) and 17 (bottom) showing that separation pattern moves up the airfoil with increasing α towards stall.

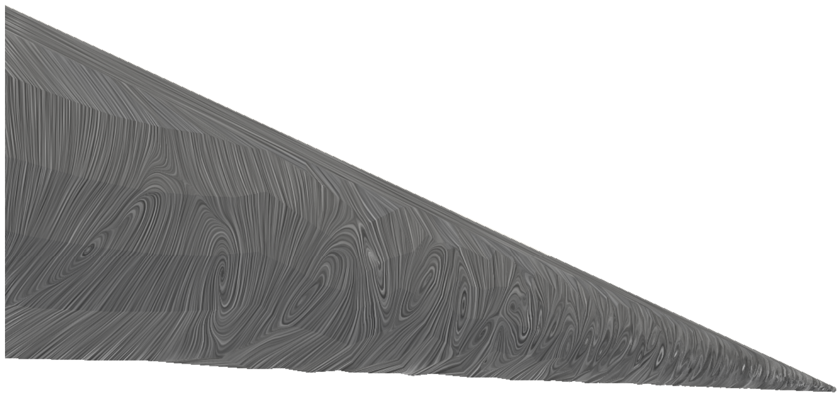

Figure 15.3: G2 oilfilm plots showing separation pattern with point stagnation for $aoa = 4$.

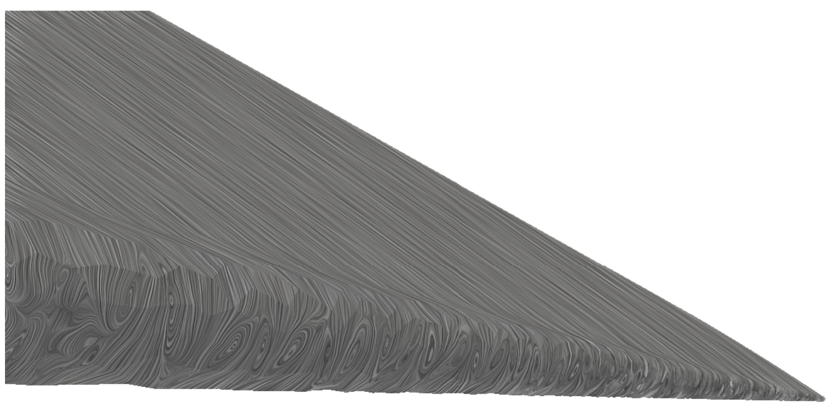

Figure 15.4: G2 oilfilm plots showing separation pattern with point stagnation $aoa = 12$.

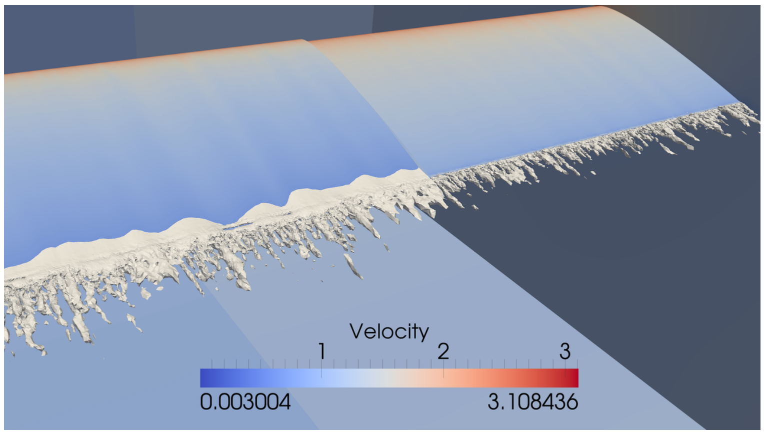

Figure 15.5: Velocity $aoa = 10$.

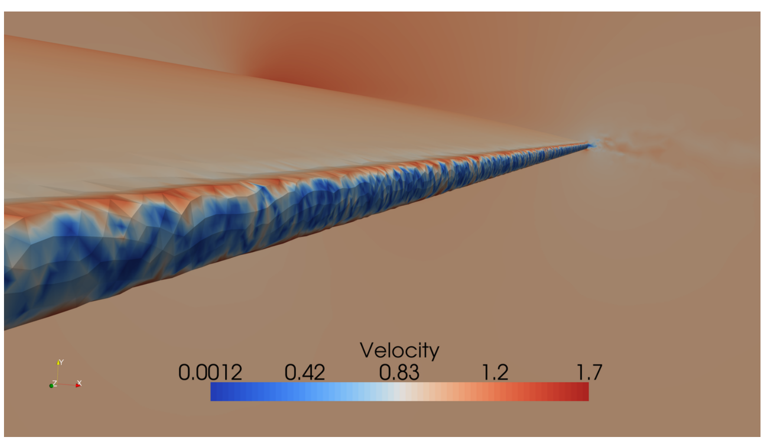

Figure 15.6: Trailing edge zig-zag velocity pattern $aoa = 04$.

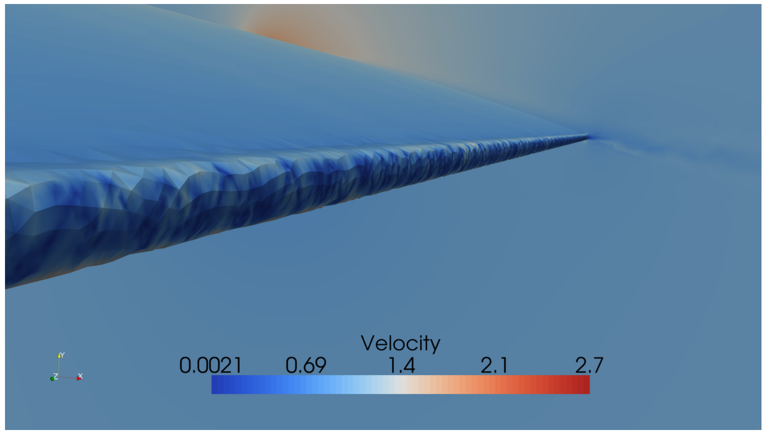

Figure 15.7: Trailing edge zig-zag velocity $aoa = 10$.

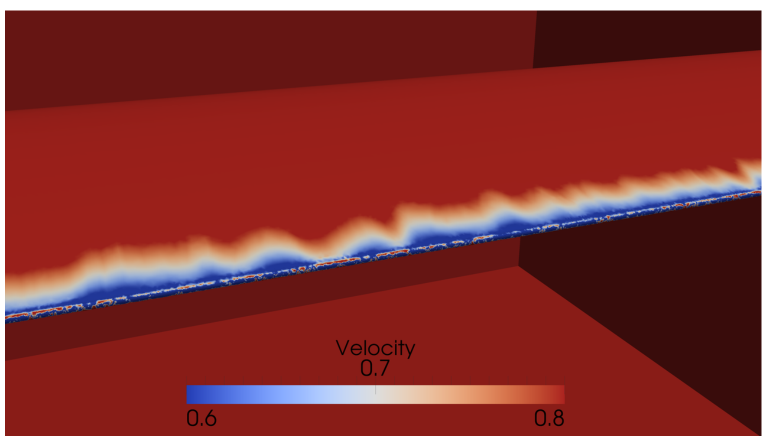

Figure 15.8: Zigzag velocity $aoa = 12$.

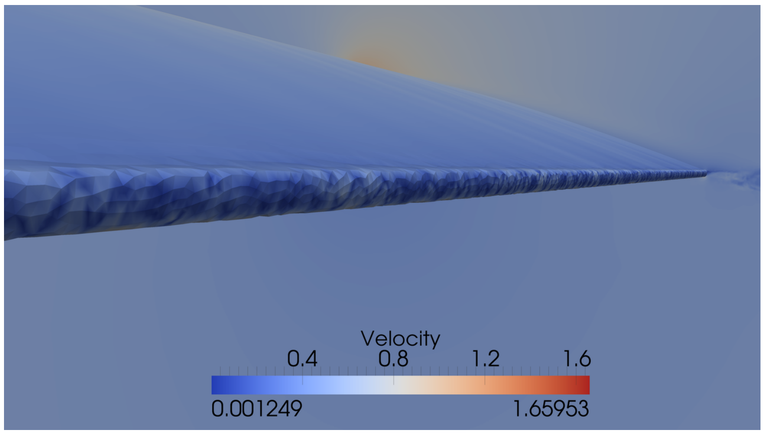

Figure 15.9: Trailing edge zig-zag velocity $aoa = 12$.

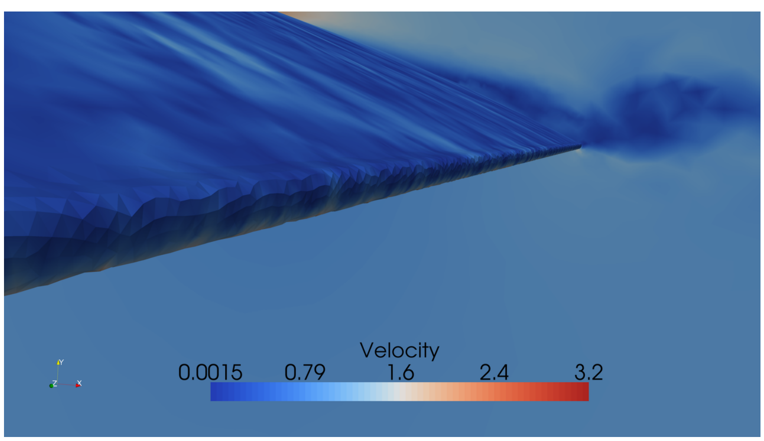

Figure 15.10: Trailing edge zig-zag velocity $aoa = 17$.

Chapter 16

Observing Vorticity

Fig. 16.1-16.3 shows side view of pressure, velocity and top view of vorticity for $\alpha = 2, 4, 8, 10, 14, 18$. We observe

- development of rolls of streamwise vorticity at separation at the trailing edge as illustrated in Fig. 13.1,
- pressure is small inside rolls of streamwise vorticity generating som drag,
- separation moves from the trailing edge to upper surface as α approches stall.

Below we will in more detail study the dynamics of the generation of streamwise vorticity as the generic structure of rotational slip separation with point stagnation.

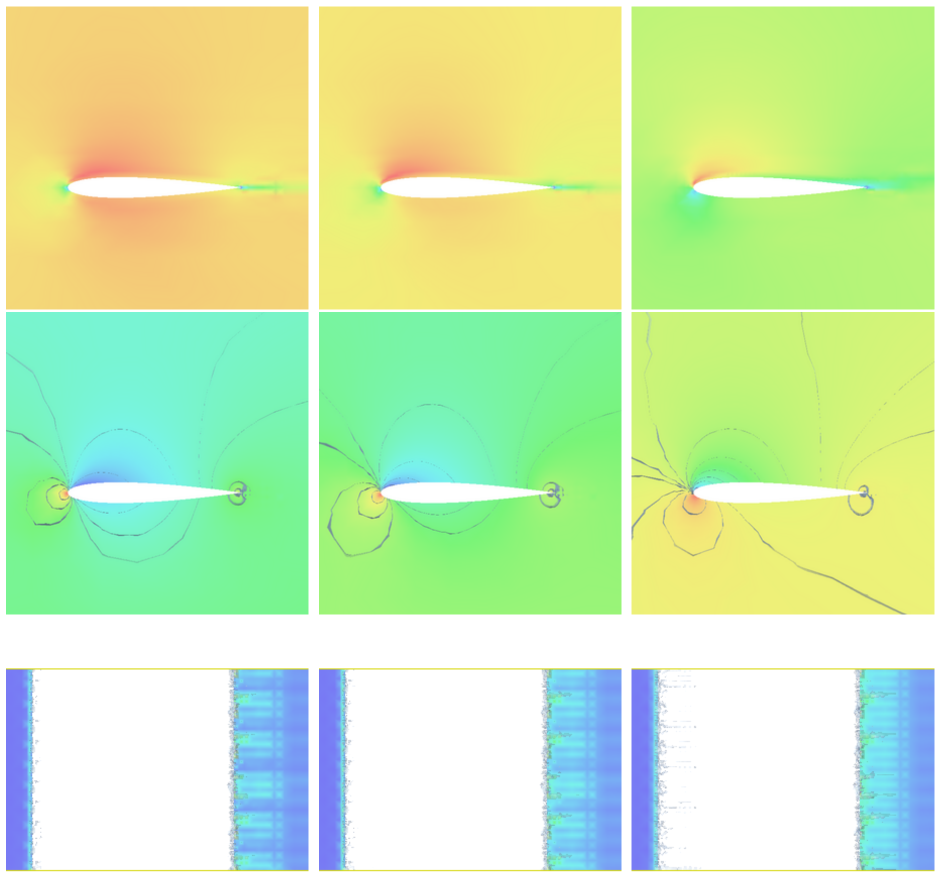

Figure 16.1: G2 computation of velocity magnitude (upper), pressure (middle), and non-transversal vorticity (lower), for angles of attack 2, 4, and 8° (from left to right). Notice in particular the rolls of streamwise vorticity at separation.

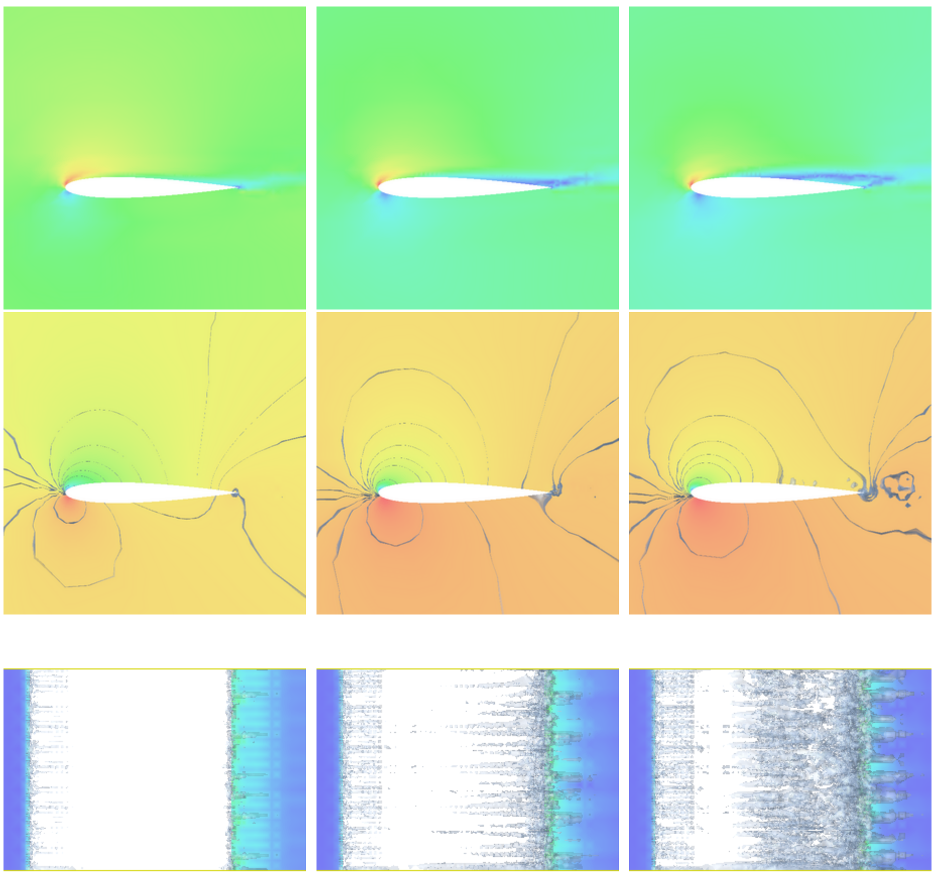

Figure 16.2: G2 computation of velocity magnitude (upper), pressure (middle), and topview of non-transversal vorticity (lower), for angles of attack 10, 14, and 18° (from left to right). Notice in particular the rolls of streamwise vorticity at separation.

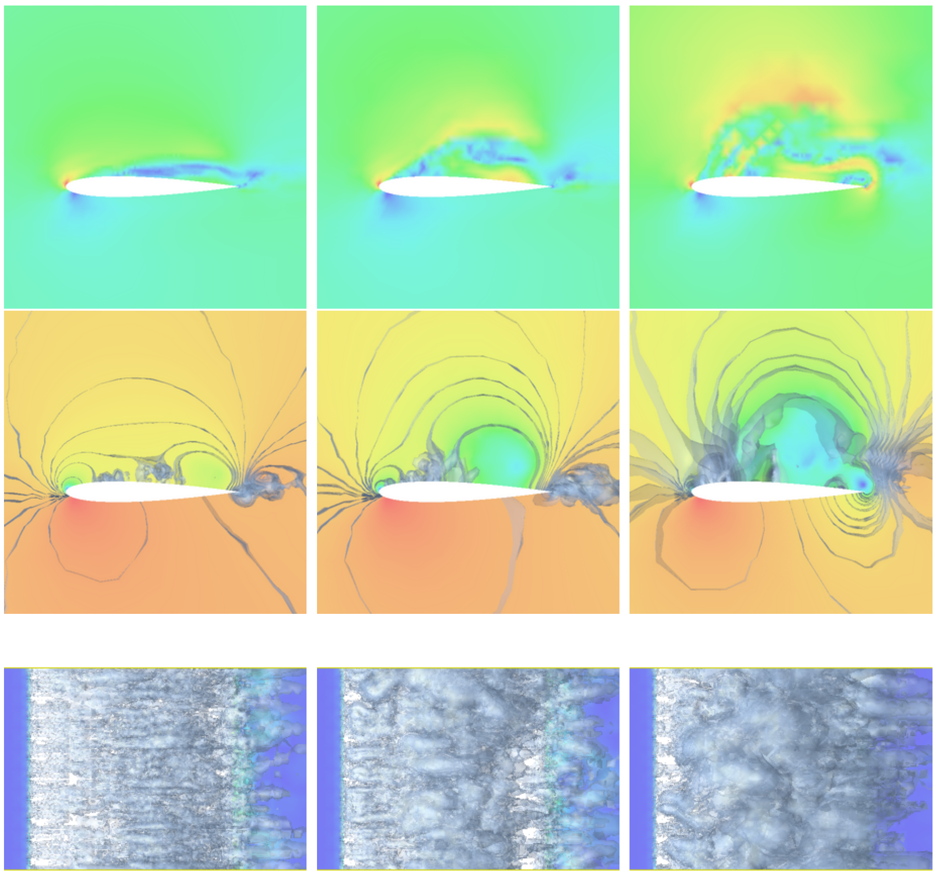

Figure 16.3: G2 computation of velocity magnitude (upper), pressure (middle), and non-transversal vorticity (lower), for angles of attack 20, 22, and 24° (from left to right).

Chapter 17

Summary of Observation

Phase 1: $0 \leq \alpha \leq 8$

At zero angle of attack with zero lift there is high pressure at the leading edge and equal low pressures on the upper and lower crests of the wing because the flow is essentially potential and thus satisfies Bernouilli's law of high/low pressure where velocity is low/high. The drag is about 0.01 and results from rolls of low-pressure streamwise vorticity attaching to the trailing edge. As α increases the low pressure below gets depleted as the incoming flow becomes parallel to the lower surface at the trailing edge for $\alpha = 6$, while the low pressure above intenisfies and moves towards the leading edge. The streamwise vortices at the trailing edge essentially stay constant in strength but gradually shift attachement towards the upper surface. The high pressure at the leading edge moves somewhat down, but contributes little to lift. Drag increases only slowly because of negative drag at the leading edge.

Phase 2: $8 \leq \alpha \leq 12$

The low pressure on top of the leading edge intensifies to create a normal gradient preventing separation, and thus creates lift by suction peaking on top of the leading edge. The slip boundary condition prevents separation and downwash is created with the help of the low-pressure wake of streamwise vorticity at rear separation. The high pressure at the leading edge moves further down and the pressure below increases slowly, contributing to the main lift coming from suction above. The net drag from the upper surface is close to zero because of the negative drag at the leading edge, known as *leading edge suction*, while the drag from the lower surface increases (linearly) with the angle of the incoming flow, with somewhat increased but still small drag slope. This explains why the line to a flying kite can be almost vertical even in strong wind, and that a thick wing can have less drag than a thin.

Phase 3: $12 \leq \alpha \leq 14$

Beginning stall with lift non-increasing while drag is increasing super-linearly.

Phase 4: $14 \leq \alpha \leq 16$

Stall with rapidly increasing drag.

17.1 Summary Lift and Drag

The lift generation in Phase 1 and 3 can rather easily be envisioned, while both the lift and drag in Phase 2 results from a (fortunate) intricate interplay of stability and instability of potential flow: The main lift comes from upper surface suction arising from a turbulent boundary layer with small skin friction combined with rear separation instability generating low-pressure streamwise vorticity, while the drag is kept small by negative drag from the leading edge.

We can thus summarize as follows:

- Substantial lift from suction on upper surface.
- Small drag from suction on leading edge.

Chapter 18

Computation vs Experiments

The computations shown are obtained by the finite element solver $G2$ with automatic mesh adaption from a posteriori error estimation of lift and drag by based on sensitivity information obtained by solving a linearized dual Navier-Stoke problem.

18.1 Meshes

We show below computational automatically adapted 3d meshes with up to 800.000 mesh points together with snapshots of computed turbulent velocities.

18.2 Data for Experiments

Ladson 1
: $Re = 8.95e6, M = 0.15$ Grit level 60W (wraparound). grit acts to trip the boundary layer.

Ladson 2
: $Re = 6.00e6, M = 0.15$ Grit level 60W (wraparound).

Ladson 3
: $Re = 8.95e6, M = 0.30$ Grit level 120W (wraparound).

Gregory/O'Reilly
: $Re = 2.88e6, M = 0.16$

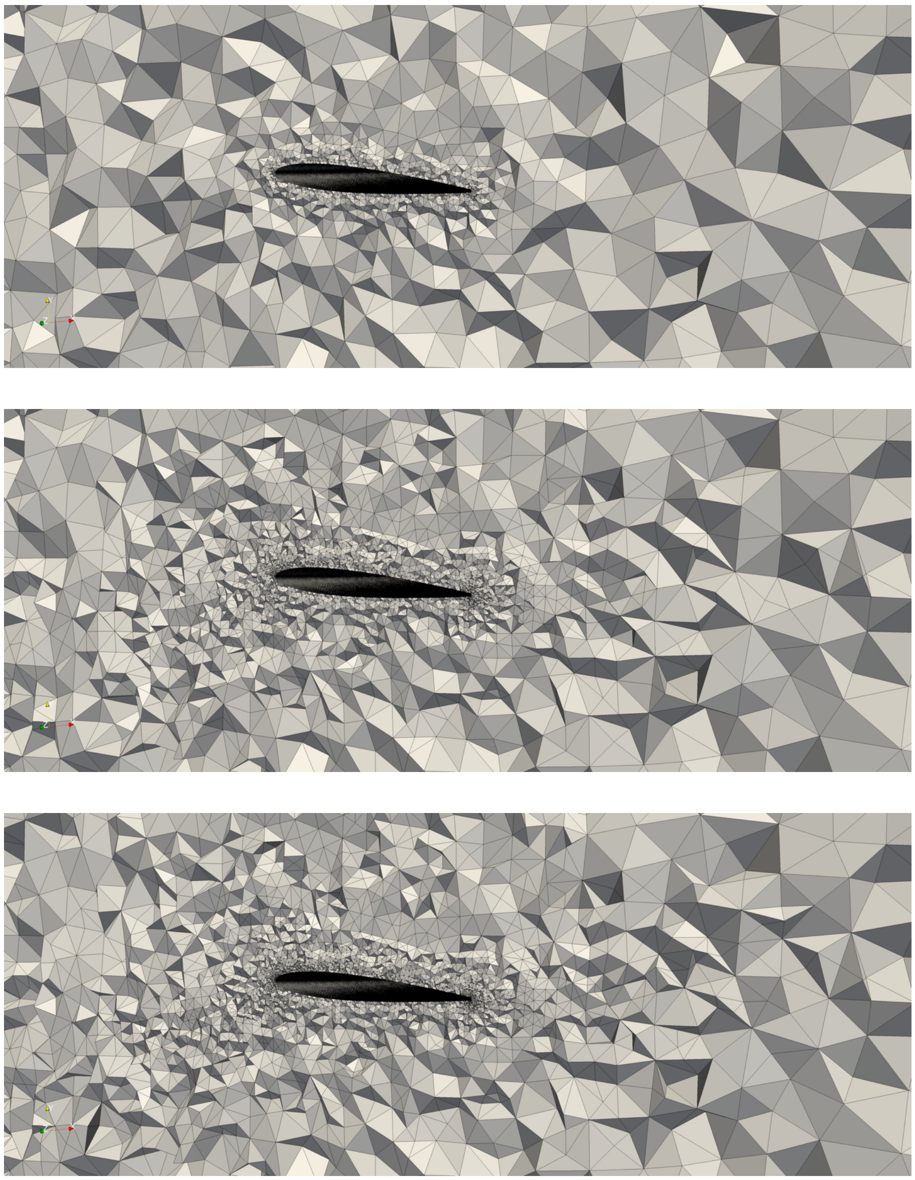

Figure 18.1: Automatically adapted meshes for $aoa = 10$, with inital mesh top, iteration 4 center, and iteration 8 bottom.

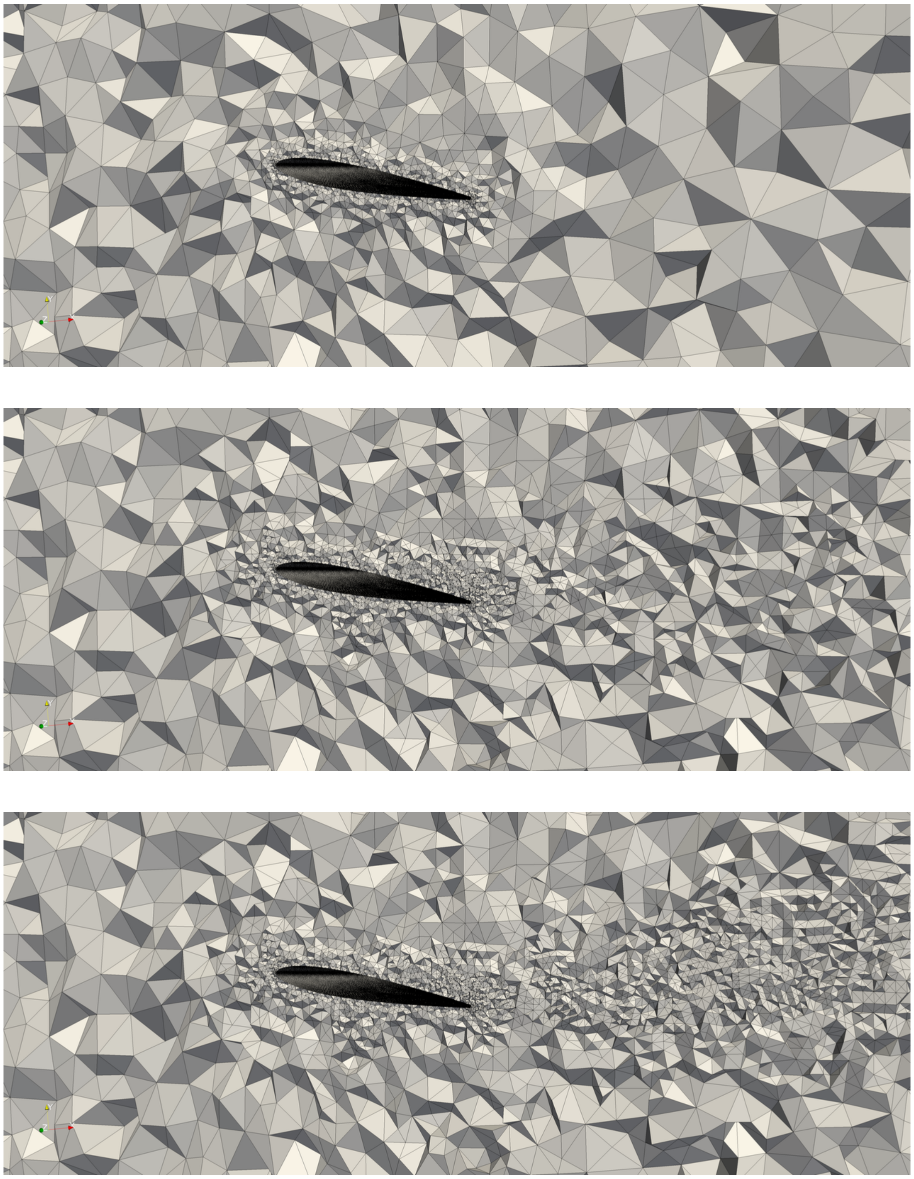

Figure 18.2: Automatically adapted meshes for $\alpha = 14$, with mesh top, iteration 4 center and iteration 8 bottom.

where the wraparound grit in the Ladson experiments acts to trip the boundary layer.

18.3 Comparing Computation with Experiment

Fig. **??** shows that G2 computations lie within variations in experiments [55, 58]. (Valid point?)

Computations more precise than experiment:

G2 with slip models a very large Reynolds number representative of e.g. a jumbojet, which cannot be attained in wind tunnel where scale model are used. Upscaling of test results is cumbersome because boundary layers do not scale. This means that computations can be closer to reality than wind tunnel experiments.

Of particular importance is the maximal lift coefficient, which cannot be predicted by Kutta-Zhukovsky nor in model experiments.

Chapter 19

Sensitivity of Lift/Drag vs Discretization

19.1 A Posteriori Error Control by Duality

G2 is equipped with automatic a posteriori error estimation in chosen output quantities such as lift and drag, which expresses the sensitivity of lift and drag with respect to the residual of a computed Navier-Stokes solution in terms of a weight function obtained by solving a dual linearized Navier-Stokes equation with the size of derivatives of the dual velocity and pressure representing the weight. G2 automatically adapts the computational mesh according to the weight so as to optimize computational resources.

19.2 Dual Pressure and Velocity

In Fig. 19.1-19.4 we show dual pressure and velocity for lift/drag indicating mesh refinement where derivatives are large.

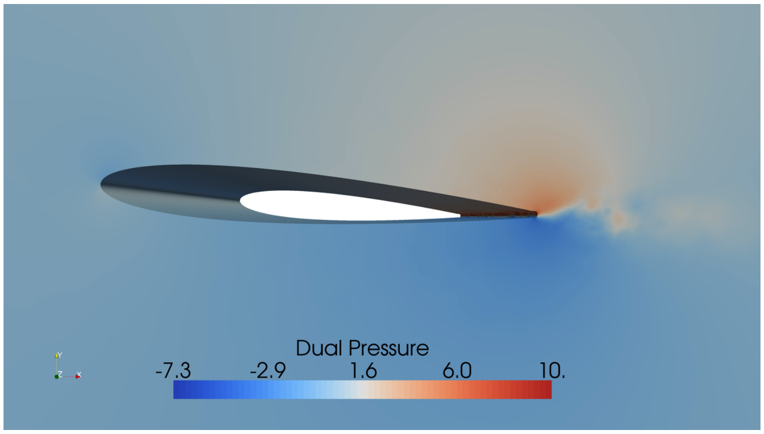

Figure 19.1: Dual pressure $\alpha = 4$.

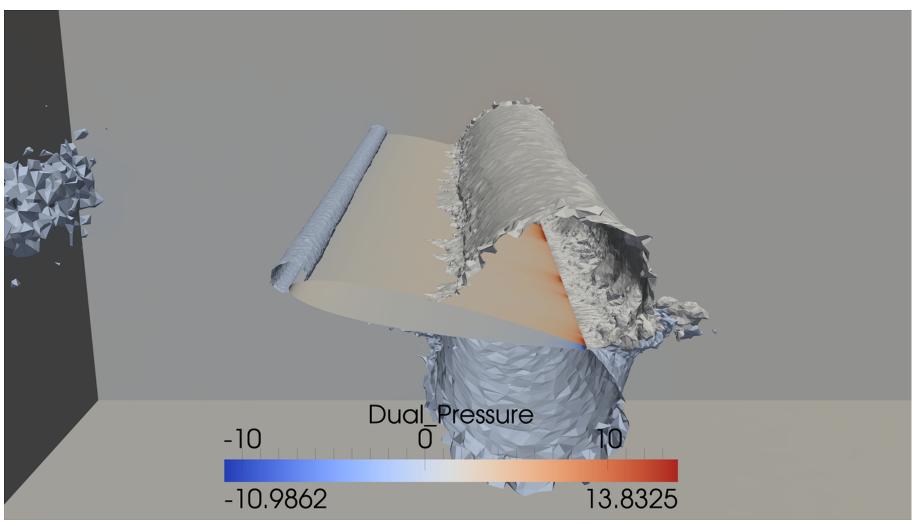

Figure 19.2: Dual pressure $\alpha = 12$.

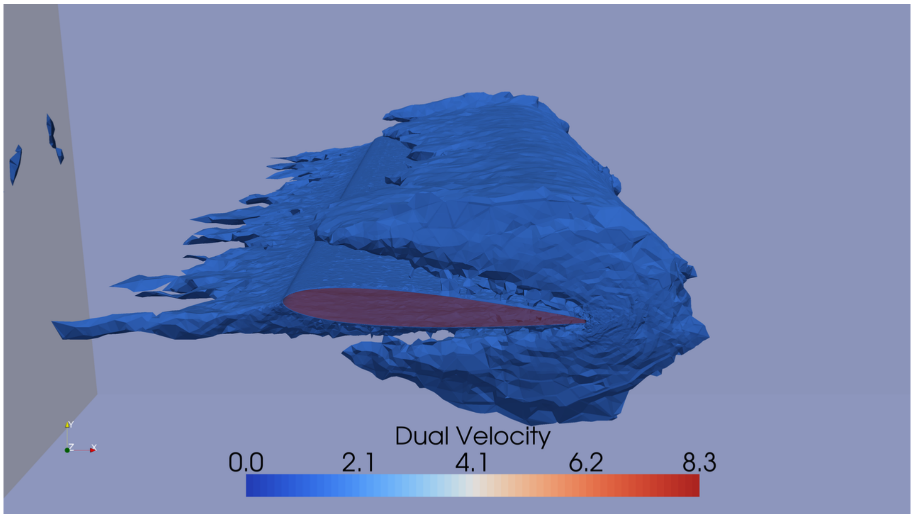

Figure 19.3: Dual velocity $\alpha = 4$.

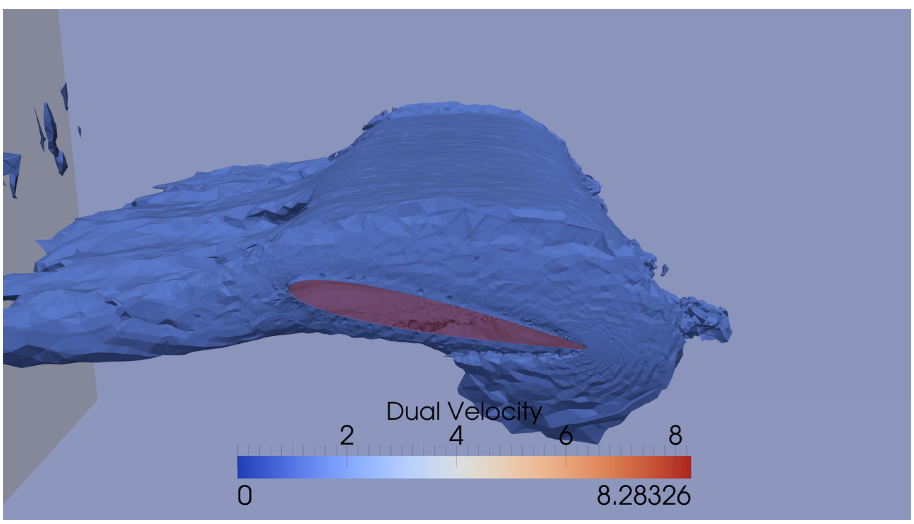

Figure 19.4: Dual velocity $\alpha = 12$.

Chapter 20

Preparing Understanding

20.1 New Resolution of d'Alembert's Paradox

We have said that the new flight theory comes out of a *new resolution* of d'Alembert's paradox [103, 104, 102]. The new resolution is based on a stability analysis showing that zero-lift/drag potential flow is *unstable* and in both computation and reality is replaced by turbulent flow with both lift and drag.

The new resolution is fundamentally different from the classical official resolution attributed to Prandtl [120, 124, 137], which disqualifies potential flow because it satisfies a *slip* boundary condition allowing fluid particles to glide along the boundary without friction force, and does not satisfy a *no-slip* boundary condition requiring the fluid particles to stick to the boundary with zero relative velocity and connect to the free-stream flow through a thin *boundary layer*, as demanded by Prandtl.

20.2 Slip/Small Friction Boundary Conditions

In contrast to Prandtl, we complement in the new theory Navier-Stokes equations with a *friction force boundary condition* for *tangential forces* on the boundary with a *small friction coefficient* as a model of the *small skin friction* resulting from a *turbulent boundary layer* of *slightly viscous flow.* In the limit of zero boundary friction this becomes a slip boundary condition, which means that potential flow can be seen as a solution of the Navier-Stokes equations subject to a small perturbation from small viscous stresses. In the new theory we then disqualify potential flow because it is unstable, that is on physical grounds, and not as Prandtl on formal grounds because it does not satisfy no-slip boundary conditions.

The Navier-Stokes equations can be complemented by no-slip or slip/friction boundary conditions, just like Poisson's equation can be complemented by Dirichlet or Neumann boundary conditions. The choice of boundary conditions depends on which data is available. In the aerodynamics of larger birds and airplanes, the skin friction is small and can be approximated by zero friction or a slip boundary condition.

For small insects viscous effects become important, which changes the physics of flight and makes gliding flight impossible. An albatross is a very good glider, while a fruit fly cannot glide at all in the syrup-like air it meets and can only move by using some form of paddling.

20.3 Computable + Correct = Secret

We solve the Navier-Stokes equations (NS) with slip/friction boundary condition using an *adaptive stabilized finite element method* with *duality-based a posteriori error control* referred to as *General Galerkin* or *G2* presented in detail in [103] and available in executable open source form from [132]. The stabilization in G2 acts as an *automatic computational turbulence model*, and the only input is the geometry of the wing. We thus find by computation that lift is not connected to circulation in contradiction to Kutta-Zhukovsky's theory and that the curse of Prandtl's laminar boundary layer theory (also questioned in [92, 93, 72]) can be circumvented. Altogether, we show in this book that *ab initio* computational fluid mechanics opens new possibilities of flight simulation ready to be explored and utilized.

- NS with no-slip: uncomputable: hides the secret,
- NS with slip: computable: reveals the secret.

20.4 No Lift without Drag

The zero-drag of potential flow has been (and still is) leading aerodynamicis to search for wings with lift but without drag [3], which we have seen is not a feature of Navier-Stokes solutions, and thus is unrealistic.

Chapter 21

Kutta-Zhukovsky-Prandtl Incorrect

The Kutta-Zhukovsky theory states that substantial lift comes from substantial circulation, but does not tell how the wing manages to cause substantial circulation of air around itself. Computing solutions of the Navier-Stokes equations shows that the wing does not do that as shown in Fig. 21.1, where the circulation is computed around the curve of the section of the section of the wing: The lift is substantial and increases linearly with the angle of attack until stall begins, while the circulation remains small. Evidently, lift does not originate from circulation.

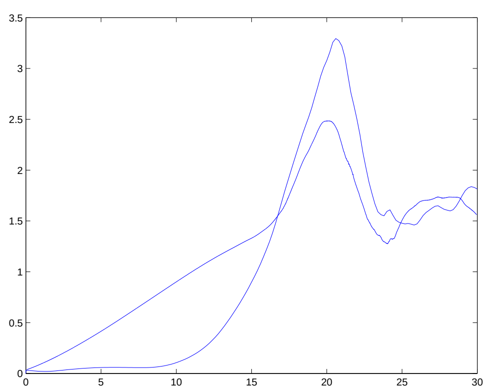

Figure 21.1: Lift coefficient and circulation as functions of the angle of attack.

Chapter 22

Mathematical Miracle of Sailing (delete)

> By denying scientific principles, one may maintain any paradox. (Galileo Galilei)

Both the sail and keel of a sailing boat under tacking against the wind, act like wings generating lift and drag, but the action, geometrical shape and angle of attack of the sail and the keel are different. The effective angle of attack of a sail is typically 15-20 degrees and that of a keel 5-10 degrees, for reasons which we now give.

The boat is pulled forward by the sail, assuming for simplicity that the beam is parallel to the direction of the boat at a minimal tacking angle, by the component $L\sin(15)$ of the lift L, as above assumed to be perpendicular to the effective wind direction, but also by the following contributions from the drag assumed to be parallel to the effective wind direction: The negative drag on the leeeward side at the leading edge close to the mast gives a positive pull which largely compensates for the positive drag from the rear leeward side, while there is less positive drag from the windward side of the sail as compared to a wing profile, because of the difference in shape. The result is a forward pull $\approx \sin(15)L \approx 0.2L$ combined with a side (heeling) force $\approx L\cos(15) \approx L$, which tilts the boat and needs to be balanced by lift from the the keel in the opposite direction. Assuming the lift/drag ratio for the keel is 13, the forward pull is then reduced to $\approx (0.2-1/13)L \approx 0.1L$, which can be used to overcome the drag from the hull minus the keel.

The shape of a sail is different from that of a wing which gives smaller drag from the windward side and thus improved forward pull, while the keel has the shape of a symmetrical wing and acts like a wing. A sail with aoa $15-20$ degrees gives maximal pull forward at maximal heeling/lift with contribution also from the rear part of the sail, like for a wing just before stall, while the drag is smaller than for a wing at 15-20 degrees aoa (for which the lift/drag ratio is 4-3), with the motivation given above. The lift/drag curve for a sail is thus different from that of wing with lift/drag ratio at aoa 15-20 much larger for a sail. On the other hand, a keel with aoa 5-10 degrees has a lift/drag ratio about 13. A sail at aoa 15-20 thus gives maximal pull at strong heeling force and small drag, which together with a keel at aoa 5-10 with strong lift and small drag, makes an efficient combination. This explains why modern designs combine a deep narrow keel acting efficiently for small aoa, with a broader sail acting efficiently at a larger aoa.

Using a symmetrical wing as a sail would be inefficient, since the lift/drag ratio is poor at maximal lift at aoa 15-20. On the other hand, using a sail as a wing can only be efficient at a large angle of attack, and thus is not suitable for cruising. This material is developed in more detail in [108].

Part III

Mathematics

Chapter 23

Navier-Stokes Equations

> Waves follow our boat as we meander across the lake, and turbulent air currents follow our flight in a modern jet. Mathematicians and physicists believe that an explanation for and the prediction of both the breeze and the turbulence can be found through an understanding of solutions to the Navier-Stokes equations. Although these equations were written down in the 19th Century, our understanding of them remains minimal. The challenge is to make substantial progress toward a mathematical theory which will unlock the secrets hidden in the Navier-Stokes equations. (Clay Mathematics Institute Millennium Problem [106])

23.1 Conservation of Mass, Momentum and Energy

The basic mathematical model of fluid mechanics takes the form of the *Navier-Stokes equations* expressing conservation of mass, momentum and energy of a viscous fluid in the conservation variables of density, momentum and energy with the viscosity as a given coefficient. For an incompressible fluid the equations can be formulated in terms velocity and pressure, referred to as the *incompressible Navier-Stokes equations*, with a decoupled energy equation.

The fluid mechanics of subsonic flight is modeled by the incompressible Navier-Stokes equations for a slightly viscous fluid, which is the focus of this book. The *Reynolds number* $Re = \frac{UL}{\nu}$ where U is a characteristic fluid velocity, L a characteristic length and ν the fluid viscosity, is used to identify the high Reynolds number flow occuring in aerodynamics with Re of size 10^8 for large airplanes.

The incompressible Navier-Stokes equations are complemented by initial values for velocity, and boundary conditions specifying either velocities or forces on the boundary. A *no-slip* boundary condition sets the fluid velocity to zero on the boundary, while a *slip* boundary condition sets the velocity normal to the boundary to zero together with the tangential (friction) force. The slip condition is a limit case of a combined normal velocity-tangential stress boundary condition with the tangential stress set to zero as a model of zero skin friction.

The Navier-Stokes equations for an incompressible fluid of unit density with *small viscosity* $\nu > 0$ and *small skin friction* $\beta \geq 0$ filling a volume Ω in $\mathbb{R}^3$ surrounding a solid body with boundary Γ over a time interval $I = [0, T]$, read as follows: Find the velocity $u = (u_1, u_2, u_3)$ and pressure p depending on $(x, t) \in \Omega \cup \Gamma \times I$, such that

$$\begin{array}{rcll} \dot{u} + (u \cdot \nabla)u + \nabla p - \nabla \cdot \sigma & = & f & \text{in } \Omega \times I, \\ \nabla \cdot u & = & 0 & \text{in } \Omega \times I, \\ u_n & = & g & \text{on } \Gamma \times I, \\ \sigma_s & = & \beta u_s & \text{on } \Gamma \times I, \\ u(\cdot, 0) & = & u^0 & \text{in } \Omega, \end{array} \tag{23.1}$$

where u_n is the fluid velocity normal to Γ, u_s is the tangential velocity, $\sigma = 2\nu\epsilon(u)$ is the viscous (shear) stress with $\epsilon(u)$ the usual velocity strain, σ_s is the tangential stress, f is a given volume force, g is a given inflow/outflow velocity with $g = 0$ on a non-penetrable boundary, and u^0 is a given initial condition.

We notice the skin friction boundary condition coupling the tangential stress σ_s to the tangential velocity u_s with the friction coefficient β with $\beta = 0$ for slip, and $\beta >> 1$ for no-slip. We note that β is related to the standard *skin friction coefficient* $c_f = \frac{2\tau}{U^2}$ with τ the tangential stress per unit area, by the relation $\beta = \frac{U}{2} c_f$. In particular, β tends to zero with c_f (if U stays bounded).

Prandtl insisted on using a no-slip velocity boundary condition with $u_s = 0$ on Γ, because his resolution of d'Alembert's paradox hinged on discriminating potential flow by this condition. On the oher hand, with the new resolution of d'Alembert's paradox, relying instead on instability of potential flow, we are free to choose instead a friction force boundary condition, if data is available. Now, experiments show [124, 28] that the skin friction coefficient decreases with increasing Reynolds number Re as $c_f \sim Re^{-0.2}$, so that $c_f \approx 0.0005$ for $Re = 10^{10}$ and $c_f \approx 0.007$ for $Re = 10^5$. Accordingly we model a turbulent boundary layer by a friction boundary condition with a friction parameter $\beta \approx 0.03URe^{-0.2}$. For very large Reynolds numbers, we can effectively use $\beta = 0$ in G2 computation corresponding to slip boundary conditions.

23.2 Wellposedness and Clay Millennium Problem

The mathematician J. Hadamard identified in 1902 [95] *wellposedness* as a necessary requirement of a solution of a mathematical model, such as the Navier-Stokes equations, in order to have physical relevance: Only *wellposed* solutions which are suitably stable in the sense that small perturbations have small effects when properly measured, have physical significance as observable pheonomena.

Leray's requirement of wellposedness is absolutely fundamental, but the question whether solutions of the Navier-Stokes equations are wellposed, has not been studied because of lack mathematical techniques for quantitative analysis. This is evidenced in the formulation of the Clay Millennium Prize Problem on the Navier-Stokes equations excluding wellposedness [106, 102].

The mathematical Garret Birkhoff became heavily criticized for posing this question in [92], which stopped him from further studies. The first step towards resolution of d'Alembert's paradox and the mathematical secret of flight is thus to pose the question if potential flow is wellposed, and then to realize that it is not. It took 256 years to take these steps.

23.3 Laminar vs Turbulent Boundary Layer

As developed in more detail in [134], we make a distinction between laminar (boundary layer) separation modeled by no-slip and turbulent (boundary layer) separation modeled by slip/small friction. Note that laminar separation cannot be modeled by slip, since a laminar boundary layer needs to be resolved with no-slip to get correct (early) separation. On the other hand, as will be seen below, in turbulent (but not in laminar) flow the interior turbulence dominates the skin friction turbulence indicating that the effect of a turbulent boundary layer can be modeled by slip/small friction, which can be justified by an posteriori sensitivity analysis as shown in [134].

We thus assume that the boundary layer is turbulent and is modeled by slip/small friction, which effectively includes the case of laminar separation followed by reattachment into a turbulent boundary layer.

Chapter 24

G2 Computational Solution

24.1 General Galerkin G2: Finite Element Method

We show in [103, 102, 104] that the Navier-Stokes equations (23.1) can be solved by a weighted least squares residual stabilized finite element referred to as *General Galerkin* or *G2*.

Writing the Navier-Stokes equations in symbolic form as $R(u, p) = 0$, the G2 method determines a piecewise linear computational solution (U, P) on a given finite element mesh such that the residual $R(U, P)$ is small in a mean-value sense (Galerkin property) and with a certain weighted control of $R(U, P)$ in a least-square sense (residual stabilization).

G2 produces turbulent solutions characterized by substantial turbulent dissipation from the least squares residual stabilization acting as an automatic turbulence model, reflecting that $R(U, P)$ cannot be made small pointwise in turbulent regions.

G2 is equipped with automatic a posteriori error control guaranteeing correct lift and drag coefficients [103, 34, 33, 38, 99, 100] up to an error tolerance of a few percent on meshes with a few hundred thousand or million mesh points number of mesh points depending on geometry complexity.

G2 with slip is thus capable of modeling slightly viscous turbulent flow with $Re > 10^6$ of relevance in many applications in aero/hydro dynamics, including flying, sailing, boating and car racing, with possible millions of mesh points, to be compared with the impossible quadrillions required [43] for boundary layer resolution.

G2 with slip works because slip is good model of the turbulent boundary layer od slightly viscous flow, and interior turbulence does not have to be resolved to physical scales to capture mean-value outputs [103].

G2 with slip thus offers a wealth of infomation at affordable cost, while Prandtl's requirement of boundary layer resolution cannot be met by any forseeable computer.

24.2 A Posteriori Error Control and Well-posedness

G2 is an adaptive finite element method with duality-residual based error control of the principal form

$$dM(U,P) \leq S\|hR(U,P)\| \tag{24.1}$$

$dM(U,P)$ is the variation of a certain mean-value output $M(U,P)$ such as lift or drag coeffiients of a computed Navier-Stokes solution (U,P) with Navier-Stokes residual $R(U,P)$ on a mesh with mesh size h and S is a stability factor measuring certain norms of an associated dual solution and $\|\cdot\|$ is a mean square integral norm.

If in a G2 computation $S\|hR(U,P) < TOL$, the output $M(U,P)$ is guaranteed to change less than TOL under any mesh refinement.

24.3 What You Need to Know

To understand flight it is not necessary to get into the details of G2; it is sufficient to understand that G2 solves the Navier-Stokes equations with an automatic control of the the computational error, which guarantees that G2 solutions are proper solutions capable of unraveling the secrets hidden in the Navier-Stokes equations, thereby offering valuable information for both understanding and design.

24.4 Turbulent Flow around a Car

In Fig. 24.1 we show computed turbulent G2 flow around a car with substantial drag in accordance with wind-tunnel experiments. We see a pattern of streamwise vorticity forming in the rear wake. We also see surface vorticity forming on the hood transversal to the main flow direction. We will discover similar features in the flow of air around a wing...

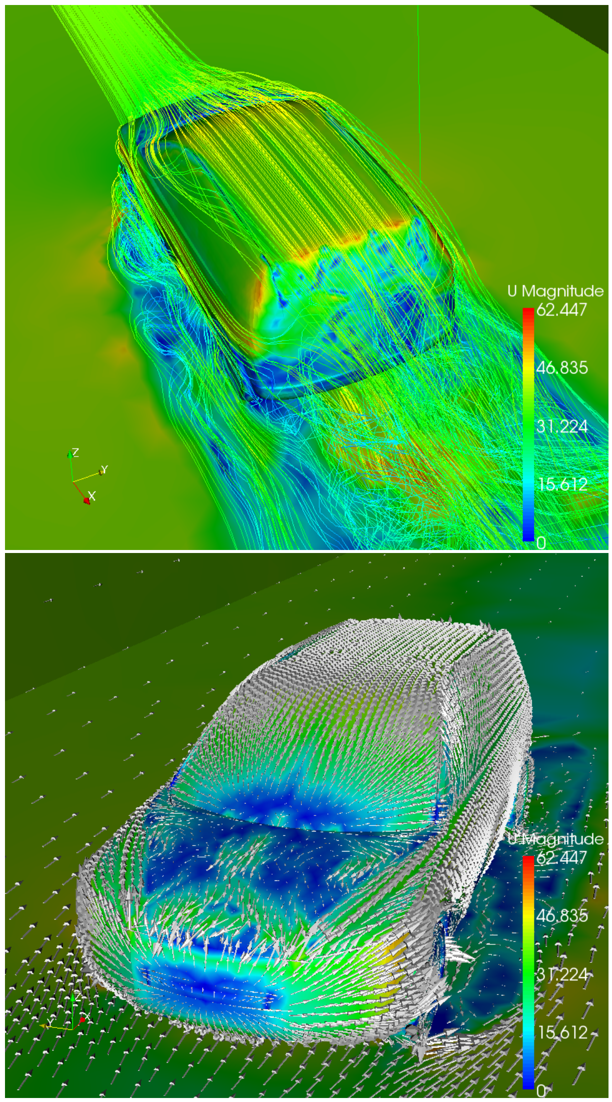

Figure 24.1: Velocity of turbulent flow around a car

Chapter 25

Potential Flow

> Because of d'Alembert's paradox) fluid mecahnics was from start split into the field of hydraulics, observing phenomena which could not be explained, and mathematical or theoretical fluid mechanics explaining phenomena which could not be observed. (Chemistry Nobel Laureate Sir Cyril Hinshelwood [63])

25.1 Euler defeated by d'Alembert

Mathematical fluid mechanics started when Euler in the 1740s discovered certain solutions in two space dimensions of the Navier-Stokes equations with vanishingly small viscosity, with velocities of the form $u = \nabla\varphi$, where the potential φ is a harmonic function satisfying $\Delta\varphi = 0$ in the fluid. These were named *potential solutions* characterized as

- inviscid: vanishingly small viscosity,
- incompressible: $\nabla \cdot u = 0$,
- irrotational: $\nabla \times u = 0$
- stationary: $\dot{u} = 0$.

This promised a fluid mechanics boom for mathematicians as experts of harmonic functions, but the success story quickly collapsed when d'Alembert in 1752 showed that both lift and drag of potential solutions are zero, which showed that the wonderful potential solutions were unphysical and thus were doomed as useless. But potential solution were essentially the only solutions which could be constructed analytically, which led to a long-lasting split of fluid mechanics into:

- practical fluid mechanics or hydraulics: observing phenomena which cannot be explained (non-zero lift and drag),
- theoretical fluid mechanics: explaining phenomena which cannot be observed (zero drag and lift),

according to the above quote.

We shall see that it took 254 years to resolve the paradox, but once it was resolved the mystery of flight could be uncovered without split between theory and reality.

25.2 Potential Flow as Near Navier-Stokes Solution

Potential flow (u, p) with velocity $u = \nabla\varphi$, where φ is harmonic in Ω and satisfies a homogeneous Neumann condition on Γ and suitable conditions at infinity, can be seen as a solution of the Navier-Stokes equations for slightly viscous flow with slip boundary condition, subject to

- perturbation of the volume force $f = 0$ in the form of $\sigma = \nabla \cdot (2\nu\epsilon(u))$,
- perturbation of zero friction in the form of $\sigma_s = 2\nu\epsilon(u)_s$,

with both perturbations being small because ν is small and a potential flow velocity u is smooth. Potential flow can thus be seen as a solution of the Navier-Stokes equations with small force perturbations tending to zero with the viscosity. We can thus express d'Alembert's paradox as the zero lift/drag of a Navier-Stokes solution in the form of a potential solution, and resolve the paradox by realizing that potential flow is unstable and thus cannot be observed as a physical flow.

Potential flow is like an inverted pendulum, which cannot be observed in reality because it is unstable and under infinitesimal perturbations turns into a swinging motion. A stationary inverted pendulum is a fictious mathematical solution without physical correspondence because it is unstable. You can only observe phenomena which in some sense are stable, and an inverted pendelum or potential flow is not stable in any sense.

25.3 Potential Flow Separates only at Stagnation

Potential flow has the following crucial property which partly will be inherited by real turbulent flow, and which explains why a flow over a wing subject to small skin friction can avoid separating at the crest and thus generate downwash, unlike viscous flow with no-slip, which separates at the crest without downwash. We will conclude that gliding flight is possible only in slightly viscous incompressible flow. For simplicity we consider two-dimensional potential flow around a cylindrical body such as a long wing (or cylinder).

Theorem. Let φ be harmonic in the domain Ω in the plane and satisfy a homogeneous Neumann condition on the smooth boundary Γ of Ω. Then the streamlines of the corresponding velocity $u = \nabla\varphi$ can only separate from Γ at a point of stagnation with $u = \nabla\varphi = 0$.
Proof. Let ψ be a harmonic conjugate to φ with the pair (φ, ψ) satisfying the Cauchy-Riemann equations (locally) in Ω. Then the level lines of ψ are the streamlines of φ and vice versa. This means that as long as $\nabla\varphi \neq 0$, the boundary curve Γ will be a streamline of u and thus fluid particles cannot separate from Γ in bounded time.

25.4 Vortex Stretching

Formally applying the curl operator $\nabla\times$ to the momentum equation of (23.1), with $\nu = \beta = 0$ for simplicity, we obtain the *vorticity equation*

$$\dot{\omega} + (u \cdot \nabla)\omega - (\omega \cdot \nabla)u = \nabla \times f \quad \text{in } \Omega, \tag{25.1}$$

which is a convection-reaction equation in the vorticity $\omega = \nabla \times u$ with coefficients depending on u, of the same form as the linearized equation (**??**), with similar properties of exponential perturbation growth $\exp(|\nabla u|t)$ referred to as *vortex stretching*. Kelvin's theorem formally follows from this equation assuming the initial vorticity is zero and $\nabla \times f = 0$ (and $g = 0$), but exponential perturbation growth makes this conclusion physically incorrect: We will see below that large vorticity can develop from irrotational potential flow even with slip boundary conditions. , by properly understanding both the physical and unphysical aspects of potential solutions.

Chapter 26

D'Alembert and his Paradox

> To those who ask what the infinitely small quantity in mathematics is, we answer that it is actually zero. Hence there are not so many mysteries hidden in this concept as they are usually believed to be. (Leonhard Euler)
>
> High office, is like a pyramid; only two kinds of animals reach the summit– reptiles and eagles. (d'Alembert)
>
> Just go on . . . and faith will soon return. (d'Alembert to a friend hesitant with respect to infinitesimals)
>
> If one looks at all closely at the middle of our own century, the events that occupy us, our customs, our achievements and even our topics of conversation, it is difficult not to see that a very remarkable change in several respects has come into our ideas; a change which, by its rapidity, seems to us to foreshadow another still greater. Time alone will tell the aim, the nature and limits of this revolution, whose inconveniences and advantages our posterity will recognize better than we can. (d'Alembert on the Enlightment)

26.1 d'Alembert and Euler and Potential Flow

Working on a 1749 Prize Problem of the Berlin Academy on flow drag, d'Alembert was led to the following contradiction referred to as *d'Alembert's paradox* [75, 76, 77, 78, 83] between observation and theoretical prediction:

- *It seems to me that the theory (potential flow), developed in all possible rigor, gives, at least in several cases, a strictly vanishing resistance, a singular paradox which I leave to future Geometers to elucidate.*

The great mathmatician *Leonard Euler*(1707-1783) had come to same conclusion of zero drag of potential flow in his work on gunnery [79] from 1745 based on the observation that in potential flow the high pressure forming in front of the body is balanced by an equally high pressure in the back, in the case of a boat moving through water expressed as

- *...the boat would be slowed down at the prow as much as it would be pushed at the poop...*

This is the idea of Aristotle adopted by da Vinci, which we met above in the form of peristaltic motion.

More precisely, d'Alembert's paradox concerns the contradiction between observations of substantial drag/lift of a body moving through a slightly viscous fluid such as air and water, with the mathematical prediction of zero drag/lift of potential flow defined as inviscid, incompressible, irrotational and stationary flow. Evidently, flying is incompatible with potential flow, and in order to explain flight d'Alembert's paradox had to be resolved. But d'Alembert couldn't do it and all the great mathematical brains of the 18th and 19th century stumbled on it: Nobody could see that any of the assumptions (i)-(iv) were wrong and the paradox remained unsolved. We shall resolve the paradox below and find the true reason that potential flow with zero drag/lift is never observed. And the true reason is not (iii).

We recall that a flow is *irrotational* if the flow velocity u has zero *vorticity*, that is if $\nabla\times u = 0$, in which case (for a simply connected domain) the velocity u is given as the gradient of a potential function: $u = \nabla\varphi$ where φ is the potential. If u is also incompressible, then

$$\Delta\varphi = \nabla\cdot\nabla\varphi = \nabla\cdot u = 0$$

and thus the potential φ is a *harmonic function* satisfying *Laplace's equation*:

$$\Delta\varphi = 0. \tag{26.1}$$

This promised to open fluid mechanics for take-over by harmonic functions in the hands of mathematicians, supported by *Kelvin's theorem* stating that

Figure 26.1: D'Alembert formulating his paradox.

without external forcing, an incompressible inviscid flow will stay irrotational if initiated as irrotational. Mathematicians thus expected to find an abundance of potential flows governed by harmonic potentials in the fluid mechanics of slightly viscous flow, but such flows did not seem to appear in reality, and nobody could understand why.

26.2 The Euler Equations

The basic equations in fluid mechanics expressing *conservation of momentum* or *Newton's 2nd law* connecting force to accelleration combined with *conservation of mass* in the form of incompressibility, were formulated by Euler in 1755 as the *Euler equations* for an *incompressible inviscid* fluid (of unit density) enclosed in a volume Ω in $\mathbb{R}^3$ with boundary Γ: Find the velocity $u = (u_1, u_2, u_3)$ and pressure p such that

$$\begin{aligned} \dot u + (u\cdot\nabla)u + \nabla p &= f &&\text{in } \Omega\times I,\\ \nabla\cdot u &= 0 &&\text{in } \Omega\times I,\\ u\cdot n &= g &&\text{on } \Gamma\times I,\\ u(\cdot,0) &= u^0 &&\text{in } \Omega, \end{aligned} \tag{26.2}$$

where the dot signifies differentiation with respect to time, n denotes the outward unit normal to Γ, f is a given volume force, g is a given inflow/outflow velocity, u^0 is a given initial condition and $I = [0, T]$ a given time interval. We notice the *slip boundary condition* $u \cdot n = 0$ modeling a non-penetrable boundary with zero friction.

The momentum equation can alternatively be formulated as

$$\dot{u} + \nabla(\frac{1}{2}|u|^2 + p) + u \times \omega = f \tag{26.3}$$

where

$$\omega = \nabla \times u$$

is the *vorticity* of the velocity u, which follows from the following calculus identity:

$$\frac{1}{2}\nabla|u|^2 = (u \cdot \nabla)u + u \times (\nabla \times u).$$

For a stationary irrotational velocity u with $\dot{u} = 0$ and $\omega = \nabla \times u = 0$, we find that if $f = 0$, then

$$\frac{1}{2}|u|^2 + p = C \tag{26.4}$$

where C is a constant, which is nothing but *Bernouilli's principle* coupling small velocity to large pressure and vice versa.

We conclude that a potential flow velocity $u = \nabla\varphi$ solves the Euler equations with the pressure p given by Bernouilli's law.

Kelvin's theorem states that if the initial velocity u^0 is irrotational and $\nabla \times f = 0$ and $g = 0$, then a smooth Euler solution velocity will remain irrotational for positive time. Below we will question the validity of Kelvin's theorem on the ground that solutions of the Euler equations in general are not smooth, even if data are.

26.3 Potential Flow around a Circular Cylinder

To understand how a wing generates lift and drag it is instructive to first consider the corresponding problem for a circular cylinder, which we can view as a wing with circular cross-section. Of course you cannot fly with such a wing, but a wing is similar to a half cylinder which can be analyzed starting with a full cylinder.

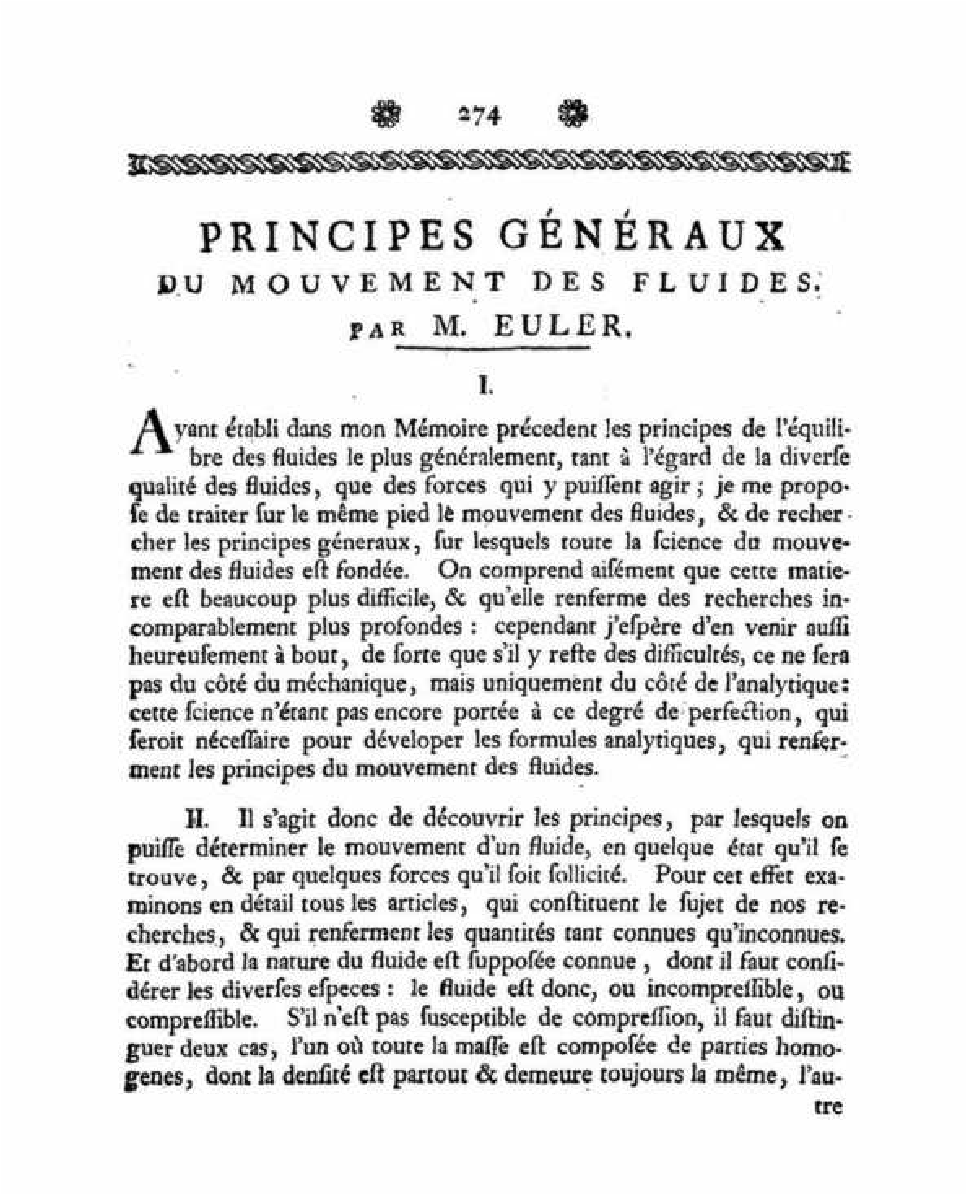

274

PRINCIPES GÉNÉRAUX
DU MOUVEMENT DES FLUIDES.
PAR M. EULER.

I.

Ayant établi dans mon Mémoire précedent les principes de l'équilibre des fluides le plus généralement, tant à l'égard de la diverſe qualité des fluides, que des forces qui y puiſſent agir; je me propoſe de traiter ſur le même pied lè mouvement des fluides, & de rechercher les principes géneraux, ſur lesquels toute la ſcience du mouvement des fluides eſt fondée. On comprend aiſément que cette matiere eſt beaucoup plus difficile, & qu'elle renferme des recherches incomparablement plus profondes : cependant j'eſpère d'en venir auſſi heureuſement à bout, de ſorte que s'il y reſte des difficultés, ce ne ſera pas du côté du méchanique, mais uniquement du côté de l'analytique: cette ſcience n'étant pas encore portée à ce degré de perfection, qui ſeroit néceſſaire pour développer les formules analytiques, qui renferment les principes du mouvement des fluides.

II. Il s'agit donc de découvrir les principes, par lesquels on puiſſe déterminer le mouvement d'un fluide, en quelque état qu'il ſe trouve, & par quelques forces qu'il ſoit ſollicité. Pour cet effet examinons en détail tous les articles, qui conſtituent le ſujet de nos recherches, & qui renferment les quantités tant connues qu'inconnues. Et d'abord la nature du fluide eſt ſuppoſée connue, dont il faut conſidérer les diverſes eſpeces : le fluide eſt donc, ou incompreſſible, ou compreſſible. S'il n'eſt pas ſusceptible de compreſſion, il faut diſtinguer deux cas, l'un où toute la maſſe eſt compoſée de parties homogenes, dont la denſité eſt partout & demeure toujours la même, l'autre

tre

Figure 26.2: First page of Euler's *General Principles concerning the Motion of Fluids* from 1757 [80].

We start considering potential flow around a circular cylinder of unit radius with axis along the x_3-axis in three-dimensional space with coordinates (x_1, x_2, x_3), assuming the flow velocity is $(1, 0, 0)$ at infinity, see Fig. 29.1 showing a section of through the cylinder with the flow horisontal from left to right. We can equally well think of the cylinder moving transversally through a fluid at rest. Potential flow around the cylinder is constant in the

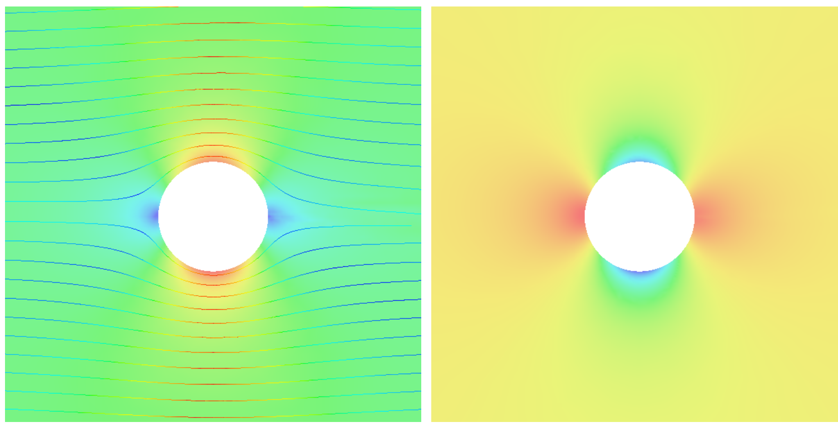

Figure 26.3: Potential flow past a circular cylinder: streamlines and fluid speed (left) and pressure (right) in a (x_1, x_2)-plane with horisontal x_1-axis in the flow direction.

x_3-direction and is symmetric in x_1 and x_2 with zero drag/lift with the flow velocity given as the gradient of the potential

$$\varphi(r, \theta) = (r + \frac{1}{r})\cos(\theta),$$

in polar coordinates (r, θ) in the (x_1, x_2)-plane. The corresponding pressure (vanishing at infinity) is determined by Bernouilli's law as:

$$p = -\frac{1}{2r^4} + \frac{1}{r^2}\cos(2\theta).$$

In its simplicity potential flow is truely remarkable: It is a solution of the Euler equations for inviscid flow with slip boundary condition, which separates at the back of cylinder at the line $(1, 0, x_3)$, with equally high pressure in the front and the back and low pressure on top and bottom (with the low pressure three times as big as the high pressure), resulting in zero drag/lift. This is d'Alembert's paradox: All experience indicates that a circular cylinder subject to air flow has substantial drag, but potential flow has zero drag.

We understand that the high pressure in the back, balancing the high pressure up front, can be seen as pushing the body through the fluid according to the principle of of motion of Aristotle and da Vinci. We shall discover that there is something which is correct in this view. But the net push from behind in real flow must be smaller than in potential flow, and so real flow must be different form potential flow in the rear, but how and why? We shall see that the correct answer to these questions hide the secret of flight.

26.4 Non-Separation of Potential Flow

Direct computation shows that on the cylinder boundary

$$\frac{\partial p}{\partial n} = \frac{U^2}{R}, \tag{26.5}$$

where n is the outward unit normal to the boundary, $\frac{\partial p}{\partial n}$ is the gradient of the pressure in the unit normal direction or *normal pressure gradient* into the fluid, U is the flow speed and $R = 1$ the radius of curvature of the boundary (positive for a concave fluid domain thus positive for the cylinder). The relation (26.5) is Newton's law expressing that fluid particles gliding along the boundary must be accellerated in the normal direction by the normal pressure gradient force in order to follow the curvature of the boundary. More generally, (26.5) is the criterion for *non-separation*: Fluid particles will stay close to the boundary as long as (26.5) is satisfied, while if

$$\frac{\partial p}{\partial n} < \frac{U^2}{R}, \tag{26.6}$$

then fluid particles will separate away from the boundary tangentially. In particular, as we will see below, laminar flow separates on the crest or top/bottom of the cylinder, since the normal pressure gradient is small in a laminar boundary layer with no-slip boundary condition [124, 134].

We sum up so far: The Euler equations express conservation of mass and momentum for an inviscid incompressible fluid. Potential flow is smooth and satisfies the Euler equations. D'Alembert's paradox compares inviscid potential flow having zero drag/lift with slightly viscous flow having substantial drag/lift. Potential flow has a positive normal pressure gradient preventing separation allowing the pressure to build up on the back to push the cylinder through the fluid without drag. We shall see that this is a bit too optimistic, but only a bit; there is some push also in real (slightly viscous) flow...

Chapter 27

Lift and Drag from Separation

> The fear of making permanent commitments can change the mutual love of husband and wife into two loves of self - two loves existing side by side, until they end in separation. (Pope John Paul II)

We now turn to a detailed mathematical analysis of flow separation, which we will find uncovers the secret of generation of both lift and drag of a body moving through air such as a wing. We know that the flow around the body *attaches* somewhere in the front, typically around a *point of stagnation*, where the flow velocity is zero, and *separates* somewhere somehow in the rear. In many cases attachment is governed by smooth (laminar) potential flow, while separation effectively is a generator of turbulence. We shall thus find that drag can be seen as a "cost of separation", which for a wing also pays for generating lift.

We will present a scenario for separation in slightly viscous turbulent flow, which is fundamentally different from the scenario for viscous laminar flow by Prandtl based on adverse pressure gradients retarding the flow to stagnation at separation. We make a distinction betweeen separation from a laminar boundary layer with no-slip boundary condition and from a turbulent boundary layer with slip. We thus make a distinction between

- **laminar separation with no-slip in (very) viscous flow**

considered by Prandtl of relevance for viscous flow, and

- **turbulent separation with slip in slightly viscous flow**

of relevance in aerodynamics.

We noted above that separation occurs if $\frac{\partial p}{\partial n} < \frac{U^2}{R}$, where $\frac{\partial p}{\partial n}$ is the pressure gradient normal to the boundary into the fluid, U is a flow speed close to the boundary and R the curvature of the boundary, positive for a convex body. We note that in a laminar boundary layer $\frac{\partial p}{\partial n} > 0$ only in contracting flow, which causes separation as soon as the flow expands after the crest of the body. We observe that in a turbulent boundary layer with slip, $\frac{\partial p}{\partial n} > 0$ is possible also in expanding flow which can delay separation. We present a basic mechanism for tangential separation with slip based on instability at rear points of stagnation generating low-pressure rolls of streamwise vorticity reducing $\frac{\partial p}{\partial n}$.

We give evidence that Prandtl's boundary layer theory for laminar separation has fallen into this trap, with the unfortunate result is that much research and effort has gone into preventing *laminar separation* in flows which effectively are turbulent with *turbulent separation*. We present a scenario for turbulent separation without stagnation supported by analysis, computation and experiments, which is radically different from Prandtl's scenario for laminar separation at stagnation. The fundamental question concerns the fluid dynamics of *separation without stagnation*, since in slightly viscous flow the friction is too small to bring fluid particles to rest. We shall find an answer which connects to the familiar experience of the rotating flow through a bathtub drain, which in reality replaces the theoretically possible but unstable fully radial flow.

We will see that laminar separation with no-slip occurs at the crest of a wing without generating lift, while turbulent separation is delayed and thereby generates lift.

Chapter 28

Separation

28.1 From Unstable to Quasi-Stable Separation

We are concerned with the fundamental problem of fluid mechanics of the motion of a solid body, such as a subsonic airplane, car or boat, through a slightly viscous incompressible fluid such as air at subsonic speeds or water. We focus on incompressible flow at large Reynolds number (of size 10^6 or larger) around both bluff and streamlined bodies, which is always partly turbulent.

The basic problem is to determine the forces acting on the surface of the body from the motion through the fluid, with the *drag* being the total force in the direction of the flow and the *lift* the total force in a transversal direction to the flow.

As a body moves through a fluid initially at rest, like a car or airplane moving through still air, or equivalently as a fluid flows around a body at rest, approaching fluid particles are deviated by the body in contracting flow, switch to expanding flow at a crest and eventually leave the body. The flow is said to *attach* in the front and *separate* in the back as fluid particles approach and leave a proximity of the body surface.

In high Reynolds number slightly viscous flow the tangential forces on the surface, or *skin friction* forces are small and both drag and lift mainly result from pressure forces and the pressure distribution at turbulent separation is of particular concern.

Separation requires *stagnation* of the flow to zero velocity somewhere in

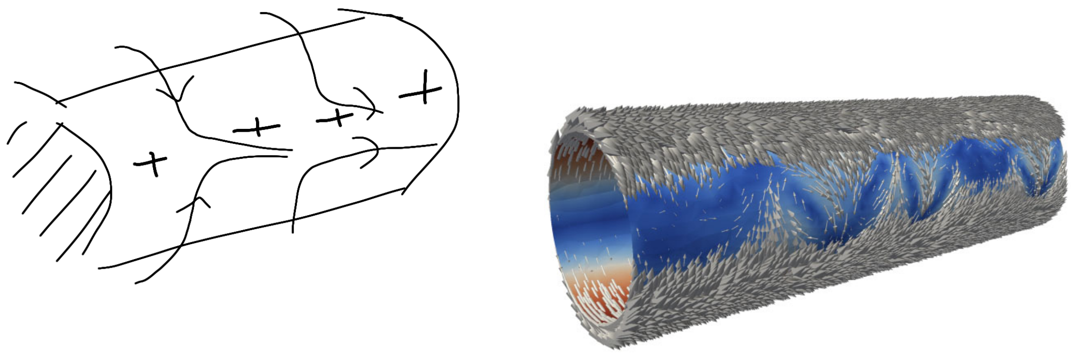

Figure 28.1: Unstable irrotational separation of potential flow around a circular cylinder (left) from line of stagnation surrounded by a high pressure zone indicated by +, with corresponding opposing flow instability (right).

the back of the body as opposing flows are meeting. Stagnation requires *retardation* of the flow, which requires a streamwise increasing pressure, or *adverse pressure gradient*. We show by a linearized stability analysis that retardation from opposing flows is exponentially unstable, which in particular shows *potential flow* to be unstable as indictaed in Fig. 28.1. Since unstable flow cannot persist over time, we expect to find a *quasi-stable* separation pattern resulting from the most unstable mode of potential flow, as a flow without streamwise retardation from opposing flows. By quasi-stable we mean a flow which is not exponentially unstable and thus may have a certain permanence over time.

Both experiment and computation show that there is such a quasi-stable separation pattern arising from transversal reorganization of opposing potential flow in the back into a set of counter-rotating vortex tubes of swirling flow (streamwise vorticity) attaching to the body, accompanied by a zig-zag pattern of alternating low and high pressure zones around points of stagnation with low pressure inside the vortex tubes. This pattern is illustrated in Fig. 2 for a cylinder along with computation and experiment, where we see how the flow finds a way to separate with unstable streamwise retardation in opposing flows replaced by quasi-stable transversal accelleration close to the surface before separation and in the swirling flow after separation. We see this phenomenon in the swirling flow in a bathtub drain, which is a stable configuration with transversal accelleration replacing the unstable opposing flow retardation of fully radial flow.

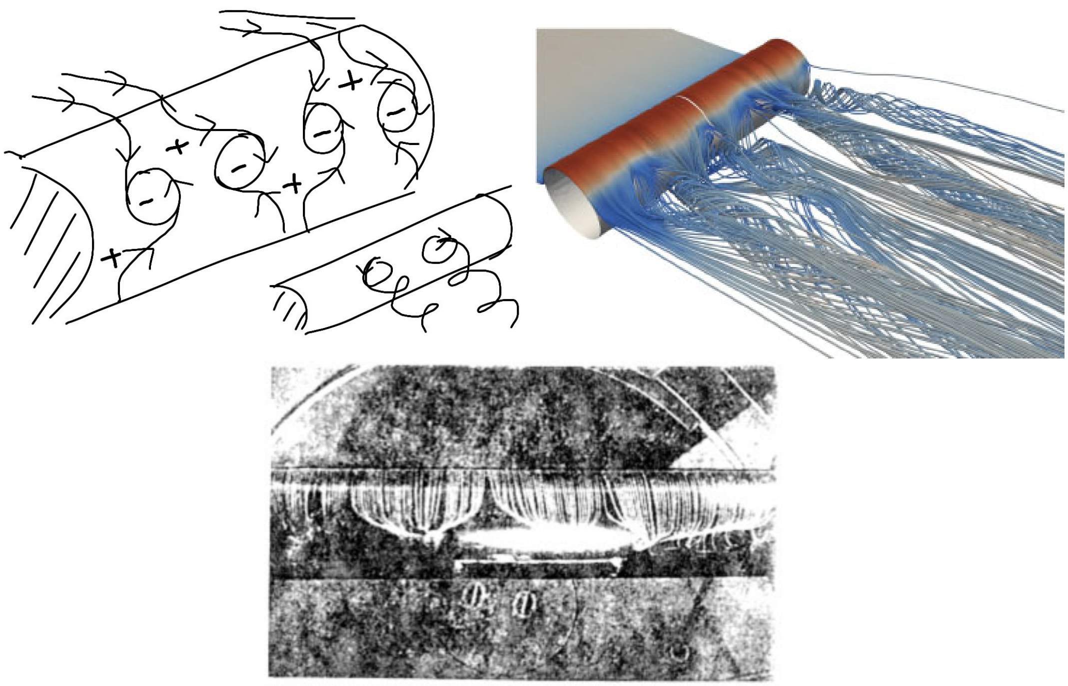

Figure 28.2: Quasi-stable 3d rotational separation from alternating high/low pressure: principle, computation and experiment

We refer to this quasi-stable pattern as *3d rotational separation.* This is a macroscopic phenomenon with the stagnation points spaced as widely as possibe. From macroscopic point of view the small skin friction of slightly viscous flow can be modeled with a *slip boundary condition* expressing vanishing skin friction. We show that computational solution of Navier-Stokes equations with slip is possible at affordable cost, because with slip there are no boundary layers to resolve, which makes it possible to compute both drag and lift of a of a car, boat or airplane arbitrary shape without the quadrillions of mesh points for boundary layer resolution commonly believed to be required [43].

The single high pressure zone stretching along the stagnation line of potential flow around a circular cylinder (creating instability) in Fig. 28.1, is thus broken down into a pattern of high and low pressure zones by the development of low pressure vortical flow in Fig. 2, which allows the fluid to separate without unstable streamwise retardation in opposing flow. The so modified pressure creates drag of a bluff body and lift of a wing from the zero drag and lift of potential flow.

28.2 Resolution of D'Alembert's Paradox

Potential flow can be viewed as an approximate solution of the Navier-Stokes equations at high Reynolds number with a slip boundary condition, but potential flow is unphysical because both drag and lift are zero, as expressed in d'Alembert's paradox [104]. Inspection of potential flow shows unstable *irrotational separation* of retarding opposing flow, which is impossible to observe as a physical flow. D'Alembert's paradox is thus resolved by observing that potential flow with zero drag and lift is unstable [104] and thus unphysical, and not by the official resolution suggested by Prandtl stating that the unphysical feature is the slip boundary condition.

Although 3d rotational separation has a macroscopic features the flow is *turbulent* at separation in the sense that the dissipation in the flow is substantial even though the viscosity is very small, following the definition of turbulent flow in [103].

28.3 Main Result

We present evidence in the form of mathematical stability analysis and computation that high Reynolds number incompressible flow around a body moving through a fluid can be described as

- quasi-stable potential flow before separation,
- quasi-stable 3d rotational separation.

This scenario is also supported by observation presented in e.g. [121, 122, ?] and our evidence thus consists of mathematical theory/computation and observation in strong accord.

We show that both drag and lift critically depend on the pressure distribution of 3d rotational separation. We remark that in the attaching flow in the front the flow is retarded by the body and not by opposing flows as in the back, which allows stable potential flow attachment. We show that drag and lift of a body of arbitrary shape can be accurately computed by solving the Navier-Stokes equations with slip.

The description and analysis of the crucial flow feature of separation presented here is fundamentally different from that of Prandtl, named the father of modern fluid mechanics, based on the idea that both drag and lift originate from a thin viscous boundary layer, where the flow speed relative to the body rapidly changes from the free stream speed to zero at the body surface corresponding to a no-slip boundary condition. Prandtl's scenario for separation, which has dominated 20th century fluid, can be described as *2d boundary layer no-slip separation*, to be compared with our entirely different scenario of *3d no-boundary layer slip separation*.

The unphysical aspect of Prandtl's scenario of separation is illuminated in [**?**]:

- *The passage from the familiar 2d to the mysterious 3d requires a complete reconsideration of concepts apparently obvious (separation and reattachment points, separated bubble, recirculation zone) but inappropriate and even dangerous to use in 3d flows.*

28.4 Navier-Stokes Equations with Slip by G2

We recall Navier-Stokes equations for incompressible flow with a slip boundary condition according to (**??**) with $\beta = 0$: Find the velocity $u = (u_1, u_2, u_3)$ and pressure p depending on $(x, t) \in \Omega \cup \Gamma \times I$, such that

$$
\begin{aligned}
\dot{u} + (u \cdot \nabla)u + \nabla p - \nabla \cdot \sigma &= f && \text{in } \Omega \times I, \\
\nabla \cdot u &= 0 && \text{in } \Omega \times I, \\
u_n &= g && \text{on } \Gamma \times I, \\
\sigma_s &= 0 && \text{on } \Gamma \times I, \\
u(\cdot, 0) &= u^0 && \text{in } \Omega,
\end{aligned}
\tag{28.1}
$$

and that solutions can be computed using G2.

We have found that that G2 with slip is capable of modeling slightly viscous turbulent flow with $Re > 10^6$ of relevance in many applications in aero/hydro dynamics, including flying, sailing, boating and car racing, with hundred thousands of mesh points in simple geometry and millions in complex geometry, while according to state-of-the-art quadrillions is required [43].

This is because a friction-force/slip boundary condition can model a turbulent boundary layer, and interior turbulence does not have to be resolved to physical scales to capture mean-value outputs [103].

28.5 Stability Analysis by Linearization

The stability of a Navier-Stokes solution is expressed by the linearized equations

$$\begin{aligned} \dot{v} + (u\cdot\nabla)v + (v\cdot\nabla)\bar{u} + \nabla q &= f - \bar{f} && \text{in } \Omega\times I, \\ \nabla\cdot v &= 0 && \text{in } \Omega\times I, \\ v\cdot n &= g - \bar{g} && \text{on } \Gamma\times I, \\ v(\cdot,0) &= u^0 - \bar{u}^0 && \text{in } \Omega, \end{aligned} \tag{28.2}$$

where (u,p) and $(\bar{u},\bar{p})$ are two Euler solutions with slightly different data, and $(v,q)\equiv(u-\bar{u},p-\bar{p})$. Formally, with u and $\bar{u}$ given, this is a linear convection-reaction problem for (v,q) with growth properties governed by the reaction term given by the 3×3 matrix $\nabla\bar{u}$. By the incompressiblity, the trace of $\nabla\bar{u}$ is zero, which shows that in general $\nabla\bar{u}$ has eigenvalues with real values of both signs, of the size of $|\nabla u|$ (with $|\cdot|$ some matrix norm), thus with at least one exponentially unstable eigenvalue, except in the neutrally stable case with purely imaginary eigenvalues, or in the non-normal case of degenerate eigenvalues representing parallel shear flow [103].

The linearized equations in velocity-pressure indicate that, as an effect of the reaction term $(v\cdot\nabla)\bar{u}$:

- streamwise retardation is exponentially unstable in velocity,
- transversal accelleration is neutrally stable,

where transversal signifies a direction orthogonal to the flow direction.

Additional stability information is obtained by applying the curl operator $\nabla\times$ to the momentum equation to give the vorticity equation

$$\dot{\omega} + (u\cdot\nabla)\omega - (\omega\cdot\nabla)u = \nabla\times f \quad \text{in } \Omega, \tag{28.3}$$

which is also a convection-reaction equation in the vorticity $\omega = \nabla\times u$ with coefficients depending on u, of the same form as the linearized equation (28.5), with a sign change of the reaction term. The vorticity is thus locally subject to exponential growth with exponent $|\nabla u|$:

- streamwise accelleration is exponentially unstable in streamwise vorticity.

We sum up as follows: The linearized equations (28.5) and (29.3) indicate exponential growth of perturbation of velocity in streamwise retardation and of streamwise vorticity in streamwise accelleration. We shall see in more detail below 3d rotational separation results from exponential instability of potential flow in retardation followed by vortex stretching in accelleration, with the retardation replaced by neutrally stable transversal accelleration.

Note that in classical analysis it is often argued that from the vorticity equation (29.3), it follows that vorticity cannot be generated starting from potential flow with zero vorticity and $f = 0$, which is *Kelvin's theorem*. But this is an incorrect conclusion, since perturbations of $\bar{f}$ of f with $\nabla \times \bar{f} \neq 0$ must be taken into account, even if $f = 0$. What you effectively see in computations is local exponential growth of vorticity on the body surface in rear retardation and by vortex stretching in accelleration, even if $f = 0$, which is a main route of instability to turbulence as well as separation.

28.6 Instability of 2d Irrotational Separation

We now analyze the stability of 2d irrotational separation considered by Planck in the following model of the potential flow around a circular cylinder studied in more detail below: $u(x) = (x_1, -x_2, 0)$ in the half-plane $\{x_1 > 0\}$ with stagnation along the line $(0, 0, x_3)$ and

$$\frac{\partial u_1}{\partial x_1} = 1 \quad \text{and} \quad \frac{\partial u_2}{\partial x_2} = -1, \tag{28.4}$$

expressing that the fluid is *squeezed* by *retardation* in the x_2-direction and *accelleration* in the x_1-direction. We first focus on the retardation with the main stability feature of (28.5) captured in the following simplified version of the v_2-equation of (28.5), assuming x_1 and x_2 are small,

$$\dot{v}_2 - v_2 = f_2,$$

where we assume $f_2 = f_2(x_3)$ to be an oscillating perturbation depending on x_3 of a certain wave length δ and amplitude h, for example $f_2(x_3) = h\sin(2\pi x_3/\delta)$, expecting the amplitude to decrease with the wave length. We find, assuming $v_2(0, x) = 0$, that

$$v_2(t, x_3) = (\exp(t) - 1)f_2(x_3).$$

We next turn to the accelleration and then focus on the ω_1-vorticity equation, for x_2 small and $x_1 \geq \bar{x}_1 > 0$ with $\bar{x}_1$ small, approximated by

$$\dot{\omega}_1 + x_1 \frac{\partial \omega_1}{\partial x_1} - \omega_1 = 0,$$

with the "inflow boundary condition"

$$\omega_1(\bar{x}_1, x_2, x_3) = \frac{\partial v_2}{\partial x_3} = (\exp(t) - 1)\frac{\partial f_2}{\partial x_3}.$$

The equation for ω_1 thus exhibits exponential growth, which is combined with exponential growth of the "inflow condition". We can see these features in principle and computational simulation in Fig. **??** showing how opposing flows at separation generate a pattern of alternating surface vortices from pushes of fluid up/down, which act as initial conditions for vorticity stretching into the fluid generating counter-rotating low-pressure tubes of streamwise vorticity.

The above model study can be extended to the full linearized equations linearized at $u(x) = (x_1, -x_2, 0)$:

$$\begin{array}{rcl} Dv_1 + v_1 & = & -\frac{\partial q}{\partial x_1}, \\ Dv_2 - v_2 & = & -\frac{\partial q}{\partial x_2} + f_2(x_3), \\ Dv_3 & = & -\frac{\partial q}{\partial x_3}, \\ \nabla \cdot v & = & 0 \end{array} \tag{28.5}$$

where $Dv = \dot{v} + u \cdot \nabla v$ is the convective derivative with velocity u and $f_2(x_3)$ as before. We here need to show that the force perturbation $f_2(x_3)$ will not get cancelled by the pressure term $-\frac{\partial q}{\partial x_2}$ in which case the exponential growth of v_2 would get cancelled. Now $f_2(x_3)$ will induce a variation of v_2 in the x_3 direction, but this variation does not upset the incompressibility since it involves the variation in x_2. Thus, there is no reason for the pressure q to compensate for the force perturbation f_2 and thus exponential growth of v_2 is secured.

We thus find streamwise vorticity generated by a force perturbation oscillating in the x_3 direction, which in the retardation of the flow in the x_2-direction creates exponentially increasing vorticity in the x_1-direction, which acts as inflow to the ω_1-vorticity equation with exponential growth by vortex stretching. Thus, we find exponential growth at rear separation in both the retardation in the x_2-direction and the accelleration in the x_1 direction, as a result of the squeezing expressed by (28.4).

Since the combined exponential growth is independent of δ, it follows that large-scale perturbations with large amplitude have largest growth, which is also seen in computations with δ the distance between streamwise rolls as seen in Fig. 29.3 which does not seem to decrease with decreasing h. The perturbed flow with swirling separation is large scale phenomenon, which we show below is more stable than potential flow.

The corresponding pressure perturbation changes the high pressure at separation of potential flow into a zig-zag alternating more stable pattern of high and low pressure with high pressure zones deviating opposing flow into non-opposing streaks which are captured by low pressure to form rolls of streamwise vorticity allowing the flow to spiral away from the body. This is similar to the vortex formed in a bathtub rain.

Notice that in attachment in the front the retardation does not come from opposing flows but from the solid body, and the zone of exponential growth of ω_2 is short, resulting in much smaller perturbation growth than at rear separation.

We shall see that the tubes of low-pressure streamwise vorticity change the normal pressure gradient to allow separation without unstable retardation, but the price is generation of drag by negative pressure inside the vortex tubes as a "cost of separation".

28.7 Quasi-Stable Rotational 3d Separation

We discover in computation and experiment that the rotational 3d separtion pattern just detected as the most unstable mode of 2d, represents a quasi-stable flow with unstable retardation in opposing flows replaced by transversal acceleration.

As a model of flow with transversal accelleration we consider the potential velocity $u = (0, x_3, -x_2)$ of a constant rotation in the x_1-direction, with corresponding linearized equations linearized problem

$$\dot{v}_1 = 0, \quad \dot{v}_2 + v_3 = 0, \quad \dot{v}_3 - v_2 = 0, \tag{28.6}$$

which model a neutrally stable harmonic oscillator without exponential growth corresponding to imaginary eigenvalues of ∇u.

Further, shear flow may represented by $(x_2, 0, 0)$, which is marginal unstable with linear perturbation growth from degenerate zero eigenvalues of ∇u, as analyzed in detail in [103].

28.8 Quasi-Stable Potential Flow Attachment

The above analysis also shows that potential flow attachment, even though it involves streamwise retardation, is quasi-stable. This is because the initial perturbation f_2 in the above analysis is forced to be zero by the slip boundary condition requiring the normal velocity to vanish. In short, potential flow attachment is stable because the flow is retarded by the solid body and not by opposing flows as in separation.

This argument further shows that a flow retarded by a high pressure zone is quasi-stable in approach because it is similar to attachment.

Chapter 29

Basic Cases

29.1 Circular Cylinder

We consider the flow around a around a long circular cylinder of unit radius with axis along the x_3-axis in $\mathbb{R}^3$ with coordinates $x = (x_1, x_2, x_3)$, assuming the flow velocity is $(1, 0, 0)$ at infinity.

29.1.1 Unstable Unphysical Potential Flow

Potential flow as inviscid, irrotational, incompressible stationary flow, is given in polar coordinates (r, θ) in a plane orthogonal to the cylinder axis by the potential function, see Fig. 29.1,

$$\varphi(r, \theta) = (r + \frac{1}{r}) \cos(\theta)$$

with corresponding velocity components

$$u_r \equiv \frac{\partial \varphi}{\partial r} = (1 - \frac{1}{r^2}) \cos(\theta), \quad u_s \equiv \frac{1}{r} \frac{\partial \varphi}{\partial \theta} = -(1 + \frac{1}{r^2}) \sin(\theta)$$

with streamlines being level lines of the conjugate potential function

$$\psi \equiv (r - \frac{1}{r}) \sin(\theta).$$

Potential flow is constant in the direction of the cylinder axis with velocity $(u_r, u_s) = (1, 0)$ for r large, is fully symmetric with zero drag/lift, attaches and separates at the lines of stagnation $(r, \theta) = (1, \pi)$ in the front and $(r, \theta) =$

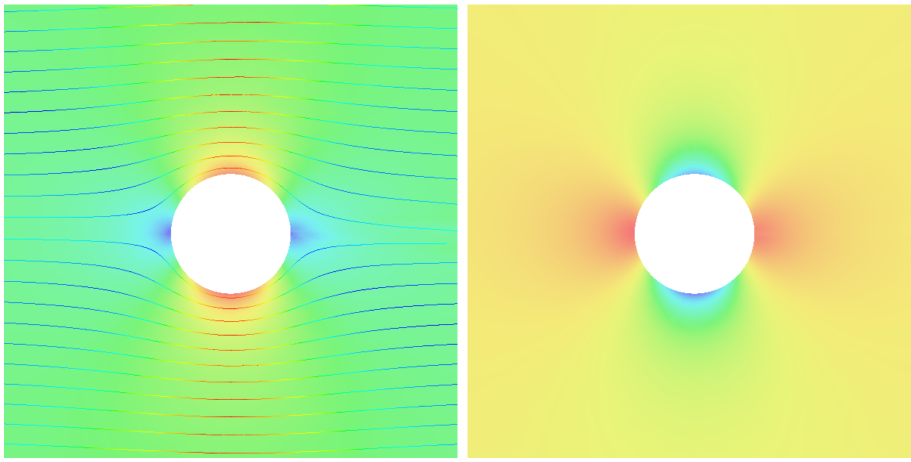

Figure 29.1: Potential flow past a circular cylinder: fully symmetric velocity (left) and pressure (right).

$(1, 0)$ in the back. Potential flow shows exponentially unstable 2d irrotational separation but quasi-stable 2d attachment. Potential flow thus represents physical flow before separation but not in separation and after separation.

By Bernouilli's principle the pressure is given by

$$p = -\frac{1}{2r^4} + \frac{1}{r^2}\cos(2\theta)$$

when normalized to vanish at infinity. We compute

$$\frac{\partial p}{\partial \theta} = -\frac{2}{r^2}\sin(2\theta)), \quad \frac{\partial p}{\partial r} = \frac{2}{r^3}(\frac{1}{r^2} - \cos(2\theta)),$$

and discover an adverse pressure gradient in the back. Further, the normal pressure gradient on the boundary

$$\frac{\partial p}{\partial r} = 4\sin^2(\theta) \geq 0$$

is precisely the force required to accelerate fluid particles with speed $2|\sin(\theta)|$ to follow the circular boundary without separation, by satisfying the condition of non-separation on a curve with curvature R

$$\frac{\partial p}{\partial n} = \frac{U^2}{R}. \tag{29.1}$$

We note, coupling to the above discussion relating to (??), that $\frac{\partial u_s}{\partial r} = \frac{2}{r^3}\sin(\theta) = 2$ at the crest. We further compute

$$\frac{\partial \psi}{\partial r} = \frac{1}{r^2}\sin(\theta)$$

which shows that fluid particles decrease their distance to the boundary in front of the cylinder and increase their distance in the rear, but the flow only separates at rear stagnation.

29.1.2 Quasi-Stable Physical Turbulent Flow

Solving Navier-Stokes equations with very small viscsoity and slip boundary condition by G2 we find the a a flow initialized as potential flow develops into a turbulent solution with rotational separation as identified above, in shown in Fig. 29.2 and 29.3.

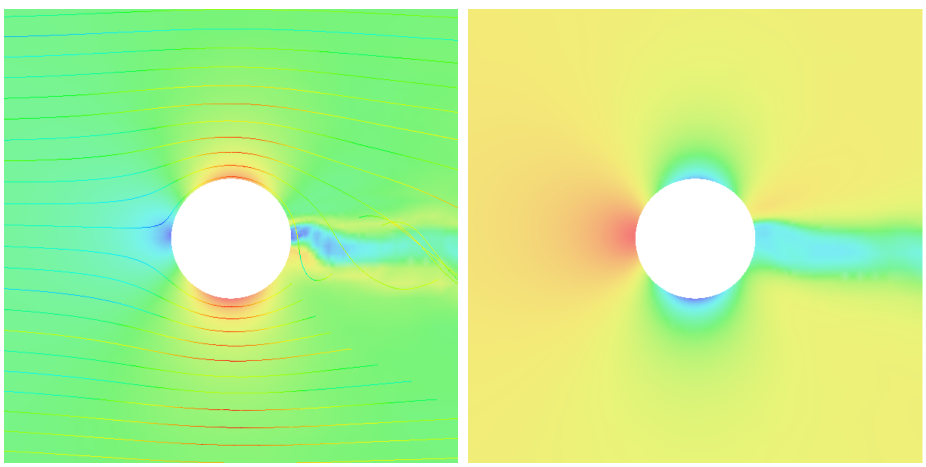

Figure 29.2: Turbulent flow past a cylinder; velocity (left) and pressure (right). Notice the low pressure wake of strong streamwise vorticity generating drag.

29.2 NACA0012 Trailing Edge Separation

The separation at the trailing edge of a wing is similar to that of a circular cylinder, as shown in Fig. 29.2 for a NACA012 wing at 5 degrees angle of attack.

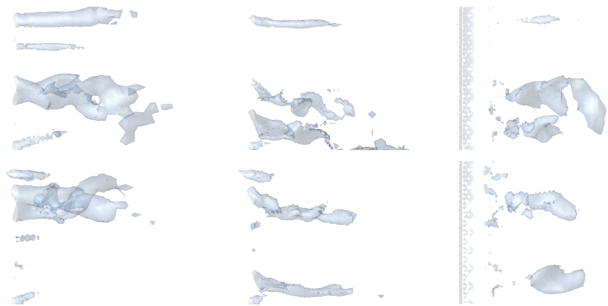

Figure 29.3: Levels surfaces of strong vorticity in EG2 solution: streamwise $|\omega_1|$ (left) and transversal $|\omega_2|$ (middle) and $|\omega_3|$ (right), at two times $t_1 < t_2$ (upper, lower), in the x_1x_3-plane.

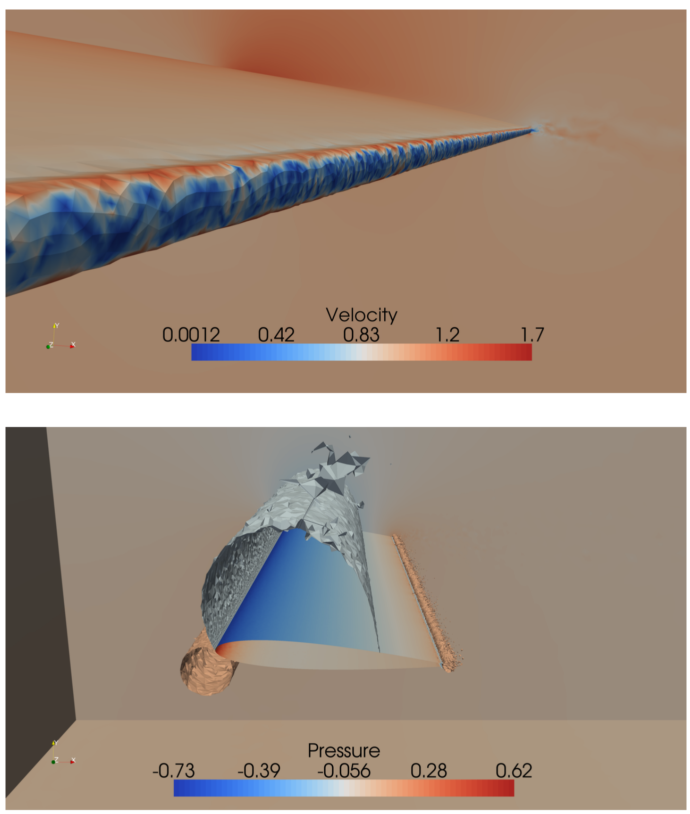

Figure 29.4: Velocity, pressure and vorticity at trailing edge separation for NACA0012 wing. Notice the zig-zag pattern of the velocity.

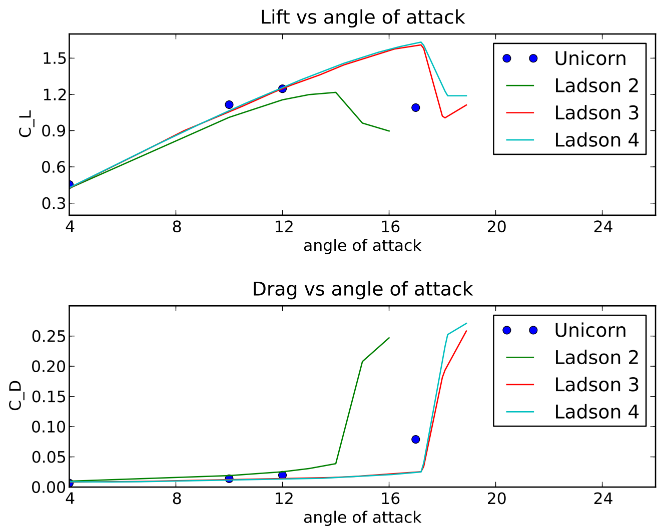

Figure 29.5: Evidence that drag and lift of a wing can be computed by solving the Navier-Stokes equations with slip without resolving any boundary layers.

29.3 Accuracte Drag and Lift without Boundary Layer

We compare in Fig. 29.6 drag and lift of a long NACA0012 wing for different angles of attack including stall computed by solving the of Navier-Stokes equations with slip using Unicorn **??**, with different experiments and notice good agreement. We conclude that drag and lift are computable without resolving and boundary layers.

29.4 Sphere

Potential flow around a sphere is exponentially unstable at its point of stagnation at separation and develops a quasi-stable separation pattern of four counterrotating rolls of streamwise vorticity as shown in Fig. 29.4.

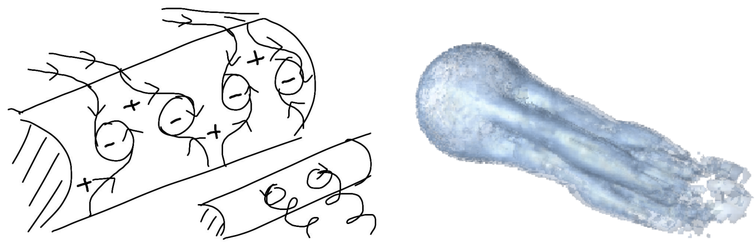

Figure 29.6: Pattern of exponential instability of potential flow around a sphere at point of stagnation forming four counterrotating rolls of streamwise vorticity, shown in computation.

29.5 Hill

In Fig. 29.7 we show turbulent Euler flow over a hill with separation after the crest by again the mechanism of tangential separation through generation of surface vorticity.

29.6 Flat Plate

The experience reported above suggests the following scenario for separation into a turbulent boundary layer over a flat plate as a representation of a smooth boundary: (i) Rolls of streamwise vorticity are formed by non-modal linear perturbation growth referred to as the *Taylor Görtler mechanism* in [103]. (ii) The rolls create opposing transversal flows (as in the back of cylinder), which generate surface vorticity which is stretched into the fluid while being bent into to streamwise direction, as evidenced in e.g. [29, 30].

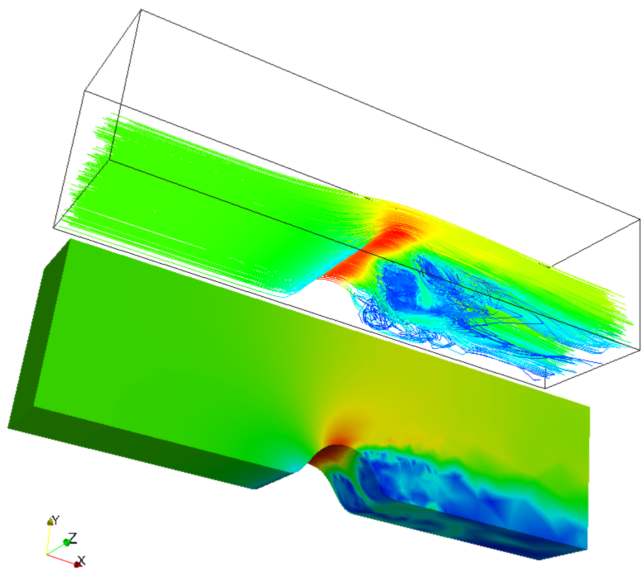

Figure 29.7: Separation after crest of hill by surface vorticity from opposing flow.

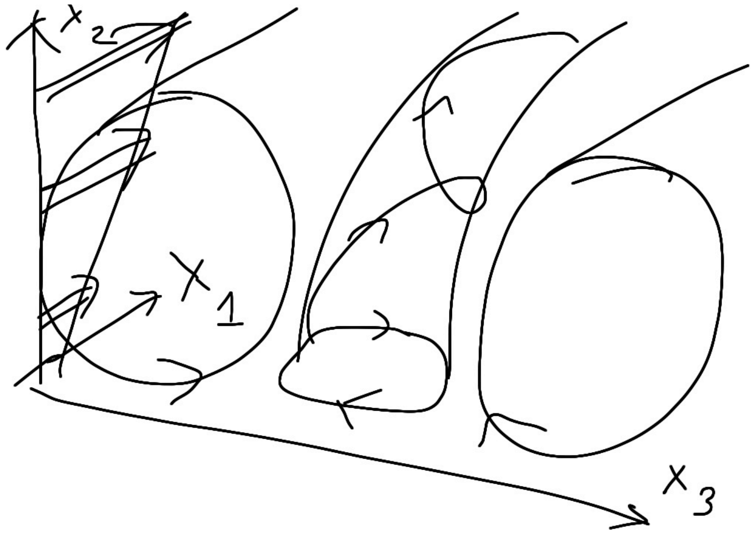

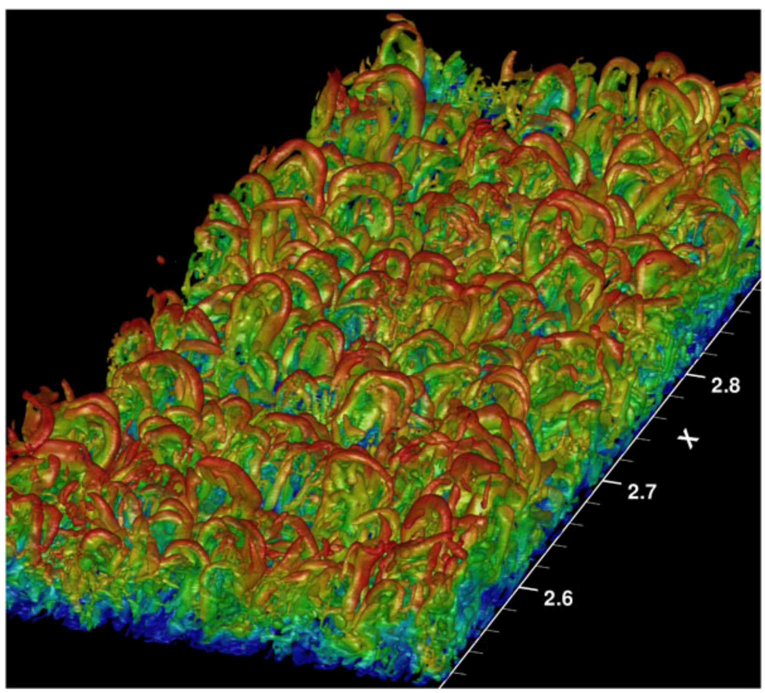

Figure 29.8: Shear flow over flat plate generates x_1 vorticity which generates secondary transversal opposing flow which generates rolls of x_2-vorticity attaching to the plate and bending into the flow, like a forest of sea tulips attaching to the sea bottom.

Chapter 30

Energy Estimate

The standard *energy estimate* for (23.1) is obtained by multiplying the momentum equation

$$\dot{u} + (u \cdot \nabla)u + \nabla p - \nabla \cdot \sigma - f = 0,$$

with u and integrating in space and time, to get in the case $f = 0$ and $g = 0$,

$$\int_0^t \int_\Omega R_\nu(u,p) \cdot u \, dxdt = D_\nu(u;t) + B_\beta(u;t) \tag{30.1}$$

where

$$R_\nu(u,p) = \dot{u} + (u \cdot \nabla)u + \nabla p$$

is the *Euler residual* for a given solution (u,p) with $\nu > 0$,

$$D_\nu(u;t) = \int_0^t \int_\Omega \nu |\epsilon(u(\bar{t},x))|^2 dxd\bar{t}$$

is the *internal turbulent viscous dissipation*, and

$$B_\beta(u;t) = \int_0^t \int_\Gamma \beta |u_s(\bar{t},x)|^2 dxd\bar{t}$$

is the *boundary turbulent viscous dissipation*, from which follows by standard manipulations of the left hand side of (30.1),

$$K_\nu(u;t) + D_\nu(u;t) + B_\beta(u;t) = K(u^0), \quad t > 0, \tag{30.2}$$

where

$$K_\nu(u;t) = \frac{1}{2}\int_\Omega |u(t,x)|^2 dx.$$

This estimate shows a balance of the *kinetic energy* $K(u;t)$ and the *turbulent viscous dissipation* $D_\nu(u;t) + B_\beta(u;t)$, with any loss in kinetic energy appearing as viscous dissipation, and vice versa. In particular,

$$D_\nu(u;t) + B_\beta(u;t) \leq K(u^0),$$

and thus the viscous dissipation is bounded (if $f = 0$ and $g = 0$).

Turbulent solutions of (23.1) are characterized by *substantial internal turbulent dissipation*, that is (for t bounded away from zero),

$$D(t) \equiv \lim_{\nu\to 0} D(u_\nu;t) >> 0, \tag{30.3}$$

which is *Kolmogorov's conjecture* [97]. On the other hand, the *skin friction dissipation* decreases with decreasing friction

$$\lim_{\nu\to 0} B_\beta(u;t) = 0, \tag{30.4}$$

since $\beta \sim \nu^{0.2}$ tends to zero with the viscosity ν and the tangential velocity u_s approaches the (bounded) free-stream velocity. We thus find evidence that the interior turbulent dissipation dominates the skin friction dissipation, which supports the use of slip as a model of a turbulent boundray layer, but which is not in accordance with Prandtl's (unproven) conjecture that substantial drag and turbulent dissipation originates from the boundary layer.

Kolmogorov's conjecture (30.3) is consistent with

$$\|\nabla u\|_0 \sim \frac{1}{\sqrt{\nu}}, \quad \|R_\nu(u,p)\|_0 \sim \frac{1}{\sqrt{\nu}}, \tag{30.5}$$

where $\|\cdot\|_0$ denotes the $L_2(Q)$-norm with $Q = \Omega \times I$. On the other hand, it follows by standard arguments from (30.2) that

$$\|R_\nu(u,p)\|_{-1} \leq \sqrt{\nu}, \tag{30.6}$$

where $\|\cdot\|_{-1}$ is the norm in $L_2(I;H^{-1}(\Omega))$. Kolmogorov thus conjectures that the Euler residual $R_\nu(u,p)$ for small ν is strongly (in L_2) large, while being small weakly (in H^{-1}).

Altogether, we understand that the resolution of d'Alembert's paradox of explaining substantial drag from vanishing viscosity, consists of realizing that the internal turbulent dissipation D can be positive under vanishing viscosity, while the skin friction dissipation B will vanish. In contradiction to Prandtl, we conclude that drag does not result from boundary layer effects, but from internal turbulent dissipation, originating from instability at separation.

Chapter 31

G2 Computational Solution

We show in [103, 102, 104] that the Navier-Stokes equations (23.1) can be solved by G2 producing turbulent solutions characterized by substantial turbulent dissipation from the least squares stabilization acting as an automatic turbulence model, reflecting that the Euler residual cannot be made pointwise small in turbulent regions. G2 has a posteriori error control based on duality and shows output uniqueness in mean-values such as lift and drag [103, 99, 100]

We find that G2 with slip is capable of modeling slightly viscous turbulent flow with $Re > 10^6$ of relevance in many applications in aero/hydro dynamics, including flying, sailing, boating and car racing, with hundred thousands of mesh points in simple geometry and millions in complex geometry, while according to state-of-the-art quadrillions is required [59]. This is because a friction-force/slip boundary condition can model a turbulent boundary layer, and interior turbulence does not have to be resolved to physical scales to capture mean-value outputs [103].

The idea of circumventing boundary layer resolution by relaxing no-slip boundary conditions introduced in [99, 103], was used in [115, 26] in the form of weak satisfaction of no-slip, which however misses the main point of using a force condition instead of a velocity condition in a model of a turbulent boundary layer.

A G2 solution (U, P) on a mesh with local mesh size $h(x,t)$ according to [103], satisfies the following energy estimate (with $f = 0$, $g = 0$ and $\beta = 0$):

$$K(U(t)) + D_h(U;t) = K(u^0), \tag{31.1}$$

where

$$D_h(U;t) = \int_0^t \int_\Omega h|R_h(U,P)|^2 \, dxdt, \qquad (31.2)$$

is an analog of $D_\nu(u;t)$ with $h \sim \nu$, where $R_h(U,P)$ is the Euler residual of (U,P). We see that the G2 turbulent viscosity $D_h(U;t)$ arises from penalization of a non-zero Euler residual $R_h(U,P)$ with the penalty directly connecting to the violation (according the theory of criminology). A turbulent solution is characterized by substantial dissipation $D_h(U;t)$ with $\|R_h(U,P)\|_0 \sim h^{-1/2}$, and

$$\|R_h(U,P)\|_{-1} \leq \sqrt{h} \qquad (31.3)$$

in accordance with (30.5) and (30.6).

31.1 Wellposedness of Mean-Value Outputs

Let $M(v) = \int_Q v\psi \, dxdt$ be a *mean-value output* of a velocity v defined by a smooth weight-function $\psi(x,t)$, and let (u,p) and (U,P) be two G2-solutions on two meshes with maximal mesh size h. Let (φ,θ) be the solution to the *dual linearized problem*

$$\begin{array}{rcll} -\dot{\varphi} - (u\cdot\nabla)\varphi + \nabla U^\top \varphi + \nabla\theta & = & \psi & \text{in } \Omega\times I, \\ \nabla\cdot\varphi & = & 0 & \text{in } \Omega\times I, \\ \varphi\cdot n & = & g & \text{on } \Gamma\times I, \\ \varphi(\cdot,T) & = & 0 & \text{in } \Omega, \end{array} \qquad (31.4)$$

where $\top$ denotes transpose. Multiplying the first equation by $u-U$ and integrating by parts, we obtain the following output error representation [103]:

$$M(u) - M(U) = \int_Q (R_h(u,p) - R_h(U,P))\cdot\varphi \, dxdt \qquad (31.5)$$

where for simplicity the dissipative terms are here omitted, from which follows the a posteriori error estimate:

$$|M(u) - M(U)| \leq S(\|R_h(u,p)\|_{-1} + \|R_h(U,P)\|_{-1}), \qquad (31.6)$$

where the stability factor

$$S = S(u,U,M) = S(u,U) = \|\varphi\|_{H^1(Q)}. \qquad (31.7)$$

In [103] we present a variety of evidence, obtained by computational solution of the dual problem, that for global mean-value outputs such as drag and lift, $S << 1/\sqrt{h}$, while $\|R_h\|_{-1} \sim \sqrt{h}$, allowing computation of of drag/lift with a posteriori error control of the output within a tolerance of a few percent. In short, mean-value outputs such as lift and drag are wellposed and thus physically meaningful.

We explain in [103] the crucial fact that $S << 1/\sqrt{h}$, heuristically as an effect of *cancellation* of rapidly oscillating reaction coefficients of turbulent solutions combined with smooth data in the dual problem for mean-value outputs. In smooth potential flow there is no cancellation, which explains why zero lift/drag cannot be observed in physical flows.

Bibliography

[1] J. D. Anderson, *A History of Aerodynamics*, Cambridge Aerospace Series 8, Cambridge University Press, 1997.

[2] John D. Anderson, Ludwig Prandtl's Boundary Layer, http://www.aps.org/units/dfd/resources/upload/prandtlvol58no12p4248.pdf

[3] H. Ashley, *Engineering Analysis of Flight Vehicles*, Addison-Wesley Aerospace Series, Addison-Wesley, Reading, Mass., 1974, Sect 4.3.4.

[4] F. Capra, The Science of Leonardo, Anchor Books, 2007.

[5] Clay Mathematics Institute, http://www.claymath.org.

[6] K. Chang, Staying Aloft; What Does Keep Them Up There?, New York Times, Dec 9, 2003.

[7] G. M. Craig, Stop Abusing Bernoulli! - How Airplanes Really Fly, Regenerative Press, 1998.

[8] G. E. Goslow Jr, K. P. Dial, F. A. Jenkins Jr, Bird Flight: Insights and Complications BioScience, Vol. 40, No. 2. (Feb., 1990), pp. 108-115.

[9] O. Chanute, *Progress in Flying Machines*, Long Beach, CA: Lorenz and Herweg, 1976 (originally published 1894).

[10] Leonardo da Vinci, Codex of Bird Flight, 1505.

[11] 3rd CFD AIAA Drag Prediction Workshop, aaac.larc.nasa.gov/ tfcab/cfdlarc/aiaa-dpw.

[12] The FEniCS Project, www.fenics.org.

[13] G.S. Jones, J.C. Lin, B.G. Allan, W.E. Milholen, C.L. Rumsey,R.C. Swanson, Overview of CFD Validation Experiments for Circulation Control Applications at NASA, $http://ntrs.nasa.gov/archive/nasa/casi.ntrs.nasa.gov/20080031119_22008030041.pdf$.

[14] D'Alembert's paradox, en.wikipedia.org/wiki/D'Alembert's_paradox.

[15] A. Hedenstrom and G. R. Spedding, Beyond robins: aerodynamic analyses of animal flight, J. Roy. Soc. Interface 5, 595-601, 2008.

[16] P. Henningsson, G. R. Spedding and A. Hedenstrom, Vortex wake and flight kinematics of a swift in cruising flight in a wind tunnel. J. Exp. Biol. 211, 717-730, 2008. (Featured on the cover, and as Inside JEB article 10.1242/jeb.017475)

[17] *How Ornithopters Fly*,http://www.ornithopter.de

[18] Experiments in Aerodynamics, Smithsonian Contributions to Knowledge no. 801, Washinton, DC, Smithsonian Institution.

[19] http://www.grc.nasa.gov/WWW/K-12/airplane/lift1.html

[20] http://www.planeandpilotmag.com/aircraft/specifications/diamond/2007-diamond-star-da40-xl/289.html

[21] A. Fage and L.F. Simmons, An investigation of the air-flow pattern in the wake of an airfoil of finite span, Rep.Memor.aero.REs.Coun.,Lond.951, 1925.

[22] http://www.aviation-history.com/theory/lift.htm

[23] http://web.mit.edu/16.00/www/aec/flight.html

[24] http://www.wright-house.com/wright-brothers/Aeronautical.html

[25] O. Lilienthal, Birdflight as the Basis of Aviation, 1889.

[26] Y. Bazilevs, C. Michler, V.M. Calo and T.J.R. Hughes, Turbulence without Tears: Residual-Based VMS, Weak Boundary Conditions, and Isogeometric Analysis of Wall-Bounded Flows, Preprint 2008.

[27] S. Cowley, Laminar boundary layer theory: A 20th century paradox, Proceedings of ICTAM 2000, eds. H. Aref and J.W. Phillips, 389-411, Kluwer (2001).

[28] A. Crook, Skin friction estimation at high Reynolds numbers and Reynolds-number effects for transport aircraft, Center for Turbulence Research, 2002.

[29] A. Ferrante, S. Elghobashi, P. Adams, M. Valenciano, D. Longmire, Evolution of Quasi-Streamwise Vortex Tubes and Wall Streaks in a Bubble-Laden Turbulent Boundary Layer over a Flat Plate, Physics of Fluids 16 (no.9), 2004.

[30] A. Ferrante and S. E. Elghobashi, A robust method for generating inflow conditions for direct numerical simulations of spatially-developing turbulent boundary layers, J. Comp. Phys., 198, 372-387, 2004.

[31] J.Hoffman, Simulation of turbulent flow past bluff bodies on coarse meshes using General Galerkin methods: drag crisis and turbulent Euler solutions, Comp. Mech. 38 pp.390-402, 2006.

[32] J. Hoffman, Simulating Drag Crisis for a Sphere using Friction Boundary Conditions, Proc. ECCOMAS, 2006.

[33] J. Hoffman, Lift and drag of a delta wing by G2.

[34] J. Hoffman and M. Nazarov, Drag of a car by G2.

[35] J. Hoffman, Computational simulation of the Magnus effect.

[36] J. Hoffman, Computational simulation of the reverse Magnus effect.

[37] J. Hoffman and C. Johnson, Blowup of Euler solutions, BIT Numerical Mathematics, Vol 48, No 2, 285-307.

[38] J. Hoffman and C. Johnson, Why its is possible to fly, submitted to Science, Dec 2008.

[39] J. Hoffman and C. Johnson, *Computational Turbulent Incompressible Flow*, Springer, 2007, www.bodysoulmath.org/books.

[40] J. Hoffman and C. Johnson, Resolution of d'Alembert's paradox, Journal of Mathematical Fluid Mechanics, Online First, Dec 10, 2008.

[41] J. Hoffman and C. Johnson, Separation in slightly viscous flow, submitted to Physics of Fluids.

[42] J. Hoffman and C. Johnson: D'Alembert's paradox, new resolution, http://knol.google.com/k/claes-johnson/dalemberts-paradox/yvfu3xg7d7wt/2.

[43] J. Kim and P. Moin, Tackling Turbulence with Supercomputer, Scientific American.

[44] F. W. Lancaster, *Aerodynamics*, 1907.

[45] Live Science, $http : //www.livescience.com/technology/060828_{h}ow_{p}lanes_{f}ly.html$.

[46] D. You and P. Moin, Large eddy simulation of separation over an airfoil with synthetic jet control, Center for Turbulence Research, 2006.

[47] How Airplanes Fly: A Physical Description of Lift, http://www.allstar.fiu.edu/
aero/airflylvl3.htm.

[48] S. Cowley, Laminar boundary layer theory: A 20th century paradox?, Proceedings of ICTAM 2000, eds. H. Aref and J.W. Phillips, 389-411, Kluwer (2001).

[49] W. Beaty, Airfoil Lifting Force Misconception Widespread in K-6 Textbooks, Science Hobbyist, http://www.eskimo.com/ billb/wing/airfoil.htm#L1.

[50] Unicorn, FEniCS, www.fenics.org.

[51] AVweb, World's Premier Independent Aviation News Resource, http://www.avweb.com/news/airman/183261-1.html.

[52] HowStuffWorks, http://science.howstuffworks.com/airplane7.htm.

[53] D'Alembert's paradox, en.wikipedia.org/wiki/D'Alembert's_paradox.

[54] S. Goldstein, Fluid mechanics in the first half of this century, in Annual Review of Fluid Mechanics, Vol 1, ed. W. R. Sears and M. Van Dyke, pp 1-28, Palo Alto, CA: Annuak Reviews Inc.

[55] N. Gregory and C.L. O'Reilly, Low-Speed Aerodynamic Characteristics of NACA 0012 Aerofoil Section, including the Effects of Upper-Surface Roughness Simulating Hoar Frost, Aeronautical Research Council Reports and Memoranda, http://aerade.cranfield.ac.uk/ara/arc/rm/3726.pdf.

[56] Experiments in Aerodynamics, Smithsonian Contributions to Knowledge no. 801, Washinton, DC, Smithsonian Institution.

[57] R. Kunzig, An old, lofty theory of how airplanes fly loses some altitude, Discover, Vol. 22 No. 04, April 2001.

[58] W. J. McCroskey, A Critical Assessment of Wind Tunnel Results for the NACA 0012 Airfoil, NASA Technical Memorandum 10001, Technical Report 87-A-5, Aeroflightdynamics Directorate, U.S. Army Aviation Research and Technology Activity, Ames Research Center, Moffett Field, California.

[59] P. Moin and J. Kim, Tackling Turbulence with Supercomputers, Scientific American Magazine, 1997.

[60] R. von Mises, Theory of Flight, McGraw-Hill, 1945.

[61] http://www.grc.nasa.gov/WWW/K-12/airplane/lift1.html

[62] G. Magnus, Über die abweichung der geschesse, Pogendorfs Ann. Der Phys. Chem., 88, 1-14, 1853.

[63] M. J. Lighthill (1956), Physics of gas flow at very high speeds, Nature 178: 343, 1956, doi:10.1038/178343a0. Report on a conference.

[64] C. Rumsey and R. Wahls, Focussed assessment of state-of-the-art CFD capabilities for predictin of subsonic fixed wing aircraft aerodynamics, NASA Langley Research Center, NASA-TM-2008-215318.

[65] B. Robins, New Principles of Gunnery Containing The Determination of The Force of Gunpowder and Investigation of The Difference in The Resisting Power of The Air to Swift and Slow Motion, 1742.

[66] http://www.planeandpilotmag.com/aircraft/specifications/diamond/2007-diamond-star-da40-xl/289.html

[67] L. Prandtl, On Motion of Fluids with Very Little, in Verhandlungen des dritten internationalen Mathematiker-Kongresses in Heidelberg 1904, A. Krazer, ed., Teubner, Leipzig, Germany (1905), p. 484. English trans. in Early Developments of Modern Aerodynamics, J. A. K. Ack- royd, B.P. Axcell, A.I. Ruban, eds., Butterworth-Heinemann, Oxford, UK (2001), p. 77.

[68] L. Prandtl and O Tietjens, *Applied Hydro- and Aeromechanics*, 1934.

[69] Prandtl: Father of Modern Fluid Mechanics, http://www.eng.vt.edu/fluids/msc/prandtl.htm.

[70] H. Schlichting, Boundary Layer Theory, McGraw-Hill, 1979.

[71] B. Thwaites (ed), *Incompressible Aerodynamics*, An Account of the Theory and Observation of the Steady Flow of Incompressible Fluid pas Aerofoils, Wings and other Bodies, Fluid Motions Memoirs, Clarendon Press, Oxford 1960, Dover 1987.

[72] F. W. Lanchester, *Aerodynamics*, 1907.

[73] Garret Birkhoff, *Hydrodynamics: a study in logic, fact and similitude*, Princeton University Press, 1950.

[74] O. Darrigol, World of Flow, A History of hydrodynamics from the Bernouillis to Prandtl, Oxford University Press.

[75] Jean le Rond d'Alembert, Theoria resistentiae quam patitur corpus in fluido motum, ex principiis omnino novis et simplissimus deducta, habita ratione tum velocitatis, figurae, et massae corporis moti, tum densitatis compressionis partium fluidi; Berlin-Brandenburgische Akademie der Wissenschaften, Akademie-Archiv call number: I-M478, 1749.

[76] Jean le Rond d'Alembert, Essai d'une nouvelle théorie de la résistance des fluides, Paris, 1752.

[77] Jean le Rond d'Alembert, Paradoxe proposé aux géomètres sur la résistance des fluides, in Opuscules mathématiques, Vol 5, Memoir XXXIV, I, 132-138, 1768.

[78] Jean le Rond d'Alembert, Sur la Résistance des fluides, in Opuscules mathématiques, Vol 8, Memoir LVII, 13, 210-230, 1780.

[79] Leonard Euler, Neue Grundsäteze der Artillerie, Berlin, 1745.

[80] Leonard Euler, Principes généraux du mouvement des fluides, Académie Royale des Sciences et des Belles-Lettres de Berlin, Mémoires 11, 274-315, 1757.

[81] Leonard Euler, Delucidationes de resistentia fluidorum, Novi Commenatrii academiae scientiarum imperialis Petropolitanae, 8, 1756.

[82] Jacques Hadamard, Sur les problmes aux dérivées partielles et leur signification physique. Princeton University Bulletin, 49-52, 1902.

[83] G. Grimberg, W. Pauls and U. Frisch, Genesis of d'Alembert's paradox and analytical elaboration of the drag problem, Physica D, to appear.

[84] Frisch, Turbulence.

[85] A. Saint-Venant, Résistance des fluides: considérations historiques, physiques et pratiques relatives au problème de l'action dynamique muteulle d'un fluide a d'un solide, dans l'état de permanence supposé acquis par leurs mouvements, Academie des Science, Mémoires 44, 1-280.

[86] J. Stoker, Bull. Amer. Math. Soc. Am. Math., Vol 57(6), pp 497-99.

[87] The Straight Dope, How Do Airplanes Fly, Really?, http://www.straightdope.com/columns/read/2214/how-do-airplanes-fly-really.

[88] K. Stewartson, D'Alembert's Paradox, SIAM Review, Vol. 23, No. 3, 308-343. Jul., 1981.

[89] http://www.aviation-history.com/theory/lift.htm

[90] AVweb, http://www.avweb.com/news/airman/183261-1.html.

[91] W. Beaty, Airfoil Lifting Force Misconception Widespread in K-6 Textbooks, Science Hobbyist, http://www.eskimo.com/ billb/wing/airfoil.htm#L1.

[92] Garret Birkhoff, *Hydrodynamics: a study in logic, fact and similitude*, Princeton University Press, 1950.

[93] S. Cowley, Laminar boundary layer theory: A 20th century paradox, Proceedings of ICTAM 2000, eds. H. Aref and J.W. Phillips, 389-411, Kluwer (2001).

[94] D'Alembert's paradox, en.wikipedia.org/wiki/D'Alembert's_paradox.

[95] J. Hadamard, Sur les problmes aux drives partielles et leur signification physique, Princeton University Bulletin, 49–52, 1902.

[96] The FEniCS Project, www.fenics.org.

[97] U. Frisch, Turbulence: The Legacy of A. N. Kolmogorov. Cambridge University Press, 1995.

[98] S. Goldstein, Fluid mechanics in the first half of this century, in Annual Review of Fluid Mechanics, Vol 1, ed. W. R. Sears and M. Van Dyke, pp 1-28, Palo Alto, CA: Annuak Reviews Inc.

[99] J.Hoffman, Simulation of turbulent flow past bluff bodies on coarse meshes using General Galerkin methods: drag crisis and turbulent Euler solutions, Comp. Mech. 38 pp.390-402, 2006.

[100] J. Hoffman, Simulating Drag Crisis for a Sphere using Friction Boundary Conditions, Proc. ECCOMAS, 2006.

[101] J.Hoffman and Niclas Jansson, A computational study of turbulent flow separation for a circular cylinder using skin friction boundary conditions, Proc. Quality and Reliability of Large Eddy Simulation, Pisa, 2009.

[102] J. Hoffman and C. Johnson, Blowup of Euler solutions, BIT Numerical Mathematics, Vol 48, No 2, 285-307.

[103] J. Hoffman and C. Johnson, *Computational Turbulent Incompressible Flow*, Springer, 2007, www.bodysoulmath.org/books.

[104] J. Hoffman and C. Johnson, Resolution of d'Alembert's paradox, Journal of Mathematical Fluid Mechanics, Online First, Dec 10, 2008.

[105] J. Hoffman and C. Johnson, Separation in slightly viscous flow, to appear.

[106] J. Hoffman and C. Johnson, Is the Clay Navier-Stokes Problem Well-posed?, NADA 2008, http://www.nada.kth.se/∼cgjoh/hadamard.pdf, http://knol.google.com/k/the-clay-navier-stokes-millennium-problem.

[107] J. Hoffman and C. Johnson, The Secret of Flight, http://www.nada.kth.se/∼ cgjoh/ambsflying.pdf

[108] J. Hoffman and C. Johnson, The Secret of Sailing, http://www.nada.kth.se/∼ cgjoh/ambssailing.pdf

[109] J. Hoffman and C. Johnson, Movies of take-off of Naca0012 wing, http://www.csc.kth.se/ctl

[110] http://knol.google.com/k/claes-johnson/dalemberts-paradox/yvfu3xg7d7wt/2.

[111] http://knol.google.com/k/claes-johnson/why-it-is-possible-to-fly/yvfu3xg7d7wt/18.

[112] G.S. Jones, J.C. Lin, B.G. Allan, W.E. Milholen, C.L. Rumsey,R.C. Swanson, Overview of CFD Validation Experiments for Circulation Control Applications at NASA.

[113] R. Kunzig, An old, lofty theory of how airplanes fly loses some altitude, Discover, Vol. 22 No. 04, April 2001.

[114] Experiments in Aerodynamics, Smithsonian Contributions to Knowledge no. 801, Washinton, DC, Smithsonian Institution.

[115] W. Layton, Weak imposition of no-slip boundary conditions in finite element methods, Computers and Mathematics with Applications, 38 (1999), pp. 129142.

[116] http://web.mit.edu/16.00/www/aec/flight.html.

[117] http://www.grc.nasa.gov/WWW/K-12/airplane/lift1.html.

[118] http://www.planeandpilotmag.com/aircraft/specifications/diamond/2007-diamond-star-da40-xl/289.html

[119] L. Prandtl, On Motion of Fluids with Very Little, in Verhandlungen des dritten internationalen Mathematiker-Kongresses in Heidelberg 1904, A. Krazer, ed., Teubner, Leipzig, Germany (1905), p. 484. English trans. in Early Developments of Modern Aerodynamics, J. A. K. Ackroyd, B.P. Axcell, A.I. Ruban, eds., Butterworth-Heinemann, Oxford, UK (2001), p. 77.

[120] L. Prandtl and O Tietjens, *Applied Hydro- and Aeromechanics*, 1934.

[121] G. Schewe, Reynold's-number effects in flow around more or less bluff bodies, 4 Intern. Colloquium Bluff Body Aerodynamics and Applications, also in Journ. Wind Eng. Ind. Aerodyn. 89 (2001).

[122] V. Theofilis, Advance in global linear instability analysis of nonparallel and three-dimensional flows, Progress in Aeropsace Sciences 39 (2003), 249-315.

[123] R. Legendre and H. Werle, Toward the elucidation of three-dimensional separation, Annu. Rev. Fluid Mech. 33 (2001), 129-54.

[124] H. Schlichting, Boundary Layer Theory, McGraw-Hill, 1979.

[125] K. Stewartson, D'Alembert's Paradox, SIAM Review, Vol. 23, No. 3, 308-343. Jul., 1981.

[126] B. Thwaites (ed), *Incompressible Aerodynamics*, An Account of the Theory and Observation of the Steady Flow of Incompressible Fluid pas Aerofoils, Wings and other Bodies, Fluid Motions Memoirs, Clarendon Press, Oxford 1960, Dover 1987, p 94.

[127] R. von Mises, Theory of Flight, McGraw-Hill, 1945.

[128] D. You and P. Moin, Large eddy simulation of separation over an airfoil with synthetic jet control, Center for Turbulence Research, 2006.

[129] O. Chanute, *Progress in Flying Machines*, Long Beach, CA: Lorenz and Herweg, 1976 (originally published 1894).

[130] Kenneth Chang, New York Times, Dec 9, 2003.

[131] 3rd CFD AIAA Drag Prediction Workshop, aaac.larc.nasa.gov/tfcab/cfdlarc/aiaa-dpw.

[132] The FEniCS Project, www.fenics.org.

[133] D'Alembert's paradox, en.wikipedia.org/wiki/D'Alembert's_paradox.

[134] J. Hoffman and C. Johnson, Separation in slightly viscous flow, to be submitted to Physics of Fluids, prel. version available on http:/www.csc.kth.se/cgjoh.

[135] J. Hoffman and C. Johnson: D'Alembert's paradox, new resolution, http://knol.google.com/k/claes-johnson/dalemberts-paradox/yvfu3xg7d7wt/2.

[136] Experiments in Aerodynamics, Smithsonian Contributions to Knowledge no. 801, Washinton, DC, Smithsonian Institution.

[137] R. von Mises, Theory of Flight, McGraw-Hill, 1945.

[138] Prandtl: Father of Modern Fluid Mechanics, http://www.eng.vt.edu/fluids/msc/prandtl.htm.